

MODEL-BASED PRELIMINARY DESIGN AND OPTIMIZATION OF
AIRCRAFTS

A THESIS SUBMITTED TO
THE GRADUATE SCHOOL OF NATURAL AND APPLIED SCIENCES
OF
MIDDLE EAST TECHNICAL UNIVERSITY

BY

MUSTAFA ÖZDEMİR

IN PARTIAL FULFILLMENT OF THE REQUIREMENTS
FOR
THE DEGREE OF MASTER OF SCIENCE
IN
AEROSPACE ENGINEERING

AUGUST 2022

Approval of the thesis:

**MODEL-BASED PRELIMINARY DESIGN AND OPTIMIZATION OF
AIRCRAFTS**

submitted by **MUSTAFA ÖZDEMİR** in partial fulfillment of the requirements for
the degree of **Master of Science in Aerospace Engineering, Middle East
Technical University** by,

Prof. Dr. Halil Kalıpçılar
Dean, Graduate School of **Natural and Applied Sciences**

Prof. Dr. Serkan Özgen
Head of the Department, **Aerospace Engineering, METU**

Prof. Dr. Dilek Funda Kurtuluş
Supervisor, **Aerospace Engineering, METU**

Examining Committee Members:

Assist. Prof. Dr. Ali Türker Kutay
Aerospace Engineering, METU

Prof. Dr. Dilek Funda Kurtuluş
Aerospace Engineering, METU

Assist. Prof. Dr. Halil Ersin Söken
Aerospace Engineering, METU

Assist. Prof. Dr. Özge Başkan Perçin
Aerospace Engineering, METU

Assoc. Prof. Dr. Munir Elfarra
Aerospace Engineering, AYBÜ

Date: 12.08.2022

I hereby declare that all information in this document has been obtained and presented in accordance with academic rules and ethical conduct. I also declare that, as required by these rules and conduct, I have fully cited and referenced all material and results that are not original to this work.

Name, Last name: Mustafa Özdemir

Signature:

ABSTRACT

MODEL BASED PRELIMINARY DESIGN AND OPTIMIZATION OF AIRCRAFTS

Özdemir, Mustafa
Master of Science, Aerospace Engineering
Supervisor: Prof. Dr. Dilek Funda Kurtuluş

August 2022, 130 pages

This study aims to create an interdisciplinary, multi-level design approach that is based on six degrees of freedom mathematical model. The model provides all disciplines to communicate with each other simultaneously, thanks to an automated process chain system. The main advantage of automatization of analyses for the design process is observing interdisciplinary effects clearly without wasting time and money. Instead of using only empirical relations, in this study, calculations are originating from trim and simulation analyses that are based on the equation of motions. Trim and simulation capability provides to increase the diversity of the analyses which can be considered in early design phases such as stability and control. However, these analyses require an integrated mathematical flight dynamic model, which is capable to solve analytical and differential equations numerically. This study explains how the model structure is created to perform analysis in the design and optimization process of the fixed-wing propeller-driven aircrafts. Throughout the whole design process, the methodologies which are followed up for the analyses

and optimization, are reported. Besides investigating aircraft design methodologies, the model validation processes are also included to the study.

Keywords: Model-Based Design, Preliminary Aircraft Design, Trim and Simulation, MAD Software, Design of Experiment.

ÖZ

HAVA ARAÇLARININ MODEL BAZLI ÖN TASARIM VE OPTİMİZASYONU

Özdemir, Mustafa

Yüksek Lisans, Havacılık ve Uzay Mühendisliği

Tez Yöneticisi: Prof. Dr. Dilek Funda Kurtuluş

Ağustos 2022, 130 sayfa

Bu çalışma, altı serbestlik dereceli matematiksel modele dayalı disiplinler arası, çok seviyeli bir tasarım yaklaşımı oluşturmayı amaçlamaktadır. Model, otomatikleştirilmiş süreç zinciri sistemi sayesinde tüm disiplinlerin aynı anda birbirleriyle iletişim kurmasını sağlar. Tasarım süreci için analizlerin otomatikleştirilmesinin temel avantajı, disiplinler arası etkilerin zaman ve para kaybetmeden net bir şekilde gözlemlenmesidir. Bu çalışmada sadece ampirik bağıntılar kullanmak yerine, hareket denklemlerine dayalı trim ve simülasyon analizlerinden hareketle hesaplamalar yapılmaktadır. Trim ve simülasyon yeteneği, stabilite ve kontrol gibi erken tasarım aşamalarında düşünülebilecek analizlerin çeşitliliğini artırmayı sağlar. Ancak bu analizler, analitik ve diferansiyel denklemleri sayısal olarak çözebilen entegre matematiksel uçuş dinamik modeli gerektirir. Bu çalışmada, sabit kanatlı pervaneli uçakların tasarım ve optimizasyon sürecinde analizlerin yapılabilmesi için model yapısının nasıl oluşturulduğu anlatılmaktadır. Tüm tasarım süreci boyunca analizler ve optimizasyon için takip edilen

metodolojiler raporlanmıřtır. Uak tasarım metodolojilerinin arařtırılmasının yanı sıra model doęrulama sreleri de bu alıřmada yer almaktadır.

Anahtar Kelimeler: Model Bazlı Tasarım, Hava Aracı n Tasarımı, Trim ve Simlasyon, MAD Yazılımı, Deney Tasarımı.

To my family and friends who were always there for me.

ACKNOWLEDGMENTS

I am grateful to my thesis advisor Prof. Dr. Dilek Funda Kurtuluş for her guidance throughout my thesis work. She was always supportive and helpful.

I owe my regard to my Mother and Father for encouraging me to succeed always.

TABLE OF CONTENTS

ABSTRACT.....	v
ÖZ.....	vii
ACKNOWLEDGMENTS	x
TABLE OF CONTENTS.....	xi
LIST OF TABLES	xiv
LIST OF FIGURES	xviii
LIST OF ABBREVIATIONS.....	xx
LIST OF SYMBOLS	xxii
CHAPTERS	
1 INTRODUCTION	1
1.1 Literature Survey.....	5
1.1.1 SUAVE.....	6
1.1.2 AGILE PROJECT.....	7
1.1.3 CEASIOM.....	9
1.1.4 AID	13
1.1.5 AAA.....	14
1.1.6 Comparison of Design Software.....	16
1.2 Thesis Scope.....	17
2 MODEL METHODOLOGY	19
2.1 Model Capabilities	19
2.2 Specifications of Cessna 172 aircraft	20

2.3	Model Blocks	24
2.3.1	Aerodynamic Block	25
2.3.2	Engine Block	34
2.3.3	Equation of Motion Block	37
2.3.4	Landing Gear Block	48
2.3.5	Atmosphere Model	50
2.3.6	Stability and Control Block	54
2.3.7	Weight and Balance	59
2.3.8	Cost Analysis	64
3	ANALYSIS CONDITIONS AND REQUIREMENTS	67
3.1	Performance Analysis	67
3.1.1	Range	68
3.1.2	Endurance	69
3.1.3	Stall Speed Calculation	70
3.1.4	Maximum Cruise Speed	72
3.1.5	Sustained Turn	72
3.1.6	Ceiling	73
3.1.7	Rate of Climb	74
3.1.8	Take of Distance	75
3.1.9	Landing Distance	78
3.2	Stability Analysis	80
3.2.1	Flight Path Stability	81
3.2.2	Flying and Handling Qualities	83
3.2.3	Spin	91
3.2.4	Departure	92

3.3	Control Surface Analysis	94
3.3.1	Nose Down Recovery	94
3.3.2	Controllability	95
3.3.3	Maximum Roll Capability	96
3.3.4	Crosswind Landing	98
3.4	Model Validation Results	100
4	PRELIMINARY DESIGN AND OPTIMIZATION METHODOLOGIES ..	101
4.1	Customer Requirements	101
4.2	Competitors	102
4.3	Configuration Selection.....	103
4.4	Quality Function Deployment Analysis	104
4.5	Overall Evaluation Criteria Equation	105
4.6	Design of Experiment.....	106
4.6.1	Design Variable Reduction (Screening)	110
4.6.2	Response Surface Function.....	112
4.7	Optimization.....	114
	CONCLUSION.....	123
	REFERENCES	125

LIST OF TABLES

TABLES

Table 1: MAD tool output parameters.....	5
Table 2: Submodules of advanced aircraft analysis software (DARcorporation, 2018).....	15
Table 3: Comparison of design software.....	17
Table 4: Legends of design software properties.....	17
Table 5: Positive sign convention.....	20
Table 6: Cessna 172 versions and updates history (Wikipedia contributors, 2022b).....	21
Table 7: Cessna 172N configuration properties	21
Table 8: Lifting surface of Cessna 172N (Cessna Aircraft Company, 1978)	22
Table 9: Mean aerodynamic chord of Cessna 172N (Fasanella & Jackson, 2016)..	22
Table 10: Control surfaces of Cessna 172N (Cessna Aircraft Company, 1978).....	22
Table 11: Cessna 172N fuselage properties (Cessna Aircraft Company, 1978)	22
Table 12: Cessna 172N landing gear properties (Cessna Aircraft Company, 1978).....	23
Table 13: Cessna 172N engine properties (Lycoming, 2007).....	23
Table 14: Inertial properties of Cessna 172N (Cessna Aircraft Company, 1978)...	23
Table 15: Cessna 172N weight breakdown (Roskam, 2018)	24
Table 16: Cessna 172 performance outputs (Cessna Aircraft Company, 1978)	24
Table 17: Datcom Aerodynamic Coefficient Predictions (Galbraith, 2004).....	26
Table 18: Aerodynamic calculation tools capability comparison	31
Table 19: Aerodynamic calculation tools comparison legends	31
Table 20: Aerodynamic analysis results of DATCOM, AVL and Open VSP	32
Table 21: Error norm comparison of aerodynamic analysis software.....	33
Table 22: Kp values for different number of blades configurations	34
Table 23: Velocity and thrust couples	37
Table 24: Equation and unknown alternatives	37
Table 25: Trim algorithm parameters	40

Table 26: Straight flight wind axis trim condition.....	42
Table 27: Straight flight body axis trim condition.....	42
Table 28: Climb trim condition.....	42
Table 29: Fixed angle of attack speed prediction trim condition.....	43
Table 30: Level flight maximum speed prediction trim condition	43
Table 31: Instant turn trim condition	43
Table 32: Steady coordinated turn trim condition	43
Table 33: Pull up trim condition	44
Table 34: Steady roll in body axis trim condition.....	44
Table 35: Crosswind landing trim condition.....	44
Table 36: Steady spin trim condition	44
Table 37: Quasi trim condition	45
Table 38: Ceiling trim condition.....	45
Table 39: Landing gear weight carriage percentages.....	48
Table 40: Friction coefficients of runways (U.S.A Department of Defense, 2003)	50
Table 41: Coefficients for prediction of atmospheric parameters (ESDU 77022, 2003)	51
Table 42: Description of linearized system equation parameters	55
Table 43: Linearized system matrix.....	56
Table 44: Flying quality parameters (Yechout et al., 2003)	57
Table 45: Inverse simulation parameter descriptions	59
Table 46: Aircraft weight estimation formulations (Roskam, 2018).....	60
Table 47 : The empirical predictions of CG point (Roskam, 2018)	61
Table 48: The weight prediction method validation of MAD with Cessna 172.....	62
Table 49: C_{GA} Coefficient Sub-Coefficients (Harris & Scully, n.d.).....	65
Table 50: Analysis capability of the MAD environment.....	67
Table 51: Definitions of ceiling types.....	73
Table 52: Take off speed definitions (Gudmundsson, 2014).....	76
Table 53: Landing performance speed definitions (Gudmundsson, 2014).....	78
Table 54: FPS levels of acceptability (U.S.A. Department of Defense, 1980).....	81
Table 55: Aircraft classes (U.S.A. Department of Defense, 1980).....	83

Table 56: Flight phase categories (U.S.A. Department of Defense, 1980)	84
Table 57: Flying quality levels (U.S.A. Department of Defense, 1980)	85
Table 58: Flight envelopes scope	85
Table 59 : Accepted levels of flying quality in related flight envelope	86
Table 60: Short period mode flying quality levels in terms of damping ratio (U.S.A. Department of Defense, 1980)	86
Table 61: Phugoid mode flying quality levels (U.S.A. Department of Defense, 1980).....	86
Table 62: Roll mode flying quality levels in terms of time constant (U.S.A. Department of Defense, 1980)	87
Table 63: Spiral mode flying quality levels in terms of time to double amplitude (U.S.A. Department of Defense, 1980)	87
Table 64: Dutch roll mode flying quality levels (U.S.A. Department of Defense, 1980).....	87
Table 65: Bihrlle-Weissman chart class definition (Mason, 2006)	92
Table 66: Nose down recovery requirements (Nguyen & Foster, 1990)	94
Table 67: Roll rate requirements for class I and II aircrafts (U.S.A. Department of Defense, 1980).....	96
Table 68: Required time to achieve 30° bank angle change for class III aircraft (U.S.A. Department of Defense, 1980)	96
Table 69: Roll rate requirements for class IV aircrafts (U.S.A. Department of Defense, 1980).....	97
Table 70: Crosswind requirement (U.S.A. Department of Defense, 1980)	98
Table 71: Comparison between MAD prediction and Cessna 172 performance data	100
Table 72: Customer requirements and importance levels	102
Table 73: Specifications of competitor aircrafts (Wikipedia contributors, 2022).	103
Table 74: Fixed wing aircraft configuration alternatives	104
Table 75: Selected configuration to optimization (Cessna Aircraft Company, 1978)	104
Table 76: Quality Function Deployment Analysis	105

Table 77: Design output parameters	106
Table 78: Statistical methodology alternatives in DOE.....	107
Table 79: All Design Input List	111
Table 80: Selected design input parameters and optimization intervals.....	112
Table 81: Considered factor interactions by response surface method.....	113
Table 82: Most affected design outputs for main design factor.....	117
Table 83: Performance enhancements of Cessna 172N aircraft	120
Table 84: Design variables of optimized Cessna 172N geometry	120
Table 85: MAD analysis and response surface function prediction comparison..	121
Table 86: Alternative customer importance levels	122
Table 87: Performance enhancements results of Cessna 172N aircraft according to alternative customer importance levels.....	122

LIST OF FIGURES

FIGURES

Figure 1: MAD software design and optimization process flowchart.....	3
Figure 2: AGILE multidisciplinary simulation workflow (Hasan et al., 2018)	7
Figure 3: CEASIOM multidisciplinary submodules (Richardson et al., 2011)	10
Figure 4: CEASIOM analysis workflow (Afsar et al., 2013).....	11
Figure 5: CEASIOM optimization process flowchart (Afsar et al., 2013).....	13
Figure 6: Positive sign convention of control surfaces (Cook, 2013)	20
Figure 7: Datcom+ Software Visualization Output.....	27
Figure 8: AVL visualization output (Drela & Youngren, 2004b).....	28
Figure 9: Aerodynamic mesh geometry of OpenVSP.....	29
Figure 10: Open VSP visualization output.....	30
Figure 11: Propeller thrust quadratic interpolation	36
Figure 12: Newton Raphson algorithm flowchart	41
Figure 13: Simulation outputs of the MAD tool	46
Figure 14: Conventional trim search method	47
Figure 15: Instant trim search method.....	47
Figure 16: Atmospheric temperature model.....	52
Figure 17: Atmospheric density model	52
Figure 18: Inverse simulation control algorithm	58
Figure 19: Inverse simulation method validation results	59
Figure 20: The comparison of weight prediction results of Cessna 172	63
Figure 21: Cessna 172N mass & CG envelope analysis results of MAD tool	64
Figure 22: Aircraft pricing relation with respect to empty weight and engine horsepower (Harris & Scully, n.d.)	65
Figure 23: Price escalation factor change in time (Harris & Scully, n.d.)	66
Figure 24: Range profile with respect to air velocity	69
Figure 25: Endurance profile with respect to air velocity	70
Figure 26: Sustain turn trimmable load factor map.....	73
Figure 27: Ceiling performance of Cessna 172N aircraft	74

Figure 28: Cessna 172N rate of climb performance	75
Figure 29: Take-off simulation procedure	76
Figure 30: Take off simulation results	77
Figure 31: Landing distance analysis visualization	78
Figure 32: Landing simulation body velocities results	79
Figure 33: Landing simulation Euler angles results.....	80
Figure 34: Landing distance simulation results	80
Figure 35: Flight path angle vs true airspeed (U.S.A. Department of Defense, 1980)	82
Figure 36: Flight path stability analysis output.....	82
Figure 37: Eigenvalues of the Cessna 172 aircraft (Çetin, 2018).....	88
Figure 38: System eigenvalues predicted by MAD software	88
Figure 39: Flying quality map for most aft (left) and forward (right) cg.....	89
Figure 40: Most unstable pole with respect to airspeed.....	89
Figure 41: Linear and nonlinear model response to vertical gust perturbation	90
Figure 42: Linear and nonlinear model response to side gust perturbation.....	90
Figure 43: Bihrlle-Weissman chart (Mason, 2006)	93
Figure 44: Controllable flight map	95
Figure 45: Bank angle response to maximum roll command	97
Figure 46: Crosswind landing analysis results.....	99
Figure 47: Central composite design structure (SAS Institute Inc, 2018b)	108
Figure 48: Pareto plot (SAS Institute Inc, 2018b)	111
Figure 49: Response surface method design space (SAS Institute Inc, 2018b)....	113
Figure 50: Design and optimization flowchart	115
Figure 51: JMP contour profiler (SAS Institute Inc, 2018b)	116
Figure 52: JMP maximum desirability results (SAS Institute Inc, 2018b).....	118
Figure 53: ROC surface plot (SAS Institute Inc, 2018b).....	119

LIST OF ABBREVIATIONS

ABBREVIATIONS

<i>AR</i>	Aspect ratio
<i>BHP</i>	Brake horsepower
<i>CCD</i>	Central composite design
<i>CG</i>	Center of gravity
<i>CW</i>	Crosswind
DLR	German aerospace center
DOE	Design of experiment
FPS	Flight path stability
<i>LCDP</i>	Lateral control departure parameter
<i>LE</i>	Leading edge
<i>LG</i>	Landing gear
<i>MAC</i>	Mean aerodynamic chord
MAD	Model based aircraft design software
MUR	Most unstable root
NDR	Nose down recovery
<i>OEC</i>	Overall evaluation criteria
<i>QFD</i>	Quality function deployment
<i>ROC</i>	Rate of climb
RSF	Response surface function

<i>RSM</i>	Response surface method
<i>SL</i>	Sea level
<i>TLAR</i>	Top level aircraft requirements
<i>TR</i>	Taper ratio
<i>VLM</i>	Vortex lattice method

LIST OF SYMBOLS

SYMBOLS

S	Wing area in ft ²
A	Wing aspect ratio
T	Temperature
n_{ult}	Design ultimate load factor
W_{TO}	Take-off weight in lbs
W_G	G weight in kg
W_{fc}	Flight control system weight
W_{els}	Electrical System weight
W_{iae}	Instrumentation, avionics, and electronics weight
W_{api}	Air-Conditioning and anti-icing system weight
W_{ox}	Oxygen system weight
W_w	Wing weight
W_h	Horizontal tail weight
W_v	Vertical tail weight
W_f	Fuselage weight
W_e	Empennage weight
$W_{mainLGs}$	Main landing gears weight
W_{noseLG}	Nose landing gear weight
S_h	Horizontal tail area in ft ²
A_H	Horizontal tail aspect ratio

t_{r_h}	Horizontal tail maximum root thickness in ft
S_v	Vertical tail area in ft ²
A_v	Vertical tail aspect ratio
t_{r_v}	Vertical tail maximum root thickness in ft
$\Lambda_v(\frac{1}{4})$	Vertical tail quarter chord sweep angle
N_{pax}	Number of passangers including the pilots
L_{fn}	Fuselage length in ft
P_{max}	Maximum fuselage perimeter in ft
W_L	Design landing weight in lbs
$n_{ult.l}$	Ultimate load factor for landing
L_{sm}	Shock strut length for main LG in ft
L_{sn}	Shock strut length for nose LG in ft
P_{to}	Required take-off power in hp
q_c	Compressible dynamic pressure
M	Mach number
P	Pressure
P_0	Sea level air pressure
ρ	Air density
ρ_{std}	Standard air density
Δ_{ISA}	Temperature difference in Kelvin
γ_{air}	<i>Adiabatic index of air</i>
R	<i>Gas constant for air</i>

T	<i>Air Temperature in Kelvin</i>
P_w	Engine power in watt
$A_{spinner}$	Spinner disc area in m ²
A_{disc}	Total propeller disc area in m ²
η_p	Propeller efficiency
d_{vs}	Maximum vertical landing gear stroke length in meters
k_{LG}	Landing gear stiffness
$P_{LG(wheel)}$	Bottom location of landing gear wrt cg in wheel axis
$P_{LG(body)}$	Bottom location of landing gear wrt cg in body axis
$V_{P_{LG}(body)}$	Velocity of P_{LG} in body axis
$V_{P_{LG}(wheel)}$	Velocity of P_{LG} in wheel axis
$h_{LGwheel}$	Bottom location of landing gear wrt ground in wheel axis
$T_{W \leftarrow B}$	Transformation matrix from body to wheel axis
ζ_{LG}	Damping coefficient of landing gear
h	Altitude referenced from cg point
μ_{rf}	Rolling friction coefficient
$F_{LGwheel}$	Landing gear forces in wheel axis
F_{LGbody}	Landing gear forces in body axis
$M_{LGwheel}$	Landing gear moments in wheel axis
M_{LGbody}	Landing gear moments in body axis
LG_{wcp}	Landing gear weight carriage percentage

u	Body x axis velocity of the aircraft
v	Body y axis velocity of the aircraft
w	Body z axis velocity of the aircraft
$(\)'$	Parameter with respect to air
$(\)^E$	Parameter with respect to earth
$\dot{(\)}$	Time derivative
V_{TAS}	True airspeed
$V_{o_{min}}$	Minimum approach speed
α	Angle of attack
β	Angle of sideslip
p	Roll rate
q	Pitch rate
r	Yaw rate
θ	Pitch angle
ϕ	Bank angle
ψ	Heading angle
γ	Flight path angle
N_x	Body x axis load factor
N_y	Body y axis load factor
N_z	Body z axis load factor
Δ_{ISA}	Air temperature difference from T_{std}
δ_{Flap}	Flap deflection angle

$\delta_{elevator}$	Elevator deflection angle
$\delta_{aileron}$	Aileron deflection angle
δ_{rudder}	Rudder deflection angle
C_{D0}	Parazite drag coefficient
C_L	Lift coefficient
C_D	Drag coefficient
C_Y	Side force coefficient
C_R	Roll moment coefficient
C_M	Pitch moment coefficient
C_N	Yaw moment coefficient
X_A	Body x axis aerodynamic force
Y_A	Body y axis aerodynamic force
Z_A	Body z axis aerodynamic force
L_A	Body x axis aerodynamic moment at cg point
M_A	Body y axis aerodynamic moment at cg point
N_A	Body z axis aerodynamic moment at cg point
X_T	Body x axis engine force
Y_T	Body y axis engine force
Z_T	Body z axis engine force
L_T	Body x axis engine moment at cg point
M_T	Body y axis engine moment at cg point
N_T	Body z axis engine moment at cg point

I_{xx}	Body x axis inertia
I_{yy}	Body y axis inertia
I_{zz}	Body z axis inertia
λ_{tcr}	Take-off fuel consumption ratio
W_c	Fuel weight for cruise
W_l	Fuel weight for landing
η_{oswald}	Oswald efficiency
K	Coefficient for lift induced drag
C_{BHP}	Horsepower specific fuel consumption for piston engines
Lph	Fuel consumption per hour in pound
Gph	Fuel consumption per hour in galon
C_t	Thrust specific fuel consumption (1/sec)
V_{TAS}	True air speed
V_{IAS}	Indicated air speed
V_{EAS}	Equavalent air speed
V_{CAS}	Calibrated air speed
P_{BHP}	Engine power in horsepower
$d_{propeller}$	Propeller diameter
τ	Track angle

CHAPTER 1

INTRODUCTION

The main objective of this study is creating an environment to conduct design and optimization process of the fixed wing aircrafts. In this scope, the analyses that are performed to observe the performance of each design concept, are based on trim and simulations. This concept is creating an alternative to use semi empirical methods in conceptual design which is not flexible and accurate enough. If calculations could be performed via fairly accurate methods for each phase of design process, then spending excess time and money could be prevented. Especially the main difference of this study from the literature is the capability of performing instant trim and simulation analysis based on six degrees of freedom model, without needing an overall aerodynamic database in preliminary design phase. Since the solver algorithm does not need an aerodynamic database to calculate trim points and perform simulations, as from the first iteration of optimization phase, all performance and stability outputs of the alternative geometries can be attained instantly. At the further steps of the design process, database which is increased fidelity level can be utilized to get more accurate force and moment values after minimizing number of design alternatives with lower fidelity level calculation methods (Böhnke et al., 2013). The main motivation of this study is determined as fixing the deficiencies of the industry in the field of aircraft design and optimization by utilizing following innovative capabilities:

- Usage of the same model structure from the first phase of the design process up to the detailed design
- Rapid initial design without needing overall aerodynamic database, with the help of instant simulation method which is created for this study. (Instant simulation method is based on the calculation of force and moments on the aircraft for each iteration of numerical solution instantly)

- Performing trim and simulation based advanced analyses in preliminary design process such as flight path stability, nose down recovery and maximum roll rate analyses
- Observing the advantages and disadvantages of all possible design alternatives in the very early phase of the design without wasting time and money
- Creating animations for simulations and visualizations for analysis results
- Getting together and revealing whole methodologies of the model creation, performance & stability analyses, and optimization process
- Creating the model structure, which is compatible to create unique and futuristic concept design alternatives e.g. (Tiltrotor VTOL), without depending on historical trends and empirical correlations
- Generating object-oriented model structure allows to use replaceable plug in-out analysis tools and methodologies inside of each discipline, which creates multi-fidelity flexible design environment

To realize the idea of rapid and accurate design, MAD (Model Based Aircraft Design Software) is developed for this study specifically as a competitor of other conceptual design tools in the literature. The analysis part of the MAD software consists of approximately 6000 lines of object-oriented code written in Python environment. The code includes six degrees of freedom dynamic model. Also, for the optimization process JMP, which is a software for statistical analysis, is benefitted from.

As a first step of the analysis part, MAD software requires to define following input parameters in detail:

- Outer Geometry Definition
- Engine Properties
- Payload / Fuel Weight
- Landing Gear Properties
- Atmospheric Conditions

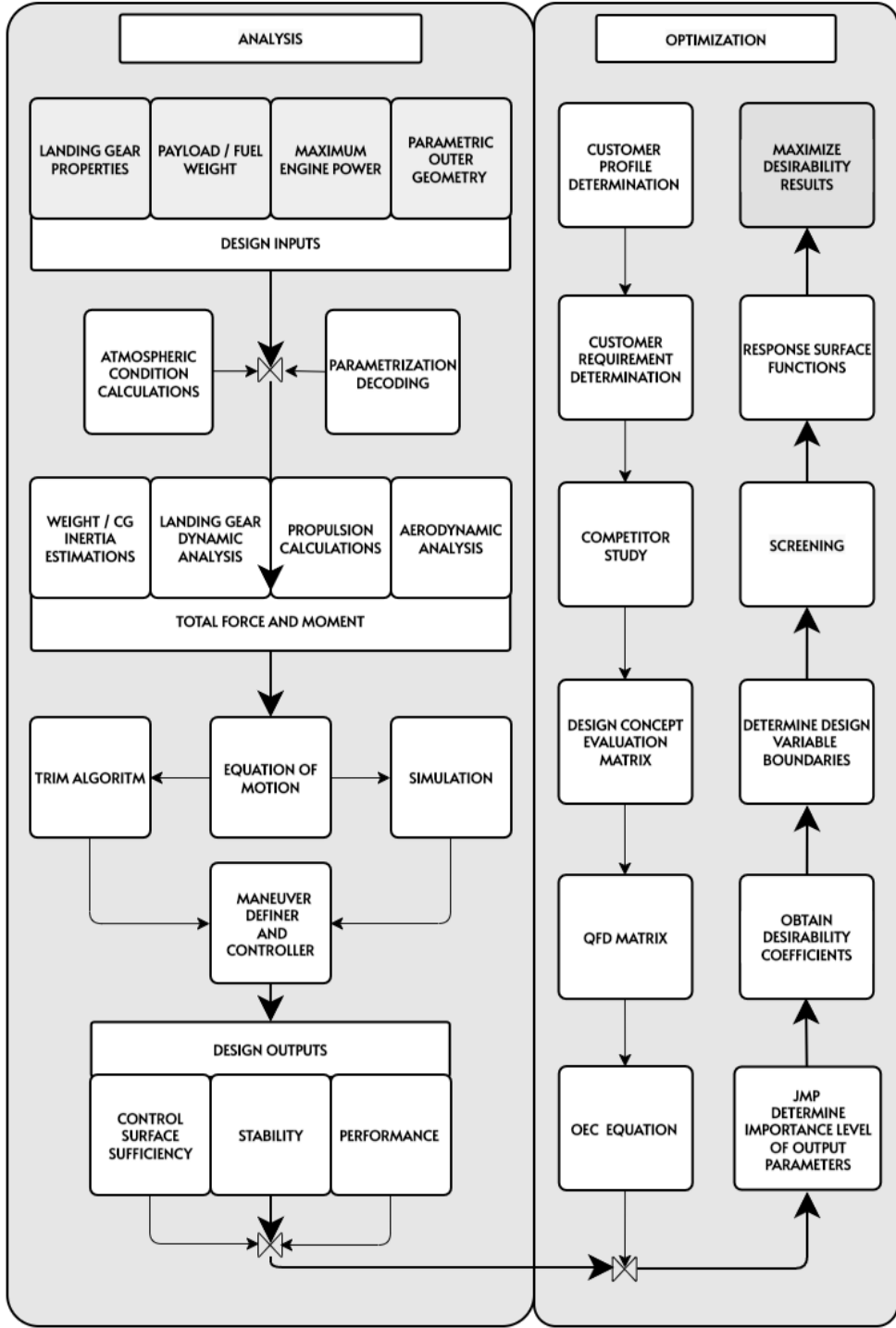


Figure 1: MAD software design and optimization process flowchart

According to input parameters specified above, force and moment calculations are performed via engine, aerodynamic, landing gear, weight and atmosphere blocks. Python-based six degrees of freedom dynamic model performs trim and simulation analyses by using related input parameters. Force and moment values are used to find the trim points by following up the equations of motion block. In the trim analysis Newton Raphson is observed as the most efficient method in point of time and accuracy issues.(Özdemir & Kurtulus, 2021)

In the design procedure, simulations are initiated from the trim points and performed by integrating differential equation of motion. MAD environment provides three choices for numerical integration which are Euler, second order and fourth order Runge Kutta methods. The user can select one of these methods according to required accuracy level. These integration methodologies that is utilized to conduct simulations, are very crucial for design process but not sufficient to get desired maneuver performance results. To obtain related maneuver performance, PID and Inverse Simulation Controllers are utilized. All above procedures enable to prepare required environment to get desired performance and stability outputs of the concept aircraft, that is stated at Table 1.

In the analysis section, each combination of input parameters gives related performance outputs with the help of sub-blocks. To obtain a relation between design inputs and outputs, numerous of analysis are performed via MAD environment. If the analysis part is regarded as black box, then MAD environment can be used for optimization process. As a result of this process, each output parameters can be represented as the set of polynomial equations which is defined in terms of design variables. By utilizing this analytical equations set, global optimum point can be achieved in the constrained design space.

Table 1: MAD tool output parameters

Stability Analysis	Departure FPS FHQ Spin
Performance Analysis	Take off Distance Landing Distance ROC Ceiling Stall Speed Maximum Cruise Speed Sustained Turn Range Endurance
Control Surface Analysis	NDR Max Roll Rate Crosswind Landing Controllability

1.1 Literature Survey

In the literature, competitor methodologies and software are investigated. In order to categorize tools and methodologies, five class are examined according to concept of (Chudoba, 2019).

- **Class I (Early Dawn):** Intuition based design where the experience is gained via trial-and-error method.
- **Class II (Manual Design Sequence):** Empirical database based, limited physical understanding methods
- **Class III (Computer Automation):** Automated Class II analysis methods
- **Class IV (Multidisciplinary Integration):** Multidisciplinary systems with opportunity to perform parameter sweeps and optimization loops. Mainly based on empirical and statistical correlations.
- **Class V (Generic Design Capability):** Conceptual design methodologies which can be used for any aircraft configurations generically. This type of tools permit to change major design variables to see the effects of them.

Mainly conducted by physic-based analyses and includes replaceable multi fidelity submodules (Liersch & Hepperle, 2011).

1.1.1 SUAVE

SUAVE is a conceptual level multi-fidelity design environment which is created by Stanford University. It allows to design conceptually futuristic aircrafts (Lukaczyk et al., n.d.).

General capability of the software is summarized below (Lukaczyk et al., n.d.):

- Weight Prediction
- Aerodynamic Calculation
- Static & Dynamic Stability Calculations
- Propulsion Model for Electric Motors or Gas Turbines
- Fundamental Performance Calculations

Above modules are used to analyze flight phase such as takeoff, landing, climb, descend and cruise. Also, SUAVE uses standard optimization packages in Python environment like SciPy, PyOpt, OpenMDAO, and Dakota. These packages provide user to obtain optimum design parameters by using gradient based multidisciplinary optimization methods. Optimization processes are mainly based on specific missions which is defined by user.

SUAVE consist of the modular set of analysis tools which provide to select different fidelity level at different phase of the design process. For aerodynamic calculations, SUAVE uses the methods having different level of accuracy like AVL, Datcom, SU2 or Lifting Line Method. For stability and performance calculations, analytical methods are used by doing some assumptions. Simulations are conducted with analytical iterations instead of integrating to differential equation of motion. Thus, SUAVE does not uses numerical solutions of equation of motion directly for stability analyses. Moreover, propulsion calculations are performed for different type of engines such as, turbofan, turbojet, ramjet or scramjet.

SUAVE serves lots of opportunity for design and optimization process but, the poor side of the program is lack of graphical user interface capability.

1.1.2 AGILE PROJECT

AGILE Project is developing the third generation MDO processes, which will support the development of the next generation aerospace products (Vecchia et al., 2018). It is conducted by DLR and cooperated with numerous institutes, includes variety of analysis submodules from different disciplines.

Each tool has own fidelity level to use different phase of design process. According to (Hasan et al., 2018), aircraft design process is highly interdisciplinary nature. All disciplines are connected to each other via multidisciplinary process chains so called simulation workflows. Using these simulation workflows, integrated multidisciplinary and multi-fidelity design studies can be performed (Hasan et al., 2018).

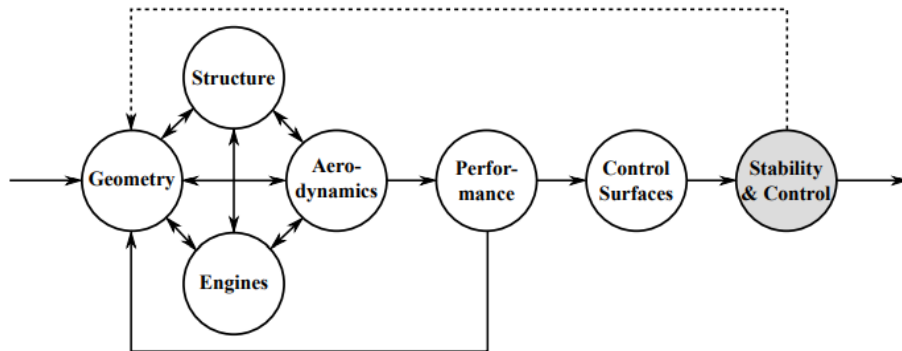


Figure 2: AGILE multidisciplinary simulation workflow (Hasan et al., 2018)

In Figure 2 optimization process is shown according to performance & stability and control disciplines. In this concept the performance outputs are used for geometry optimization in the inner loop without including control surface effects (point mass). In the outer loop, stability and control parameters are utilized to get the alternative geometry which provide optimum performance and stability outputs by including

control surface dynamics. In the AGILE project, the preliminary aircraft design process includes following independent disciplinary analysis modules, which is used for physics-based simulations and sensitivity analyses:

- Aerodynamic analysis
- Propulsion system analysis
- Mass and balance analysis
- Structural analysis
- Flight performance and stability analysis

Moreover, design and optimization steps of AGILE paradigm are listed as follows:

- Determination of TLAR (Top Level Aircraft Requirements)
- Determination of baseline aircraft
- Creating input file in CPACS format
- Performing analyses via submodules
- Getting outputs in CPACS format
- Performing optimization and sensitivity analyses

In the project there is not any specific list of tools to integrate to overall system. Any tool can be integrated to design process if the input and output format (CPACS) are arranged as compatible with RCE environment. RCE (Remote Component Environment) is an integration environment to analyze, design and simulate complex systems such as aircraft or satellites. RCE is developed by DLR, and it is used for multidisciplinary collaboration (Zur, 2013). CPACS (Common Parametric Aircraft Configuration Schema) is a hierarchic XML-structure developed by DLR for usage in multidisciplinary aircraft design processes. CPACS structure includes all information about the aircraft configuration to be designed (Rocca et al., 2013). Besides a detailed, parametrized definition of the aircraft geometry, data for various analyses (aerodynamics, mission analysis, climate impact, loads, structures) is included to CPACS structure (Böhnke et al., 2013). In summary, RCE and CPACS is used to provide a coordination between tools from different disciplines. Some of these tools can be listed as follows (Hasan et al., 2018):

- **VAMPzero**: enables the generation of initial CPACS data enough to trigger higher level methods, using a minimum amount of input data (TLAR). Output format contains aircraft's outer geometry, performance data and its mass breakdown (Moerland et al., 2012).
- **EMWET**: is used as weight estimation.
- **Tornado & AVL**: are used to calculate aerodynamic coefficient, which is based on vortex lattice method.
- **TWDat**: is used to create engine performance map.
- **WAB**: is used to estimate weight and CG.
- **LCG**: is used to generate Vn diagrams.
- **TRIM_VL**: is used to trigger AVL for generating aerodynamic polars or calculate the wing load distribution for pre-provided load case (Moerland et al., 2012).
- **MONA**: is used for structural analysis and sizing.
- **SMS**: is used for straightforward mission simulation.
- **FSMS** is used to perform mission analysis.
- **MisSim**: is used to simulate an autopiloted flight on a given flight plan.
- **DOC**: is used to predict operational cost.

1.1.3 CEASIOM

CEASIOM (Computerized Environment for Aircraft Synthesis and Integrated Optimization Methods) that is developed within the European Program SimSAC (Simulating Aircraft Stability and Control Characteristics for Use in Conceptual Design), is a framework tool for conceptual aircraft design that integrates discipline-specific tools like: CAD & mesh generation, CFD, stability & control analysis, aeroelastic analysis, etc., all for the purpose of early preliminary design (Böhnke et al., 2013). CEASIOM is suitable to perform the analyses having the variety of fidelity level. Moreover, it includes optimization tools to get global optimum point

between different design alternatives. One of the advantages of the CEASIOM is having graphical user interface.

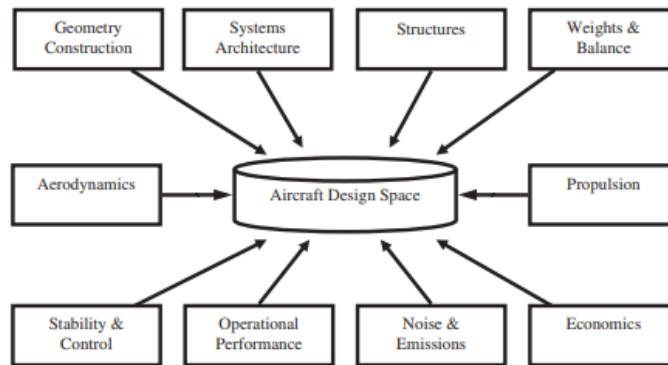


Figure 3: CEASIOM multidisciplinary submodules (Richardson et al., 2011)

Figure 3 shows all disciplines which are connected to CEASIOM environment. According to figure CEASIOM can be classified as multidisciplinary design software which has multi-level hierarchy.

The analysis workflow of CEASIOM software is shown in Figure 4. The variety of tools, which are used in workflow, are listed in following part (Pester, 2010).

ACBuilder

The aircraft builder module allows user to define a parameterized geometry of an aircraft and visualize it. Thanks to this module, data importing, or exporting is possible in *.xml format. Input file AMB, NeoCass and FCSDT modules can be generated via AcBuilder. The sub-tasks of AcBuilder are listed as follows:

- Geometry Definition,
- Weight & Balance accommodations,
- Centre of Gravity computation,
- Technology Definitions.

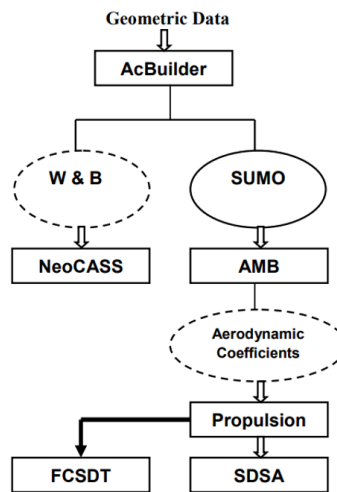


Figure 4: CEASIOM analysis workflow (Afsar et al., 2013)

SUMO

SUMO is a graphical tool aimed at rapid creation of aircraft geometries and automatic surface mesh generation.

AMB

The Aerodynamic Model Builder controls the calculation and displays of the aerodynamic aircraft characteristics. For RANS solver, CFD mesh must be prepared using the tool SUMO previously. CEASIOM uses below methodologies to create overall aerodynamic database in different phase of design process for the further analysis of the aircraft:

- Tornado - Datcom
- Euler
- Rans

PROPULSION

The Propulsion tool calculates engine performance for different Mach number and altitude that are required for the SDSA tool.

SDSA

The SDSA (Simulation and Dynamic Stability Analysis) module is useful for dealing with stability analysis based on JAR/FAR, ICAO and MIL standards. Also, six degree of freedom simulation is possible via this tool. Overall capabilities of SDSA tool are stated as follows:

- Trim & Simulation analysis
- Linearization & stability characteristics analysis
- LQR controller integration
- Performance analysis (Range, Endurance, Takeoff & Landing Distance)

NeoCass

NeoCass tool is utilized to analyze weight, structure and aeroelastic properties of the aircraft. It is a combination of modules that gets together computational, analytical, and semi-empirical methods to overcome all the aspects of the aero-structural analysis of a design layout at conceptual design stage.

FCSDT

Flight Control System Design Toolkit has two main capabilities: The first function is to design the FCS itself while the second function is to perform some analyses which affect design of other sub-spaces in the aircraft design space. The FCSDT includes five modules known as:

- FCSEA-Flight Control System Architecture,
- SCAA- Stability & Control Analyzer & Assessor,
- LTIS-Linear Time Invariant Synthesis,
- CLD-Control Laws Definition,
- FSim-Desktop Flight Simulator.

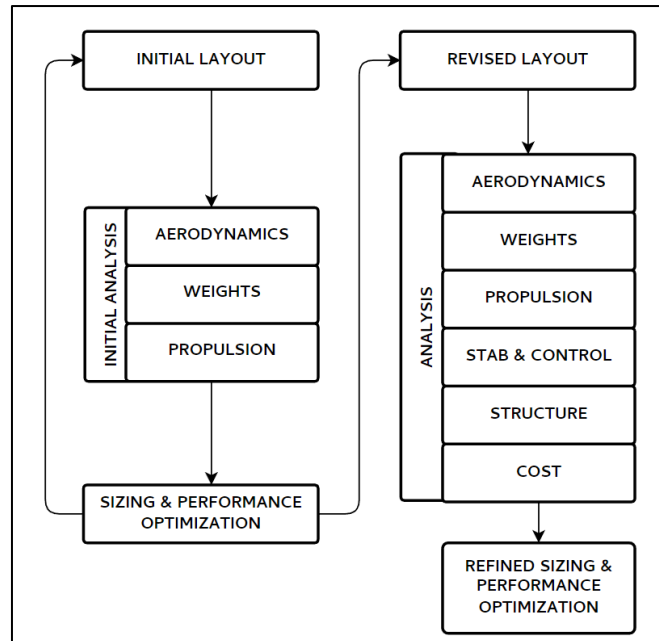


Figure 5: CEASIOM optimization process flowchart (Afsar et al., 2013)

Figure 5 shows initial and secondary optimization loops. The inner loop represents initial guess optimization which is based on low fidelity calculations. The following loop has more accurate calculation methods with respect to first optimization loop. The output of the secondary loop is resultant design decision of the preliminary design phase.

1.1.4 AID

Aircraft Intuitive Design is a Matlab based design tool. AID includes several methods for predicting fixed wing aircraft stability and control parameters. The motivations of AID tool can be stated as follows:

- Unify basic analysis tools for aircraft stability and control
- Provide an intuitive understanding of various design components.
- Create an interface between geometric and aerodynamic parameters
- Quick optimization of an aircraft for a given mission and set of requirements.

Although AID is quite user-friendly tool, it serves wide range of analysis capability such as performing airfoil analysis, detecting the trim points for point mass configuration at a given condition, calculating wake considerations for tail effectiveness, analyzing profile, and induced drag coefficients, and simultaneous visualization of the geometry. Aerodynamic calculation methods are based on analytical methods supplemented by semi-empirical data (DATCOM) and potential flow solvers (AVL, Tornado, Panel Methods).

1.1.5 AAA

Advanced Aircraft Analysis software is created by Dar Corporation to provide a framework to support the iterative process of the aircraft preliminary design. It allows to evolve a preliminary aircraft configuration from early sizing phase through open-loop and closed-loop dynamic stability and sensitivity analysis (DARcorporation, 2018).

The submodules of Advanced Aircraft Analysis software are shown in Table 2, which is based on methods in Jan Roskam's books (Airplane Design Part I-VIII, Flight Dynamics Part I-II, Airplane Aerodynamics and Performance)(Roskam, 1997).

Table 2: Submodules of advanced aircraft analysis software (DARcorporation, 2018)

Application Button	Calculation Modules
Weight	<ul style="list-style-type: none"> • Class I take-off weight and fuel calculation • Class I and Class II weight & balance analysis, center of gravity calculation and moment of inertia calculation for current loading • Radii of Gyration calculation based on Class II moment of inertia
Aerodynamics	<ul style="list-style-type: none"> • Class II lifting surface and airplane lift calculation • Class I and Class II drag polar calculation • Class II lifting surface and airplane moment calculation • Airplane aerodynamic center calculation • Dynamic Pressure Ratio • Power effects on airplane lift and pitching moment • Ground effects of airplane lift and pitching moment • Airplane deep stall angles • Airplane pitch break • Airfoil aerodynamic characteristic definition
Performance	<ul style="list-style-type: none"> • Class I performance sizing • Class II performance analysis
Geometry	<ul style="list-style-type: none"> • Class I wing, fuselage, and empennage layout • Aero-Pack Interface • Lateral tip-over analysis • Scale
Propulsion	<ul style="list-style-type: none"> • Class I installed thrust/power calculation • Inlet/Nozzle sizing
Stability and Control	<ul style="list-style-type: none"> • Longitudinal and lateral-directional stability and control derivatives, including thrust/power • Control surface and trim tab hinge moment derivatives • Class I stability & control empennage sizing • Class II longitudinal and lateral-directional trim, including stick force and pedal force calculations
Dynamics	<ul style="list-style-type: none"> • Open loop dynamics analysis • Automatic control system analysis
Loads	<ul style="list-style-type: none"> • Velocity-Load Factor (V-n) diagram generation • Structural component internal load estimation
Structures	<ul style="list-style-type: none"> • Material property tables • Class I component structural sizing
Cost	<ul style="list-style-type: none"> • Airplane program cost estimation

AAA tool consists of Class I and Class II design methodologies which is dominated by empirical data and supported by physic-based analytical methods. The software provides to manipulate equations which is based on empirical correlations. Moreover, according to analysis results, user can classify the output parameters by using certification standards which is stated as follows (DARcorporation, 2018):

- FAR 23: Federal Aviation Regulations, Part 23
- JAR 23: Joint Airworthiness Requirements, Part 23
- FAR 25: Federal Aviation Regulations, Part 25
- VLA: Very Light Aircraft
- Mil Specs: Military Specifications (MIL-F-8785C and MIL-STD 1797A)
- AS Specs: Naval Air Systems Command Specifications
- Light Sport: Light Sport Requirements

1.1.6 Comparison of Design Software

Table 3 shows the capability of the aircraft design software which is stated in this chapter. Between five different competitor software, the most powerful ones are determined as AGILE and CEASIOM from the aspects of accuracy, tool flexibility, ease of usage and selectable level of fidelity. However, any software apart from MAD, does not have the capability of performing instant trim and simulation via six degrees of freedom dynamic model. This capability provides user to analyze any unconventional unique design without needing a precalculated database in the early design phase of the aircraft. Thus, in MAD environment all analysis methods are compatible with instant trim and simulation concept. MAD software is created for this thesis study in object-oriented python environment to provide different aspect of view to the aircraft design and optimization process.

Table 3: Comparison of design software

	SUAVE	AGILE	CEASIOM	AID	AAA	MAD
Empirical Formulas	v	v	v	v	v	v
Physics Based Calculations	v	v	v	v	v	v
Integrated CFD Solver	v	v	v	x	x	x
Vortex Lattice Method	v	v	v	v	x	v
Graphical User Interface	x	o	v	v	v	x
Open Source	v	o	o	x	x	v
Handling Quality Analysis	v	v	v	x	v	v
Performance Analyses	v	v	v	x	v	v
Maneuver Controller	x	v	v	x	x	v
Optimization	v	v	v	x	x	v
Instant 6 DOF Trim & Simulation Capability	x	x	x	x	x	v
Database Based 6 DOF Trim & Simulation Capability	x	v	v	x	x	v

Table 4: Legends of design software properties

v	Included
x	Not Included
o	Partially included

1.2 Thesis Scope

In this study, by creating MAD software, it is aimed to get an environment which all disciplines work in cooperation with improved prediction technics to obtain performance, stability, and control capabilities of a unique conceptual aircraft. Moreover, the software provides an opportunity to conduct the optimization process systematically.

Chapter 1 gives a general knowledge about literature study and thesis workflow. Literature study includes competitor conceptual design software and capabilities of each tool in detail.

Chapter 2 explains model structure and capabilities of MAD software. The prediction methods and required equations for physic-based calculations are elaborated. Moreover, specifications of the aircraft which is utilized for model validation are stated in detail.

Chapter 3 describes analysis methods for performance, stability, and control surface sufficiency calculations. For all these disciplines, model validation is performed with Cessna 172N aircraft in this chapter.

Chapter 4 express procedure which is applied for design and optimization process of the aircraft according to customer requirements and certification standards. In this chapter, statistical methods are utilized to apply the optimization technics to the aircraft design process.

CHAPTER 2

MODEL METHODOLOGY

The MAD software is mainly consisting of two sections as analysis and optimization. In order to get desired performance and stability outputs from the software in the analysis section, model structure is created as suitable to perform the trim and simulations. Thanks to the generic trim and simulation capability, in MAD environment, the base model structure does not need to be changed for performing an additional type of analysis. This capability gains flexibility to the model. The flexible model structure, which is used for analysis section, will be elaborated in this section in detail.

2.1 Model Capabilities

In order to perform user defined analyses without needing to change model structure, it is required to have some base modules inside of the model. The capabilities of base modules of MAD software are stated as follows.

- Weight, inertia, center of gravity estimations
- Cost analysis
- Primary and secondary control surface effect analysis
- Hinge moment prediction
- Static and dynamic coefficient effect analysis
- Stall prediction
- Parasite drag calculations
- System linearization and mode analysis
- Maneuver controller via PID and inverse simulation controller
- Atmospheric condition calculation
- Propulsion calculations

- Trim and simulation analysis
- Landing gear dynamic calculations
- Visualization of simulation results and animations

2.2 Specifications of Cessna 172 aircraft

In order to validate studies of MAD tool, short range version of Cessna 172N (40-gallon fuel capacity) aircraft is based. All specifications of the aircraft are stated accordingly. The distances are given with respect to datum point. Datum point is located on the tip of the spinner. Also, Positive sign conventions are tabulated at Table 5 and Figure 6.

Table 5: Positive sign convention

Positive Sign Convention of the Coordinate System		
X	Y	Z
From Tip to Tail	From Left to Right	From Down to Up

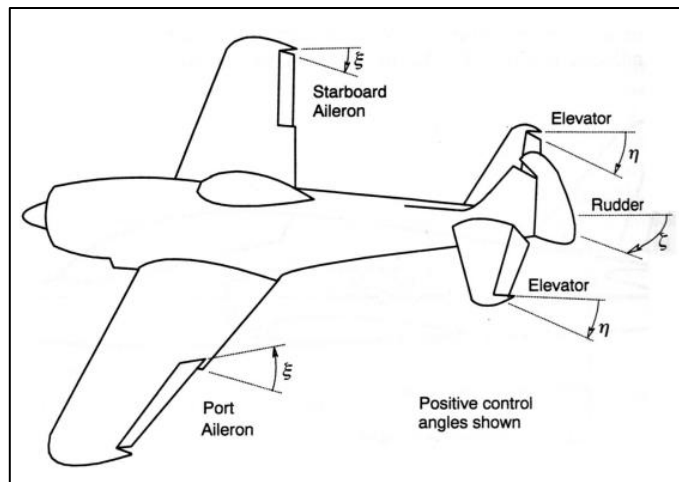


Figure 6: Positive sign convention of control surfaces (Cook, 2013)

Historical versions of the Cessna 172 model aircraft are shown in Table 6. 1977 model Cessna 172, which has 160 horsepower engine and 2300 lb. gross weight, is selected for validation study.

Table 6: Cessna 172 versions and updates history (Wikipedia contributors, 2022b)

CESSNA 172	MAX HP	Gross Weight (lb.)	Year	Specification Addition
Toowoomba	145	2200	1955	Base model
A	145	2200	1960	Tailfin
B	145	2250	1961	Painting and shorter LG
C	145	2250	1962	Autopilot and child seats
D	175	2300	1963	Changed engine and rudder
E	175	2300	1964	Redesigned instrument panel
F	175	2300	1965	Electric operated flap
G	175	2300	1966	Changed spinner
H	175	2300	1967	Shorter nose LG and pneumatic stall warning
I	150	2300	1968	Changed engine
K	150	2300	1969	197 L fuel tank relocation (Fuselage to wing)
L	150	2300	1971	Increased LG width & plastic dorsal fin
M	150	2300	1973	Increased baggage compartment size
N	160	2300	1977	Changed engine + rudder trim option
P	160	2400	1981	Flap deflection decreased from 40 to 30 Fuel capacity increased to 235 L
Q	180	2550	1983	Changed engine
R	160	2450	1996	Changed engine and improvements in interior
S	180	2550	1998	Changed engine + updated avionics
RG	180	2650	1980	Retractable LG Variable pitch constant speed propeller

Table 7: Cessna 172N configuration properties

CESSNA 172 N CONFIGURATION	
Wing Location	High
Tail Type	Conventional Tail
Engine Type	Piston Prop
Landing Gear Type	Tricycle / Fixed
Material	Aluminum
Fuel Tank Location	Wing

Table 8: Lifting surface of Cessna 172N (Cessna Aircraft Company, 1978)

		Span (m)	AR	TR	Sref (m ²)	Incidence (deg)	LE Sweep	Dihedral (deg)	Twist (deg)	Airfoil	LE Pos (x,z) (m)
Wing	Root	11.00	7.50	1.00	16.11	1.50	0.00	1.73	-3.00	NACA 2412	[2.00, 0.65]
	Tip			0.68			3.00			NACA 0012	
Horizontal Tail		3.35	3.13	0.62	3.59	0.00	10.00	0.00	0.00	NACA 0012	[6.41, 0.21]
Vertical Tail		1.50	1.32	0.52	1.71	0.00	42.00	0.00	0.00	NACA 0009	[6.15, 0.08]

Table 9: Mean aerodynamic chord of Cessna 172N (Fasanella & Jackson, 2016)

MAC Forward Point Position (m)			Mean Aerodynamic Chord Length (m)
X	Y	Z	
2.03	2.59	0.00	1.48

Table 10: Control surfaces of Cessna 172N (Cessna Aircraft Company, 1978)

	Chord ratio %		Span ratio %		Deflection Limits (deg)	Type
	Root Side	Tip Side	Root Side	Tip Side		
Flap	33	33	11	48	0 Up 20 Down (Take Off) 40 Down (Landing)	Single Slotted
Aileron	30	30	49	95	20 Up 15 Down	Plain
Elevator	40	40	10	95	28 Up 23 Down	Plain
Rudder	40	40	10	90	16 Right 16 Left	Plain

Table 11: Cessna 172N fuselage properties (Cessna Aircraft Company, 1978)

FUSELAGE PROPERTIES	
Max Width (m)	1.10
Length (m)	7.51
Max Height (m) (Lower Surf to Upper Surf)	1.52
Max Height (m) (Ground to Upper Surf)	1.98
Number of Passenger	4 (Crew Included)

Table 12: Cessna 172N landing gear properties (Cessna Aircraft Company, 1978)

LANDING GEAR PROPERTIES		
	NOSE LG	MAIN LG
Ground Contact Point X Position(m)	1.20	2.80
Ground Contact Point Y Position(m)	0.00	[-1.3 /+1.3]
Ground Contact Point Z Position(m)	- 1.28	1.20

Table 13: Cessna 172N engine properties (Lycoming, 2007)

ENGINE PROPERTIES	
Max RPM	2700
Max Take Off HP	160
Gph	7
Lph	42
Propeller Type	Fix Pitch
Propeller Material	Metal
Number of Blade	2
Propeller Diameter (m)	1.91
Hub diameter (m)	0.35
Engine Type	Lycoming O-320-H2AD

Table 14: Inertial properties of Cessna 172N (Cessna Aircraft Company, 1978)

Center of Gravity Position and Inertia Values				
CG X (m)	2.40	IXX (kgm²)	1395	
CG Y (m)	0.00	IYY (kgm²)	1825	
CG Z (m)	0.16	IZZ (kgm²)	2667	
CG X MAC%	25% MAC		IXZ (kgm²)	123
Most Forward CG X	15.5% MAC	2.23 m	IXY (kgm²)	0
Most Aft CG X	36.5% MAC	2.54 m	IYZ (kgm²)	0

Table 15: Cessna 172N weight breakdown (Roskam, 2018)

Cessna 172N Weight Breakdown	
Gross Weight (kg)	1040
Empty Weight (kg)	660
Wing Group (kg)	107
Empennage Group (kg)	27
Fuselage Group (kg)	166
LG Group (kg)	52
Power Plant (kg)	163
Fuel Weight (kg)	109
(Short Range Version)	
Passenger Weight (kg)	255
Payload Weight (kg)	20
Fixed Equipment (kg)	75

Table 16: Cessna 172 performance outputs (Cessna Aircraft Company, 1978)

PERFORMANCE PROPERTIES	
Take Off Distance 15°C (ft)	1440
Landing Distance 15°C (ft)	1250
Rate of Climb (fpm)	770
Service Ceiling (ft)	14200
Stall Speed (kts)	50 kts for 0° Flap Deflection 47 kts for 10° Flap Deflection 44 kts for 40° Flap Deflection
Maximum Cruise Speed (kts)	125
Max Crosswind Capability (kts)	15
Max Range 90 kts SL 2300 lb	1064 km
Max Endurance SL 2300 lb	6.4 hr
Load Factors	+3.8g / -1.5g

2.3 Model Blocks

In order to create multidisciplinary workflow for design and optimization process, each discipline should have connected each other. In this scope, base structure of MAD tool consists of seven submodules which can work collaboratively. Disciplines that are represented by submodules, are listed as follows:

- Aerodynamic
- Engine

- Equation of Motion
- Landing Gear
- Atmosphere
- Control
- Weight and Balance
- Cost

2.3.1 Aerodynamic Block

In the traditional modeling analogy, to operate 6-DOF trim and simulation analysis, overall database is required which is a very long process. However, in this study in order to get aerodynamic force and moments, a unique methodology is developed which let user perform trim and simulation analysis without needing overall aerodynamic database. The methodology is based on calculating the aerodynamic force and moments simultaneously for a specific state combination of each iteration of Newton Raphson and Runge Kutta methods. Using this method instead of obtaining aerodynamic data by interpolating pre-calculated aerodynamic database, gains model flexibility. Thanks to this concept, 6-DOF model can be utilized even each phase of design process for a futuristic unique aircraft design.

2.3.1.1 Aerodynamic Coefficient Prediction Tools

In order to calculate force and moments instantly in the process of numeric iterations to solve equations of motions, it is required to have rapid aerodynamic calculation methods such as vortex lattice, panel or empirical methods. To have the capability of instant aerodynamic calculation, possible method and software alternatives are investigated. To decide most suitable alternative, the same analysis is repeated for each tool which is defined below:

- DATCOM
- AVL
- Open VSP

2.3.1.1.1 DATCOM

Digital Datcom is a computer program which incorporates the methods contained in the USAF Stability and Control DATCOM (Data Compendium) (Finck et al., 1978). The fundamental purpose of the USAF Stability and Control DATCOM is to provide a systematic summary of methods for estimating stability and control characteristics in preliminary design applications. DATCOM is contained in a series of notebooks with over 3100 pages (Galbraith, 2004). In 1979, the DATCOM was written in FORTRAN computer language. It was originally coded in FORTRAN 77 but later upgraded to FORTRAN 90 (Siddiqui et al., 2010). Table 17 shows the prediction capability of Datcom program.

Table 17: Datcom Aerodynamic Coefficient Predictions (Galbraith, 2004)

DATCOM	CL	CD	CY	CR	CM	CN
Angle of Attack	v	v			v	
Angle of Sideslip			v	v		v
Pitch Rate	v				v	
Roll Rate			v	v		v
Yaw Rate			v	v		v
Flap Deflection	v	v			v	
Rudder Deflection						
Aileron Deflection				v		v
Elevator Deflection	v	v			v	

The general properties of Datcom program are stated as follows:

- Utilizes analytical equations instead of numerical solution. Thus, analyses are performed very fast.
- Compressibility effect is included. Datcom gives acceptable results for even hypersonic speeds.
- Predicts stall condition and maximum lift coefficient
- Calculates parasite drag coefficient

- Engine properties can be defined in input file. So, engine effects can be considered in analysis.
- Flap, slat, spoiler and differential horizontal tail effects can be included to calculations
- Fuselage forces are calculated with Jorgensen method
- Elevator and aileron effects included however, there is no rudder effect in Datcom analysis
- In Datcom+ version, geometry visualization capability is available

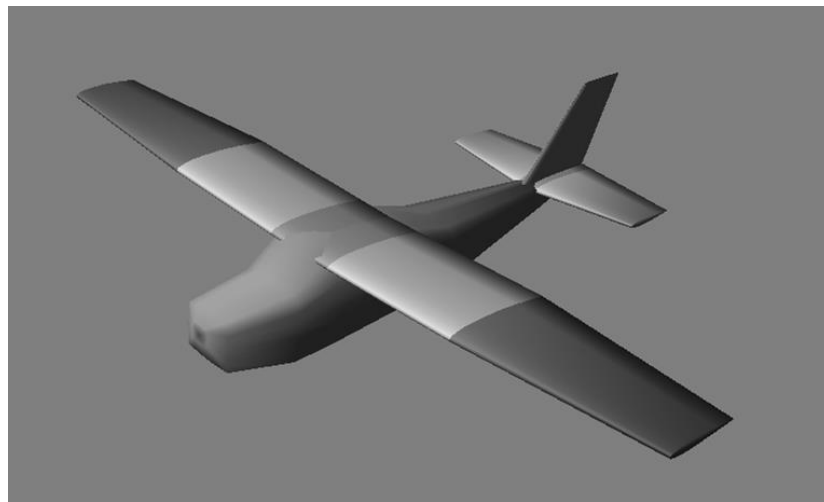


Figure 7: Datcom+ Software Visualization Output

2.3.1.1.2 AVL

AVL (Athena Vortex Lattice) is a tool for aerodynamic and flight dynamic analysis of rigid aircrafts (Budziak, 2015). Influence of all state and input (control surface) variables over aerodynamic coefficients can be observed via AVL. However, effects of viscosity are neglected in the software. AVL provides user to have flexible configuration definition capability. It uses extended vortex lattice method for lifting surface and slender body model for fuselage. In VLM the wing is modeled with horseshoe vortices distributed along span and chord. (Drela & Youngren, 2004b)

In AVL for fuselage analysis, slender body theory is utilized, but modeling of bodies should be done with caution. If the fuselage has a small effect on aerodynamic coefficients, then it is more reasonable to perform analysis with only lifting surfaces without including fuselage.

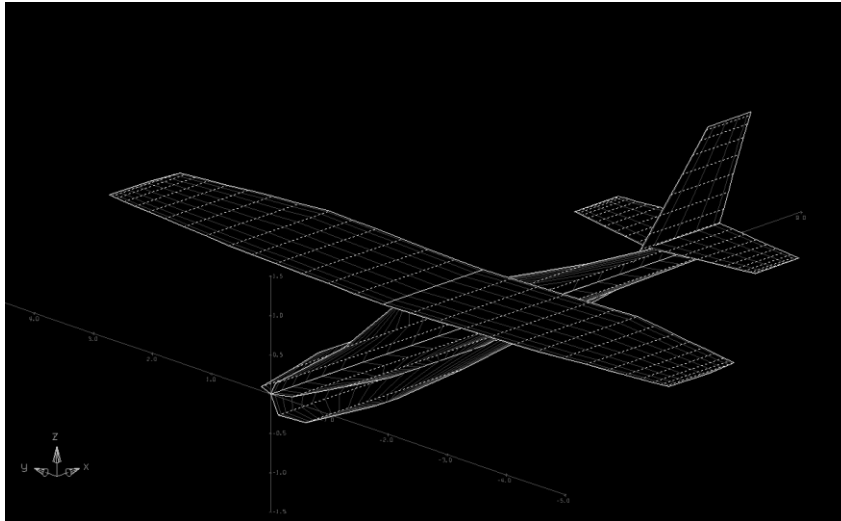


Figure 8: AVL visualization output (Drela & Youngren, 2004b)

Results of AVL is best suited for the thin lifting surface configurations and small angle of attack & sideslip conditions. In order to consider compressibility effect for analyses, Prandtl-Glauert transformation is used in AVL. According to Drela, AVL provides valid results up to 0.7 Mach speeds by considering compressibility effects. However, performing the analysis at the speeds more than 0.7 Mach, is not suggested. (Drela & Youngren, 2004)

2.3.1.1.3 OpenVSP

OpenVSP is a tool for creating parametric aircraft geometry and performing aerodynamic analysis during conceptual design. In the scope of geometry creation, OpenVSP is utilized to not only visualize an aircraft concept in three dimensions, but also to create structural and aerodynamic mesh to feed external high-fidelity analysis tools. Figure 9 shows aerodynamic mesh which is created by OpenVSP.

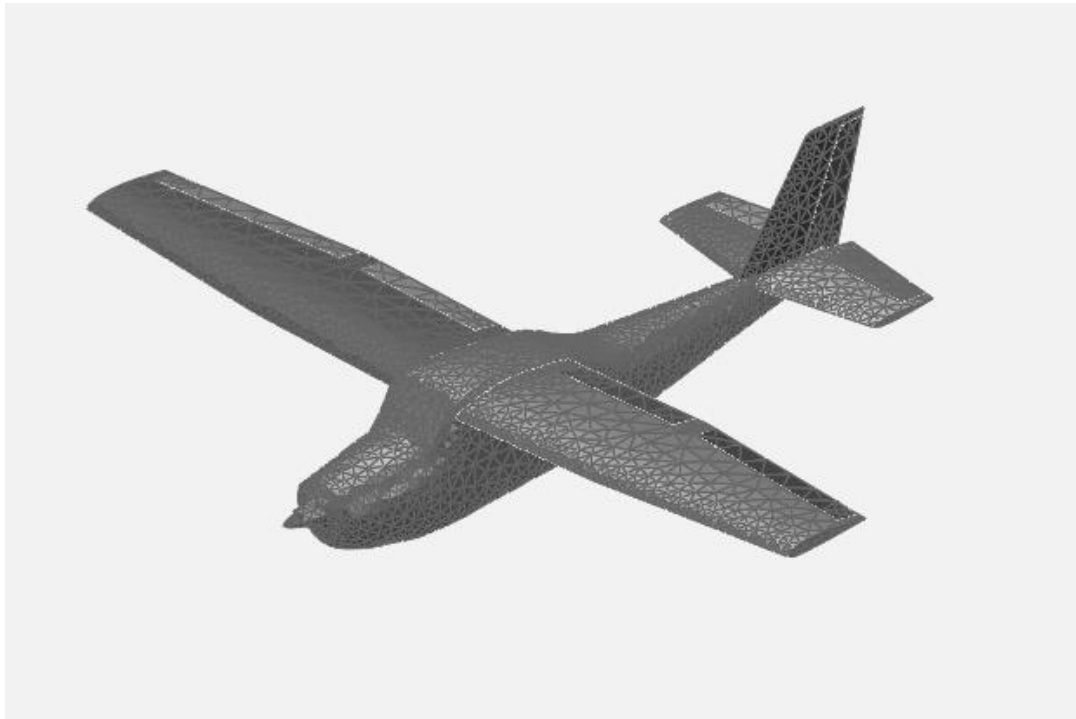


Figure 9: Aerodynamic mesh geometry of OpenVSP

Besides visualization and mesh creation capability, OpenVSP can also be used as aerodynamic solver via submodule so called VSPAERO. VSPAERO was designed to utilize the thin-plate and camber surface representations by including control surface deflections. User can select the solver as panel method or vortex lattice method. VLM method which is used in VSPAERO has some additional formulation and manipulation. These manipulations differentiate the method from classical VLM codes.

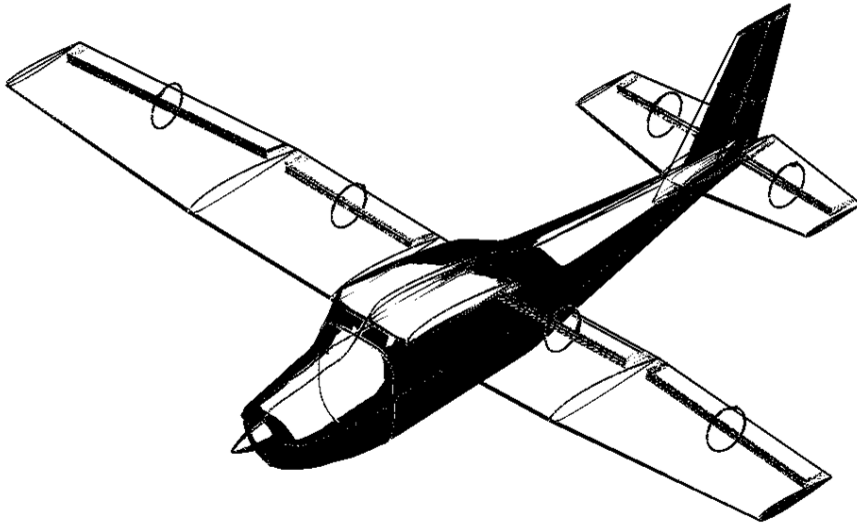


Figure 10: Open VSP visualization output

VSPAERO could calculate subsonic and supersonic flow by including wave drag and parasite drag analysis. In addition, the VSPAERO solver involves an actuator disk and ground effect model. Thanks to these completeness, static and hover cases induced by rotors or propellers, can be modelled via OpenVSP. Moreover, VSPAERO module provide the capability to calculate static and dynamic stability derivatives (McDonald & Gloude-mans, 2022).

2.3.1.2 Aerodynamic Coefficient Prediction Tool Comparison and Validation

In the light of the information provided about most popular aerodynamic coefficient prediction methods, the completeness of the tools is evaluated. Table 18 shows general comparisons of the software.

Table 18: Aerodynamic calculation tools capability comparison

	DATCOM	AVL	OPEN VSP
Control Surface Effect	o	v	v
Rapid Analysis Capability	v	o	x
Parasite Drag Calculation	v	x	v
Stall Prediction	v	x	x
Engine Calculations	v	x	v
Geometry Visualization	o	o	v
High Mach Number Analysis	v	o	o
Analysis Capability for Variety of Aerodynamic Coefficients	o	v	v
Ground Effect	v	v	v
Hinge Moment Calculation	v	v	x

Table 19: Aerodynamic calculation tools comparison legends

Legends	
v	Included
o	Partially included
x	Excluded

According to Table 18, DATCOM is capable to perform most of analysis however, capability to obtain variety of aerodynamic coefficient is limited for DATCOM. On the other hand, Open VSP has wide range of coefficient analysis capability but, analysis time is an important disadvantage of the tool when compared to Datcom and AVL. The last alternative, AVL has both wide range of coefficient analysis capability and less calculation time however, stall and parasite drag prediction is not possible with AVL. In order to adopt analysis software to MAD, the best choice may be combining analysis software according to their strong skills.

In addition to general capability comparison study of three competitor analyses software, they are also compared according to analysis accuracy by referencing NASA flight test results of Cessna 172 aircraft (Suit & Cannaday, 1979).

Table 20: Aerodynamic analysis results of DATCOM, AVL and Open VSP

	DATCOM		AVL		OPENVSP		NASA Flight Test
	With Fuselage	Without Fuselage	With Fuselage	Without Fuselage	With Fuselage	Without Fuselage	
C_{M_α}	-1.0630	-1.2400	-1.1789	-1.3992	-1.0423	-1.2058	-0.6800
$C_{M_{\dot{\alpha}}}$	-6.1010	-6.1010					
C_{M_q}	-13.6000	-13.6000	-14.6021	-14.5197	-13.5991	-13.7031	-15.3400
C_{L_α}	5.6200	5.4130	5.2355	5.1840	4.9000	4.9215	5.1800
$C_{L_{\dot{\alpha}}}$	2.0540	2.0540					
C_{L_q}	6.8120	6.8120	9.8111	9.4834	9.0448	8.9526	8.6500
C_{D_α}					0.0898	0.0908	
$C_{L_{\delta_{elevator}}}$	0.4560	0.4560	0.5404	0.5471	0.5103	0.5085	0.4050
$C_{D_{\delta_{elevator}}}$	0.0221	0.0221			0.0035	0.0038	
$C_{M_{\delta_{elevator}}}$	-1.3156	-1.3156	-1.5689	-1.6001	-1.4532	-1.4532	-1.1900
C_{R_β}	-0.0771	-0.0659	-0.0601	-0.0410	-0.0466	-0.0277	-0.0780
C_{R_p}	-0.4364	-0.4364	-0.5020	-0.5007	-0.4981	-0.4956	-0.4700
C_{R_r}	0.0339	0.0274	0.0532	0.0532	0.0526	0.0506	0.0700
$C_{R_{\delta_{aileron}}}$	-0.0940	-0.0940	-0.1089	-0.1086	-0.1063	-0.1060	-0.1100
$C_{R_{\delta_{rudder}}}$			0.0060	0.0059	0.0066	0.0066	0.0058
C_{N_β}	0.0251	0.0045	0.0379	0.0823	0.0594	0.1196	0.0480
C_{N_p}	-0.0130	-0.0130	-0.0131	-0.0084	-0.0254	-0.0171	-0.0500
C_{N_r}	-0.0562	-0.0054	-0.0815	-0.0821	-0.1085	-0.1097	-0.1000
$C_{N_{\delta_{aileron}}}$			-0.0027	-0.0013	-0.0007	0.0019	-0.0030
$C_{N_{\delta_{rudder}}}$			-0.0532	-0.0532	-0.0823	-0.0810	-0.0530
C_{Y_β}	-0.6196	-0.0373	-0.3289	-0.2180	-0.3143	-0.2892	-0.5900
C_{Y_p}	-0.0485	-0.0485	-0.0654	-0.0353	-0.0495	-0.0417	-0.0450
C_{Y_r}			0.2211	0.1947	0.2970	0.2646	
$C_{Y_{\delta_{rudder}}}$			0.1166	0.1159	0.1865	0.1831	0.1100

Table 21: Error norm comparison of aerodynamic analysis software

	DATCOM		AVL		OPENVSP		NASA Flight Test
	With Fuselage	Without Fuselage	With Fuselage	Without Fuselage	With Fuselage	Without Fuselage	
C_{M_α}	56.32	82.35	73.36	105.76	53.28	77.32	REFERENCE
C_{M_q}	11.34	11.34	4.81	5.35	11.35	10.67	
C_{L_α}	8.49	4.50	1.07	0.08	5.41	4.99	
C_{L_q}	21.25	21.25	13.42	9.63	4.56	3.50	
$C_{L_{\delta_{elevator}}}$	12.59	12.59	33.44	35.10	26.00	25.55	
$C_{M_{\delta_{elevator}}}$	10.55	10.55	31.84	34.46	22.12	22.11	
C_{R_β}	1.19	15.50	22.92	47.42	40.25	64.45	
C_{R_p}	7.15	7.15	6.81	6.53	5.98	5.44	
C_{R_r}	51.51	60.93	24.00	24.03	24.87	27.65	
$C_{R_{\delta_{aileron}}}$	14.56	14.56	1.04	1.30	3.38	3.60	
$C_{R_{\delta_{rudder}}}$			3.19	2.21	14.08	14.33	
C_{N_β}	47.67	90.54	20.94	71.50	23.72	149.14	
C_{N_p}	74.04	74.04	73.78	83.22	49.20	65.77	
C_{N_r}	43.76	94.62	18.51	17.88	8.51	9.75	
$C_{N_{\delta_{aileron}}}$			8.80	58.20	76.22	164.80	
$C_{N_{\delta_{rudder}}}$			0.45	0.34	55.29	52.89	
C_{Y_β}	5.02	93.68	44.26	63.05	46.72	50.98	
C_{Y_p}	7.67	7.71	45.33	21.51	10.10	7.27	
$C_{Y_{\delta_{rudder}}}$			5.97	5.40	69.57	66.49	
Mean Error	20.73	33.41	21.70	29.65	25.03	37.58	

According to Table 20 and Table 21, it can be observed that the error norms of Datcom and AVL is close to each other for both with and without fuselage versions. From the tables it is observed that OpenVSP has larger error norms than the other tools. Moreover, from Table 21, it is clearly seen that the configuration with fuselage gives more accurate results with respect to the configuration without fuselage. When considering the accuracy level and scope of capabilities of the software, it is reasonable to use AVL software as a base aerodynamic calculation tool by supporting it with Datcom. In this scope, Datcom is used to support to AVL in the analysis of parasite drag and stall prediction which AVL is not capable to perform.

2.3.2 Engine Block

In the MAD environment, the main aim of engine block is to calculate thrust force in terms of engine horsepower, true airspeed, and altitude. To predict thrust force, quadratic polynomial curve fitting method is implemented. For each engine horsepower and altitude values, the coefficients of second degrees of polynomial is calculated separately. To set a relation between true airspeed and thrust force for a specific altitude and horsepower, three point is referenced as maximum speed, cruise speed and zero speed (static thrust). The relation used for calculation of thrust at maximum speed and cruise speed is based on Equation(5). Moreover, static thrust is obtained with the relation introduced at Equation (4). In order to include the atmospheric effects of altitude changes, Gagg and Ferrar model is utilized which is stated at Equation (1) (Gudmundsson, 2014). By using these methodologies, MAD tool calculates the thrust force for different horsepower, airspeed, and altitude conditions.

$$P_{BHP} = P_{BHP_{SL}}(1.132 \sigma - 0.132) \quad (1)$$

In the Equation(1), σ represents density ratio between a specific altitude and sea level condition, which is formulated at Equation (2).

$$\sigma = \frac{\rho}{\rho_{SL}} \quad (2)$$

Table 22: Kp values for different number of blades configurations

Type of Propeller	K _p for British Unit System
Two- bladed	20.4
Three - bladed	19.2
Four or more blades	18.0

Equation (3) gives a relation to predict propeller diameter in inches by utilizing Table 22.

$$d_{propeller} = K_p (P_{BHP})^{0.25} \quad (3)$$

$$T_{Static} = 0.85(P_w)^{\frac{2}{3}}(2\rho A_{disc})^{\frac{1}{3}}\left(1 - \frac{A_{spinner}}{A_{disc}}\right) \quad (4)$$

Equation (4) enable to predict maximum static thrust of the propulsion system. However, it does not calculate tip losses. This formula calculates thrust as if force distribution on blade is uniform and maximum. So, the result gives maximum attainable thrust. According to real data of the engine, a correlation factor can be applied to formula as between 50% and 90%. For Cessna 172 N aircraft with 160 horsepower, 60% correlation factor is applied to get realistic static thrust values (Mingtai, 2012).

$$T_{Actual} = 745.7 \frac{P_{BHP}\eta_p}{V_{TAS}} \quad (5)$$

To get maximum attainable speed, Equation (6) and (7) are solved explicitly in order to obtain to V_{MS} parameter. So, the maximum speed parameter is achieved by solving the equality between the forces for minimum drag coefficient condition and a specific horsepower condition at wind x axis direction.

$$\left[745.7 \frac{P_{BHP}\eta_p}{V_{MS}} = \frac{1}{2}\rho(V_{MS})^2 S(C_{Dmin})\right] \quad (6)$$

$$V_{MS} = \left(1491.4 \frac{P_{BHP}\eta_p}{\rho S C_{D_{min}}} \right)^{\frac{1}{3}} \quad (7)$$

The actual thrust value for maximum speed and cruise speed conditions are calculated by using Equations(8).

$$T_{VMS} = 745.7 \frac{P_{BHP}\eta_p}{V_{MS}} \quad (8)$$

$$T_{Cruise} = 745.7 \frac{P_{BHP}\eta_p}{V_{Cruise}}$$

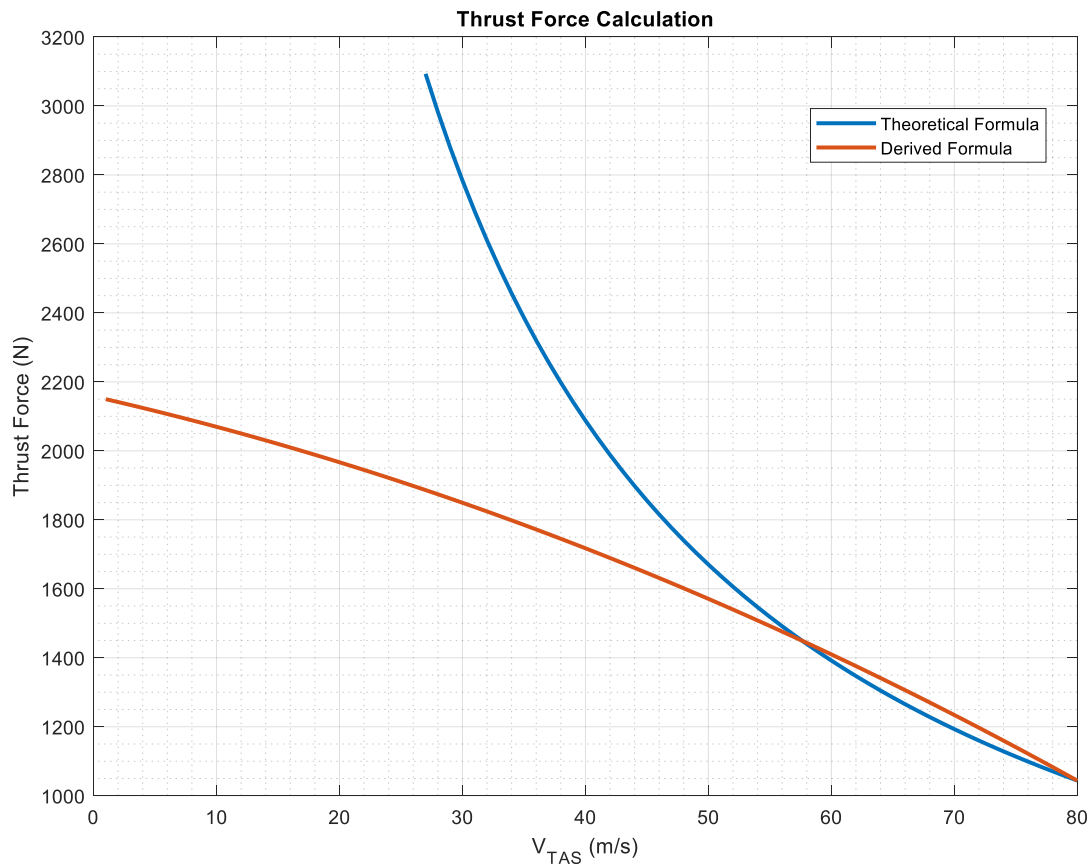


Figure 11: Propeller thrust quadratic interpolation

Thanks to clarified thrust and airspeed values, thrust equation is assumed as a form of Equation (9).

$$T = AV^2 + BV + C \quad (9)$$

By using three data points at Table 23, which is already known; A, B and C coefficients can be calculated for a specific altitude and throttle level.

Table 23: Velocity and thrust couples

Point 1	Point 2	Point 3
(V_{MS}, T_{VMS})	(V_{Cruise}, T_{Cruise})	$(V_{Static=0}, T_{Static})$

After getting A, B, and C coefficients of the Equation (9), the relation between velocity and thrust value can be set with ease.

2.3.3 Equation of Motion Block

Equation of motion block can be regarded as the main block of the dynamic model. The block contains all required differential and analytical formulations. Trim and simulation studies are based on the equations in this module. All unknowns and equation alternatives, that are used in the block, are tabulated at Table 24.

Table 24: Equation and unknown alternatives

UNKNOWNNS	EQUATIONS	
	State Derivative Equations	Constrained Equations
u, v, w, α, β	$\dot{u}, \dot{v}, \dot{w}, \dot{\alpha}, \dot{\beta}, \dot{V}_{TAS}, \dot{p}, \dot{q}, \dot{r}$	$\gamma, N_x, N_y, N_z, \text{Track Angle}$
$V_{TAS}, p, q, r, \theta, \phi$	$\dot{\theta}, \dot{\phi}, \dot{\psi}, \dot{x}, \dot{y}, \dot{z}, \dot{h}$	$\alpha, \beta, V_{TAS}, p_w, q_w, r_w$
ψ, x, y, z, h		

Equations utilized in the module are stated at the formulations from Equation (10) to Equation (34) (Chudoba & Cook, 2003).

$$X_A + X_T - mg\sin\theta = m(\dot{u}^E + qw^E - rv^E) \quad (10)$$

$$Y_A + Y_T - mg\cos\theta\sin\phi = m(\dot{v}^E + ru^E - pw^E) \quad (11)$$

$$Z_A + Z_T - mg\cos\theta\cos\phi = m(\dot{w}^E + pv^E - qu^E) \quad (12)$$

$$\begin{aligned} L_A + L_T = I_x\dot{p} - I_{yz}(q^2 - r^2) - I_{zx}(\dot{r} + pq) \\ - I_{xy}(\dot{q} - rp) - (I_y - I_z)qr \end{aligned} \quad (13)$$

$$\begin{aligned} M_A + M_T = I_y\dot{q} - I_{zx}(r^2 - p) - I_{xy}(\dot{p} + qr) \\ - I_{yz}(\dot{r} - pq) - (I_z - I_x)rp \end{aligned} \quad (14)$$

$$\begin{aligned} N_A + N_T = I_z\dot{r} - I_{xy}(p^2 - q^2) - I_{yz}(\dot{q} + rp) \\ - I_{zx}(\dot{p} - qr) - (I_x - I_y)pq \end{aligned} \quad (15)$$

$$\dot{\phi} = p + q(\sin\phi + r\cos\phi)\tan\theta \quad (16)$$

$$\dot{\theta} = q\cos\phi - r\sin\phi \quad (17)$$

$$\dot{\psi} = (q\sin\phi + r\cos\phi)\sec\theta \quad (18)$$

$$\begin{bmatrix} \dot{x} \\ \dot{y} \\ \dot{z} \end{bmatrix} = \begin{bmatrix} c\theta c\psi & s\phi s\theta c\psi - c\phi s\psi & c\phi s\theta c\psi + s\theta s\psi \\ c\phi s\psi & s\phi s\theta s\psi + c\phi c\psi & c\phi s\theta s\psi - s\phi c\psi \\ -s\theta & s\phi c\theta & c\phi c\theta \end{bmatrix}_{E \leftarrow B} \begin{bmatrix} u^E \\ v^E \\ w^E \end{bmatrix} \quad (19)$$

$$\begin{bmatrix} p_w \\ q_w \\ r_w \end{bmatrix} = \begin{bmatrix} c(\alpha) c(\beta) & s(\beta) & s(\alpha) c(\beta) \\ -c(\alpha) s(\beta) & c(\beta) & -s(\alpha) s(\beta) \\ -s(\alpha) & 0 & c(\alpha) \end{bmatrix}_{W \leftarrow B} \begin{bmatrix} p \\ q \\ r \end{bmatrix} \quad (20)$$

$$N_x = \frac{(X_A + X_T)}{mg} \quad (21)$$

$$N_y = \frac{(Y_A + Y_T)}{mg} \quad (22)$$

$$N_z = \frac{-(Z_A + Z_T)}{mg} \quad (23)$$

$$\dot{h} = -\dot{z} \quad (24)$$

$$\gamma = \text{Arctan}\left(\frac{\dot{h}}{\dot{x}}\right) \quad (25)$$

$$\text{Track Angle} = \text{Arctan}\left(\frac{\dot{y}}{\dot{x}}\right) \quad (26)$$

$$\begin{bmatrix} u' \\ v' \\ w' \end{bmatrix} = \begin{bmatrix} u^E \\ v^E \\ w^E \end{bmatrix} + \begin{bmatrix} u_{CW} \\ v_{CW} \\ w_{CW} \end{bmatrix} \quad (27)$$

$$\begin{bmatrix} \dot{u}' \\ \dot{v}' \\ \dot{w}' \end{bmatrix} = \begin{bmatrix} \dot{u}^E \\ \dot{v}^E \\ \dot{w}^E \end{bmatrix} + \begin{bmatrix} \dot{u}_{CW} \\ \dot{v}_{CW} \\ \dot{w}_{CW} \end{bmatrix} \quad (28)$$

$$\alpha = \text{Arctan}\left(\frac{w'}{u'}\right) \quad (29)$$

$$\beta = \text{Arctan}\left(\frac{v'}{\sqrt{u'^2 + w'^2}}\right) \quad (30)$$

$$V_{TAS} = \sqrt{u'^2 + v'^2 + w'^2} \quad (31)$$

$$\dot{V}_{TAS} = \frac{u'\dot{u}' + v'\dot{v}' + w'\dot{w}'}{V_{TAS}} \quad (32)$$

$$\dot{\alpha} = \frac{u'\dot{w}' - w'\dot{u}'}{u'^2 + w'^2} \quad (33)$$

$$\dot{\beta} = \frac{\dot{v}'V_{TAS} - v'\dot{V}_{TAS}}{V_{TAS}\sqrt{u'^2 + w'^2}} \quad (34)$$

2.3.3.1 Numeric Trim and Simulation Algorithm

In order to perform trim analysis, MAD software uses Newton Raphson algorithm which is an analytical equation solver. Newton Raphson Method is found to be more suitable for trim calculations when compared to the other numerical methods because of high accuracy level, less computing time and easy applicability advantages (Özdemir & Kurtulus, 2021). The workflow of the Newton Raphson method is given in Figure 12. The parameters used in the figure are explained in Table 25.

Table 25: Trim algorithm parameters

J	Jacobian Matrix
X	Trim Unknowns
Y	Trim Equation Outputs

The critical point in the trim algorithm is the fact that the number of trim unknowns and trim equations should be equal. Because in the solution process, the inverse of the Jacobian matrix can be calculated if only it is a square matrix. Moreover, each equation which is included to the Jacobian matrix should be linearly independent from each other. Otherwise, rank of the matrix is decreased which prevents to solve equations.

In addition, MAD software allows the user to select different unknown sets defined in wind or body axis. To illustrate u, v, w states can be chosen as unknown parameters instead of α, β and V_{TAS} . Also, the unknown parameters which is defined in wind axis, includes external gust effects. Thanks to this capability crosswind and gust analysis can be performed with ease.

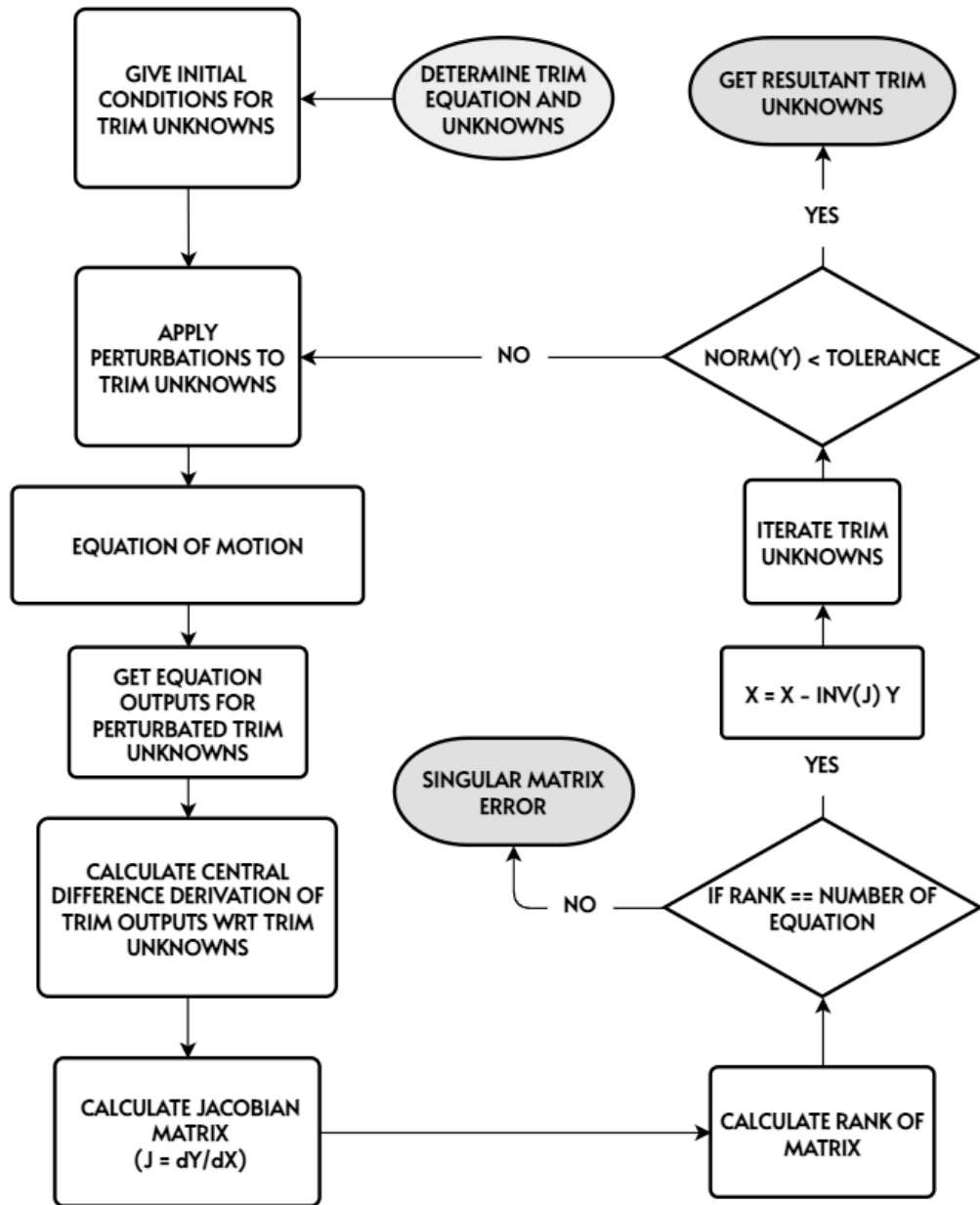


Figure 12: Newton Raphson algorithm flowchart

To simulate all type of maneuvers and detect equilibrium conditions of the aircraft, trim unknowns and equations should be defined accordingly. In MAD software pre-defined trim conditions provide initial condition to simulate the desired maneuver easily. Trim manipulations, that are included in MAD environment are tabulated from Table 26 to Table 38.

Table 26: Straight flight wind axis trim condition

		Straight Flight Wind Axis Trim Parameters
Flight Conditions		$V_{TAS}, h, W_G, \Delta_{ISA}$
States & Inputs	Freeze	$\delta_{flap(landing)}$
	Zero	p, q, r
	Unknowns	$\alpha, \beta, \theta, \phi, \psi, \delta_{elevator}, \delta_{aileron}, \delta_{rudder}, \delta_{throttle}$
Constrained Equations	Freeze	τ, γ
	Zero	$(\dot{V}_{TAS}, \dot{\alpha}, \dot{\beta}, \dot{p}, \dot{q}, \dot{r}, N_y)$ or $(\dot{u}, \dot{v}, \dot{w}, \dot{p}, \dot{q}, \dot{r}, N_y)$

Table 27: Straight flight body axis trim condition

		Straight Flight Body Axis Trim Parameters
Flight Conditions		$V_{TAS}, h, W_G, \Delta_{ISA}$
States & Inputs	Freeze	$\delta_{flap(landing)}$
	Zero	p, q, r
	Unknowns	$u, v, w, \theta, \phi, \psi, \delta_{elevator}, \delta_{aileron}, \delta_{rudder}, \delta_{throttle}$
Constrained Equations	Freeze	$\tau, \gamma, V_{TAS}(V_{TAS} = \sqrt{u^2 + v^2 + w^2})$
	Zero	$(\dot{V}_{TAS}, \dot{\alpha}, \dot{\beta}, \dot{p}, \dot{q}, \dot{r}, N_y)$ or $(\dot{u}, \dot{v}, \dot{w}, \dot{p}, \dot{q}, \dot{r}, N_y)$

Table 28: Climb trim condition

		Climb Trim Parameters
Flight Conditions		$V_{TAS}, h, W_G, \Delta_{ISA}$
States & Inputs	Freeze	$\delta_{throttle(maximum)}, \delta_{flap}$
	Zero	p, q, r
	Unknowns	$\alpha, \beta, \theta, \phi, \psi, \delta_{elevator}, \delta_{aileron}, \delta_{rudder}$
Constrained Equations	Freeze	τ
	Zero	$\dot{V}_{TAS}, \dot{\alpha}, \dot{\beta}, \dot{p}, \dot{q}, \dot{r}, N_y$

Table 29: Fixed angle of attack speed prediction trim condition

Flight Conditions		Level Flight Speed Prediction Trim Parameters
States & Inputs	Freeze	h, W_G, Δ_{ISA}
	Zero	$\delta_{flap(landing)}, \alpha_{user\ defined\ value}$
Constrained Equations	Unknowns	p, q, r
	Freeze	$V_{TAS}, \beta, \theta, \phi, \psi, \delta_{elevator}, \delta_{aileron}, \delta_{rudder}, \delta_{throttle}$
Constrained Equations	Zero	τ
	Zero	$\dot{V}_{TAS}, \dot{\alpha}, \dot{\beta}, \dot{p}, \dot{q}, \dot{r}, N_y, \gamma$

Table 30: Level flight maximum speed prediction trim condition

Flight Conditions		Max Speed Prediction Trim Parameters
States & Inputs	Freeze	h, W_G, Δ_{ISA}
	Zero	$\delta_{throttle_{max}}$
Constrained Equations	Unknowns	p, q, r
	Freeze	$V_{TAS}, \alpha, \theta, \phi, \psi, \delta_{elevator}, \delta_{aileron}, \delta_{rudder}$
Constrained Equations	Zero	τ
	Zero	$\dot{V}_{TAS}, \dot{\alpha}, \dot{\beta}, \dot{p}, \dot{q}, \dot{r}, \gamma$

Table 31: Instant turn trim condition

Flight Conditions		Instant Turn Trim Parameters
States & Inputs	Freeze	$V_{TAS}, h, W_G, \Delta_{ISA}$
	Zero	$\delta_{throttle\ (user\ defined)}, \phi_{\phi=Arccos(\frac{1}{N_z})}$
Constrained Equations	Unknowns	<i>Not Available</i>
	Freeze	$\alpha, \beta, \theta, \psi, p, q, r, \delta_{elevator}, \delta_{aileron}, \delta_{rudder}$
Constrained Equations	Zero	τ
	Zero	$\dot{\alpha}, \dot{\theta}, \dot{\phi}, \dot{p}, \dot{q}, \dot{r}, N_y, N_z, \gamma$

Table 32: Steady coordinated turn trim condition

Flight Conditions		Steady Coordinated Turn Trim Parameters
States & Inputs	Freeze	$V_{TAS}, h, W_G, \Delta_{ISA}$
	Zero	$\phi_{user\ defined}$
Constrained Equations	Unknowns	<i>Not Available</i>
	Freeze	$\alpha, \beta, \theta, \psi, p, q, r, \delta_{elevator}, \delta_{aileron}, \delta_{rudder}, \delta_{throttle}$
Constrained Equations	Zero	τ
	Zero	$\dot{V}_{TAS}, \dot{\alpha}, \dot{\beta}, \dot{\theta}, \dot{\phi}, \dot{p}, \dot{q}, \dot{r}, N_y, \gamma$

Table 33: Pull up trim condition

Pull Up Trim Parameters		
Flight Conditions		$V_{TAS}, h, W_G, \Delta_{ISA}$
States & Inputs	Freeze	$\delta_{throttle}(\text{user defined})$
	Zero	p, r, ϕ
Inputs		Unknowns
		$\alpha, \beta, \theta, \psi, q, \delta_{elevator}, \delta_{aileron}, \delta_{rudder}$
Constrained Equations	Freeze	τ
	Zero	$\dot{V}_{TAS}, \dot{\alpha}, \dot{\beta}, \dot{p}, \dot{q}, \dot{r}, N_z$

Table 34: Steady roll in body axis trim condition

Steady Roll Trim Parameters		
Flight Conditions		$V_{TAS}, h, W_G, \Delta_{ISA}$
States & Inputs	Freeze	$p(\text{user defined})$
	Zero	q, r, ϕ
Inputs		Unknowns
		$\alpha, \beta, \theta, \delta_{elevator}, \delta_{aileron}, \delta_{rudder}, \delta_{throttle}$
Constrained Equations	Freeze	τ
	Zero	$\dot{V}_{TAS}, \dot{\alpha}, \dot{\beta}, \dot{p}, \dot{q}, \dot{r}, \gamma$

Table 35: Crosswind landing trim condition

Crosswind Landing Trim Parameters		
Flight Conditions		$V_{TAS}, V_{crosswind}, h, W_G, \Delta_{ISA}$
States & Inputs	Freeze	$\delta_{flap(\text{landing})}, \psi_{\text{user defined}}$
	Zero	p, q, r
Inputs		Unknowns
		$\alpha, \beta, \theta, \phi, \delta_{elevator}, \delta_{aileron}, \delta_{rudder}, \delta_{throttle}$
Constrained Equations	Freeze	τ, γ
	Zero	$\dot{u}, \dot{v}, \dot{w}, \dot{p}, \dot{q}, \dot{r}$

Table 36: Steady spin trim condition

Spin Trim Parameters		
Flight Conditions		h, W_G, Δ_{ISA}
States & Inputs	Freeze	$\delta_{elevator}, \delta_{aileron}, \delta_{rudder}, \delta_{throttle}$
	Zero	Not Available
Inputs		Unknowns
		$V_{TAS}, \alpha, \beta, \theta, p, q, r$
Constrained Equations	Freeze	γ
	Zero	$\dot{V}_{TAS}, \dot{p}, \dot{q}, \dot{r}, q_{wind_axis}, r_{wind_axis}$

Table 37: Quasi trim condition

		Quasi Trim Parameters
Flight Conditions		$V_{TAS}, h, W_G, \Delta_{ISA}$
States & Inputs	Freeze	$\alpha, \beta, \phi, p, q, r, \delta_{throttle}$
	Zero	<i>Not Available</i>
	Unknowns	$\theta, \delta_{elevator}, \delta_{aileron}, \delta_{rudder}$
Constrained Equations	Freeze	γ
	Zero	$\dot{p}, \dot{q}, \dot{r}$

Table 38: Ceiling trim condition

		Ceiling Trim Parameters
Flight Conditions		$V_{TAS}, W_G, \Delta_{ISA}$
States & Inputs	Freeze	<i>Not Available</i>
	Zero	p, q, r
	Unknowns	$\alpha, \beta, \theta, \phi, \psi, \delta_{elevator}, \delta_{aileron}, \delta_{rudder}, h$
Constrained Equations	Freeze	τ, \dot{h}
	Zero	$\dot{u}, \dot{v}, \dot{w}, \dot{p}, \dot{q}, \dot{r}, N_y$

In the simulation part, as well as Euler method, second, third and fourth order Runge Kutta methods are used for time integration process. The type of solver for integration are arranged as selectable by users. Thanks to MAD software, the time history of the maneuver simulations can be visualized and exported in *.gif or *.png formats. Some of the outputs of the simulations are given in Figure 13. In order to define aircraft attitudes, quaternion and Euler angle definitions are used. Moreover, in the process of calculating bounded Euler angles, DCM method is implemented to integration concept.

The critical point during the time integration of the equations, is the selection of the model frequency. In MAD tool, three different level of frequencies are defined to use as: 10 Hz ,20 Hz and 30 Hz. In this scope, 10 Hz is used for normal flight, 20 Hz is used for landing analysis and 30 Hz is used for take-off analysis in the simulations.

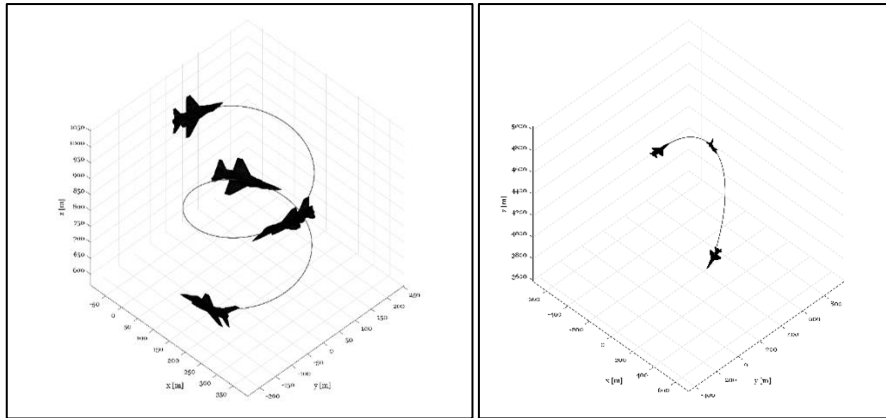


Figure 13: Simulation outputs of the MAD tool

Instant trim and simulation method:

In the conventional trim search methodology, overall pre-calculated aerodynamic database is needed. The model reads the related aerodynamic coefficients from database for each Newton Raphson iteration by performing interpolation between nearest two breakpoints. This method is only useful for the analysis of mature geometries. Because, in this method, all aerodynamic database of each geometric alternative should be analyzed to obtain trim point, which is very time-consuming issue. On the other hand, in the instant trim and simulation algorithm, it is aimed to perform trim and simulation analysis without needing precalculated aerodynamic database. Figure 14 and Figure 15 shows the difference of the methodologies from the point of database needs. In order to find trim points, aerodynamic analysis can be performed quickly for the required state conditions at each Newton Raphson iteration. By utilizing empirical and vortex lattice-based solvers, different geometric alternatives can be trimmed and simulated to use in the optimization process. In this scope 402 different geometric alternatives are evaluated by using instant trim and simulation algorithm that is developed specifically for the thesis study.

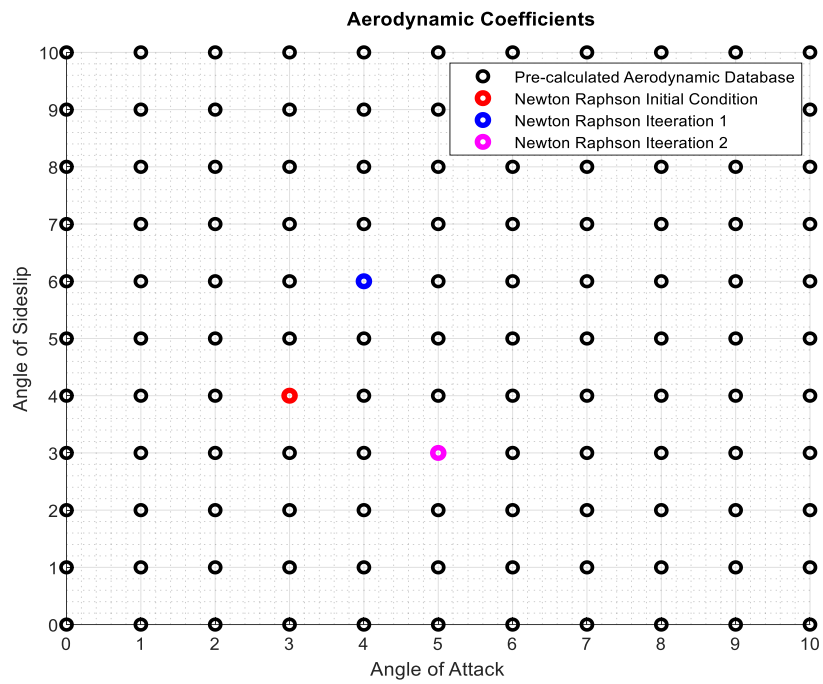


Figure 14: Conventional trim search method

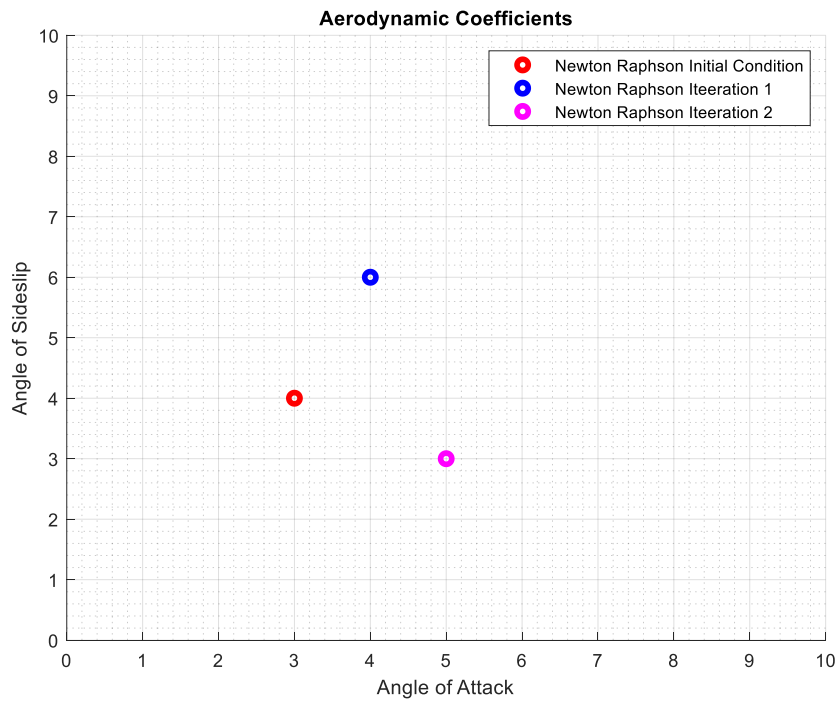


Figure 15: Instant trim search method

2.3.4 Landing Gear Block

Most of the conceptual aircraft design tool use empirical and theoretical relations to predict landing and take-off distance parameters. In MAD software landing and take-off analysis are performed by using six degrees of freedom dynamic model. This concept provides to perform high fidelity analysis without changing model structure at the further phases of design. During time integration of ground simulations, in order to support mathematical model, landing gear dynamics are included to calculations. This capability enables to consider the contribution of damping and spring effects of the landing gear to the ground simulation analysis. Detailed validation cases will be investigated in the landing and take-off distance performance analysis part.

Table 39: Landing gear weight carriage percentages

LG_{wcp}	Landing	Take Off
Weight Carriage Percentage Nose LG	33%	15 %
Weight Carriage Percentage Right LG	33%	42.5 %
Weight Carriage Percentage Left LG	33%	42.5 %

In the landing gear module, the response of the ground is calculated according to acceptances which is tabulated in Table 39 and Table 40. In addition, Equation (36) and (43) assumed as the stroke length equal to 20 cm and damping ratio equal to 2.5 times W_{TO} . The spring coefficient of the landing gear are calculated for the condition of the fact that maximum stroke level is reached when the landing gears carry three times of gross weight.

$$k_{LG} = 3 \frac{W_{TO} LG_{wcp}}{d_{vs}} \quad (35)$$

$$d_{vs} = 0.2 \quad (36)$$

$$T_{W \leftarrow B} = \begin{bmatrix} c\theta & s\phi s\theta & c\phi s\theta \\ 0 & c\phi & -s\phi \\ -s\theta & s\phi c\theta & c\phi c\theta \end{bmatrix}_{W \leftarrow B} \quad (37)$$

$$T_{B \leftarrow W} = [T_{W \leftarrow B}]^T \quad (38)$$

Equation (37) shows the transformation matrix from body axis to wheel axis. Interaction between landing gear and ground is analyzed in wheel axis to make calculations independent from attitude of the body.

$$P_{LG(wheel)} = T_{W \leftarrow B}(P_{LG body}) \quad (39)$$

$$h_{LG wheel} = h - P_{LGz(wheel)} \quad (40)$$

$$V_{P_{LG}(body)} = [u, v, w] + [p, q, r] (P_{LG(body)}) \quad (41)$$

$$V_{P_{LG}(wheel)} = T_{W \leftarrow B} (V_{P_{LG}(body)}) \quad (42)$$

$$\zeta_{LG} = W_{TO} * 2.5 \quad (43)$$

if $h_{LG wheel} < 0$:

$$F_{Z_{LG wheel}} = k_{LG} h_{LG wheel} - \zeta_{LG} V_{P_{LG}(wheel)} \quad (44)$$

Equation (44) reveals the main reaction force of the ground to the landing gear in wheel z axis. In addition, the friction force can be calculated by using Equation (45) which is required to know reaction force and friction coefficient.

Table 40: Friction coefficients of runways (U.S.A Department of Defense, 2003)

Runway Condition	$\mu_{rf\text{ Braked}}$	$\mu_{rf\text{ Unbraked}}$
Dry	0.30	0.025
Wet	0.20	0.050
Snow	0.14	0.090
Ice	0.09	0.050

$$F_{X_{LG\text{ wheel}}} = F_{Z_{LG\text{ wheel}}} \mu_{rf} \quad (45)$$

$$F_{LG\text{ wheel}} = \begin{bmatrix} F_{X_{LG\text{ wheel}}} \\ F_{Y_{LG\text{ wheel}}} \\ F_{Z_{LG\text{ wheel}}} \end{bmatrix} \quad (46)$$

$$M_{LG\text{ wheel}} = P_{LG(\text{wheel})} F_{LG\text{ wheel}} \quad (47)$$

$$M_{LG(\text{body})} = T_{B \leftarrow W}(M_{LG\text{ wheel}}) \quad (48)$$

$$F_{LG(\text{body})} = T_{B \leftarrow W}(F_{LG\text{ wheel}}) \quad (49)$$

Equation (48) and (49) gives resultant moments and forces in body axis, which are originated from landing gears. By adding these components to the total moment and force values, it is possible to include the ground dynamics in the mathematical 6-DOF model.

2.3.5 Atmosphere Model

In MAD tool, most of the modules are utilized to calculate force and moment values created by a component of the aircraft such as aerodynamic, engine and landing gear. However, atmosphere model provides to observe effect of air density, pressure and temperature over the total force and moment on the aircraft.

Table 41: Coefficients for prediction of atmospheric parameters (ESDU 77022, 2003)

ATMOSPHERIC CONDITION COEFFICIENTS			
Sea Level < h < 36090 ft		36090 ft < h < 65616 ft	
A	288.15	A	216.65
B	-1.9815e-3	B	0
I	0.2418e+0	M	4.0012e-3
J	-1.6625e-6	N	48.0634e-6
L	0.4256e+1		
$\rho_{std} = I + J (h)^L$		$\rho_{std} = M e^{N(h)}$	
$T_{(std)} = A + B(h)$			

In order to get standard density and temperature at related altitude, the coefficients, which is indicated at Table 41, are utilized.

$$T = (T)_{std} + \Delta_{ISA} \quad (50)$$

$$\rho = \frac{\rho_{std}}{1 + \frac{\Delta_{ISA}}{(T)_{std}}} \quad (51)$$

Equation (50) and (51) calculates actual temperature and density by including temperature deviation from standard values. As a result of the relations which are used to create atmospheric model, temperature and density map are figured out at Figure 16 and Figure 17.

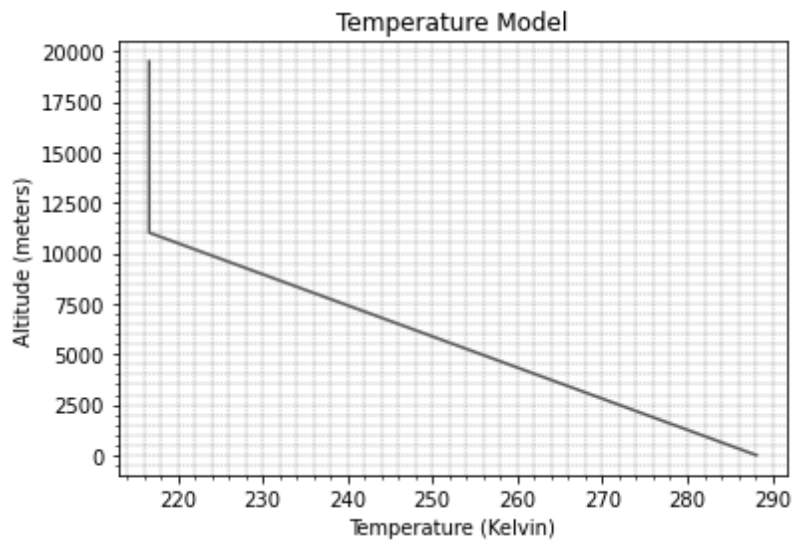


Figure 16: Atmospheric temperature model

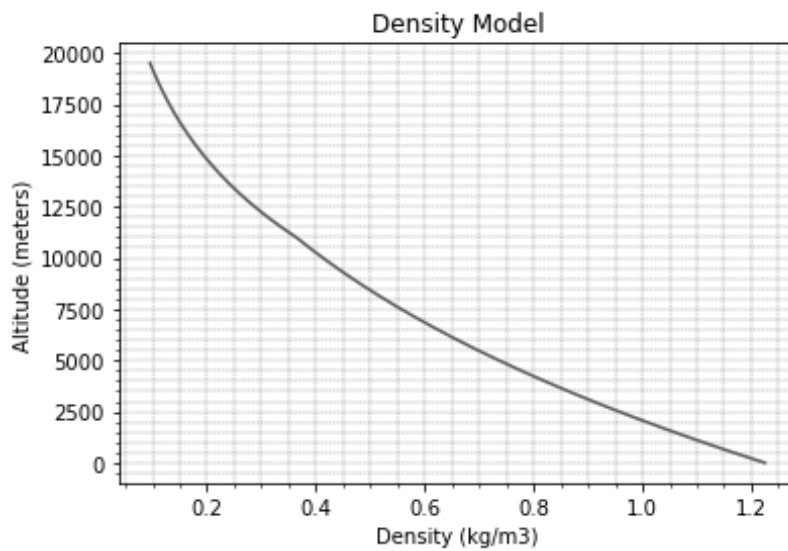


Figure 17: Atmospheric density model

To obtain Mach number for related atmospheric conditions, Equations from (52) to (55) are applied.

$$V_{sound} = \sqrt{\gamma_{air}RT} \quad (52)$$

$$\gamma_{air} = 1.4 \quad (53)$$

$$R = 287.053 \text{ J} \cdot \text{K}^{-1} \cdot \text{kg}^{-1} \quad (54)$$

$$Mach = \frac{V_{TAS}}{\text{Speed of Sound}} \quad (55)$$

Equations from (56) to (59) indicates definitions of air speeds with respect to body reference frame.

$$V_{CAS} = V_{IAS} - \Delta\text{error} \quad (56)$$

Indicated air speed is the speed which can be read from aircraft indicator panel. Calibrated air speed is obtained by eliminating instrument and position error from the indicated airspeed as shown in Equation (56). However, there is no exact formulation to get indicated air speed by using calibrated air speed, since instrument and position error may vary aircraft to aircraft.

$$V_{EAS} = V_{CAS} \sqrt{\frac{P}{P_0}} \sqrt{\frac{\left(\frac{q_c}{P} + 1\right)^{0.286} - 1}{\left(\frac{q_c}{P_0} + 1\right)^{0.286} - 1}} \quad (57)$$

$$q_c = P[(1 + 0.2M^2)^{3.5} - 1] \quad (58)$$

Equivalent airspeed is obtained by correcting compressibility effect inside of the calibrated airspeed. For this calculation impact pressure parameter is utilized. The related equalities are stated at Equation (57) and (58).

$$V_{TAS} = V_{EAS} \sqrt{\frac{\rho_{SL}}{\rho}} \quad (59)$$

True airspeed can be reached by correcting pressure altitude and Δ_{ISA} effects inside of the equivalent airspeed. Moreover, thanks to equivalent air speed concept, analysis can be performed by fixing dynamic pressure. The relation between equivalent and true airspeed is given at Equation (59) (Gudmundsson, 2014).

2.3.6 Stability and Control Block

Stability and control module is created in order to analyze flight characteristics and control the aircraft while performing desired maneuver. To observe flight characteristics, MAD software benefits from linearization and mode analysis methods. Moreover, in control part inverse simulation and PID methods are utilized.

2.3.6.1 Flight Character Analysis

In order to do an assessment about flight characteristics of the aircraft, initially equilibrium points should be obtained, since stability is a property of trim point. If the states is not in equilibrium, then stability would be a meaningless term for that point. To get a Linear Time Independent (LTI) system, it is required that states of the system should not change in time. Derivatives of the following states ($V_{TAS}, \alpha, \beta, p, q, r, \theta, \phi$) should be zero to be sure of the fact that system can be represented as LTI. After determining the trim values of the states, stability and control matrices can be attained by linearizing the system at the equilibrium point.

$$\dot{X} = AX + BU \quad (60)$$

Equation (60) and Table 42 express equations of linearized system, which is followed up for flight characteristics analysis.

Table 42: Description of linearized system equation parameters

\dot{X}	State derivatives vector
X	States vector
U	Inputs vector
A	System matrix
B	Control matrix

Derivatives of the states can be expressed in terms of state and input parameters of the system, thanks to linearized system & control matrices. According to this concept, system and control matrices can be written as Equation (61) and (62).

$$\text{System Matrix: } A = \left. \left(\frac{\delta \dot{X}}{\delta X} \right) \right|_{\substack{(U=U_{trim}) \\ (X=X_{trim})}} \quad (61)$$

$$\text{Control Matrix: } B = \left. \left(\frac{\delta \dot{X}}{\delta U} \right) \right|_{\substack{(U=U_{trim}) \\ (X=X_{trim})}} \quad (62)$$

In MAD environment, while calculating derivatives of the equations, central difference derivation method is used. Moreover, in case of evaluation of the pre-calculated database integrated system, perturbation is arranged as equal to half of the breakpoint differences of the database for the related state. It guaranties that effect of all data points are included to derivation process.

Table 43: Linearized system matrix

System Matrix [$X = X_{trim}$] [$U = U_{trim}$]	V_{TAS}	α	β	p	q	r	θ	ϕ
\dot{V}_{TAS}	$\left(\frac{\delta(\dot{V}_{TAS})}{\delta(V_{TAS})}\right)$	$\left(\frac{\delta(\dot{V}_{TAS})}{\delta(\alpha)}\right)$	$\left(\frac{\delta(\dot{V}_{TAS})}{\delta(\beta)}\right)$	$\left(\frac{\delta(\dot{V}_{TAS})}{\delta(p)}\right)$	$\left(\frac{\delta(\dot{V}_{TAS})}{\delta(q)}\right)$	$\left(\frac{\delta(\dot{V}_{TAS})}{\delta(r)}\right)$	$\left(\frac{\delta(\dot{V}_{TAS})}{\delta(\theta)}\right)$	$\left(\frac{\delta(\dot{V}_{TAS})}{\delta(\phi)}\right)$
$\dot{\alpha}$	$\left(\frac{\delta(\dot{\alpha})}{\delta(V_{TAS})}\right)$	$\left(\frac{\delta(\dot{\alpha})}{\delta(\alpha)}\right)$	$\left(\frac{\delta(\dot{\alpha})}{\delta(\beta)}\right)$	$\left(\frac{\delta(\dot{\alpha})}{\delta(p)}\right)$	$\left(\frac{\delta(\dot{\alpha})}{\delta(q)}\right)$	$\left(\frac{\delta(\dot{\alpha})}{\delta(r)}\right)$	$\left(\frac{\delta(\dot{\alpha})}{\delta(\theta)}\right)$	$\left(\frac{\delta(\dot{\alpha})}{\delta(\phi)}\right)$
$\dot{\beta}$	$\left(\frac{\delta(\dot{\beta})}{\delta(V_{TAS})}\right)$	$\left(\frac{\delta(\dot{\beta})}{\delta(\alpha)}\right)$	$\left(\frac{\delta(\dot{\beta})}{\delta(\beta)}\right)$	$\left(\frac{\delta(\dot{\beta})}{\delta(p)}\right)$	$\left(\frac{\delta(\dot{\beta})}{\delta(q)}\right)$	$\left(\frac{\delta(\dot{\beta})}{\delta(r)}\right)$	$\left(\frac{\delta(\dot{\beta})}{\delta(\theta)}\right)$	$\left(\frac{\delta(\dot{\beta})}{\delta(\phi)}\right)$
\dot{p}	$\left(\frac{\delta(\dot{p})}{\delta(V_{TAS})}\right)$	$\left(\frac{\delta(\dot{p})}{\delta(\alpha)}\right)$	$\left(\frac{\delta(\dot{p})}{\delta(\beta)}\right)$	$\left(\frac{\delta(\dot{p})}{\delta(p)}\right)$	$\left(\frac{\delta(\dot{p})}{\delta(q)}\right)$	$\left(\frac{\delta(\dot{p})}{\delta(r)}\right)$	$\left(\frac{\delta(\dot{p})}{\delta(\theta)}\right)$	$\left(\frac{\delta(\dot{p})}{\delta(\phi)}\right)$
\dot{q}	$\left(\frac{\delta(\dot{q})}{\delta(V_{TAS})}\right)$	$\left(\frac{\delta(\dot{q})}{\delta(\alpha)}\right)$	$\left(\frac{\delta(\dot{q})}{\delta(\beta)}\right)$	$\left(\frac{\delta(\dot{q})}{\delta(p)}\right)$	$\left(\frac{\delta(\dot{q})}{\delta(q)}\right)$	$\left(\frac{\delta(\dot{q})}{\delta(r)}\right)$	$\left(\frac{\delta(\dot{q})}{\delta(\theta)}\right)$	$\left(\frac{\delta(\dot{q})}{\delta(\phi)}\right)$
\dot{r}	$\left(\frac{\delta(\dot{r})}{\delta(V_{TAS})}\right)$	$\left(\frac{\delta(\dot{r})}{\delta(\alpha)}\right)$	$\left(\frac{\delta(\dot{r})}{\delta(\beta)}\right)$	$\left(\frac{\delta(\dot{r})}{\delta(p)}\right)$	$\left(\frac{\delta(\dot{r})}{\delta(q)}\right)$	$\left(\frac{\delta(\dot{r})}{\delta(r)}\right)$	$\left(\frac{\delta(\dot{r})}{\delta(\theta)}\right)$	$\left(\frac{\delta(\dot{r})}{\delta(\phi)}\right)$
$\dot{\theta}$	$\left(\frac{\delta(\dot{\theta})}{\delta(V_{TAS})}\right)$	$\left(\frac{\delta(\dot{\theta})}{\delta(\alpha)}\right)$	$\left(\frac{\delta(\dot{\theta})}{\delta(\beta)}\right)$	$\left(\frac{\delta(\dot{\theta})}{\delta(p)}\right)$	$\left(\frac{\delta(\dot{\theta})}{\delta(q)}\right)$	$\left(\frac{\delta(\dot{\theta})}{\delta(r)}\right)$	$\left(\frac{\delta(\dot{\theta})}{\delta(\theta)}\right)$	$\left(\frac{\delta(\dot{\theta})}{\delta(\phi)}\right)$
$\dot{\phi}$	$\left(\frac{\delta(\dot{\phi})}{\delta(V_{TAS})}\right)$	$\left(\frac{\delta(\dot{\phi})}{\delta(\alpha)}\right)$	$\left(\frac{\delta(\dot{\phi})}{\delta(\beta)}\right)$	$\left(\frac{\delta(\dot{\phi})}{\delta(p)}\right)$	$\left(\frac{\delta(\dot{\phi})}{\delta(q)}\right)$	$\left(\frac{\delta(\dot{\phi})}{\delta(r)}\right)$	$\left(\frac{\delta(\dot{\phi})}{\delta(\theta)}\right)$	$\left(\frac{\delta(\dot{\phi})}{\delta(\phi)}\right)$

In order to perform mode analysis of the aircraft, eigenvalues of the system matrix can be obtained by solving Equation (63) for λ .

$$Det|A - \lambda I| = 0 \quad (63)$$

The formulations to attain the parameters based on eigenvalues that define flight characteristics, is tabulated at Table 44. These formulations are used to get physical expressions of stability concept.

Table 44: Flying quality parameters (Yechout et al., 2003)

FLYING QUALITY PARAMETERS	
Time Constant (τ)	$\frac{-1}{\lambda_{real}}$
Time to Double (T_2)	$\frac{\ln 2}{\lambda_{real}}$
Time to half ($T_{\frac{1}{2}}$)	$\frac{-\ln 2}{\lambda_{real}}$
Natural Frequency (ω_N)	$\sqrt{(\lambda_{real})^2 + (\lambda_{imag})^2}$
Damping Ratio (ζ)	$\frac{-\lambda_{real}}{\omega_N}$
Damped Frequency (ω_D)	$\omega_D = \omega_N \sqrt{1 - \zeta^2}$

2.3.6.2 Inverse Simulation Controller

During the performance and stability analysis process, inverse simulation controller is utilized to simulate maneuvers within desired conditions which is specified in requirements. Inverse simulation method is based on Newton Raphson solver. To get a desired model output for a specific time step, the controller applies different control surface deflections and integrates the differential equations during this timestep. At the end of the integration process for a specific timestep with fixed control surface deflection, algorithm calculates the difference between actual and desired model outputs, so called error norm. If the related control surface deflection provides the error norm to decrease up to under the level of error tolerance, then Newton Raphson algorithm stops to iterations and stores the control surface deflection value for related timestep. For next timestep the same procedures are repeated until whole time history of desired and actual maneuver equalizes. As a result of the process, time history of the control surface deflections is obtained for desired model output (Jafari & Shahmiri, 2019).

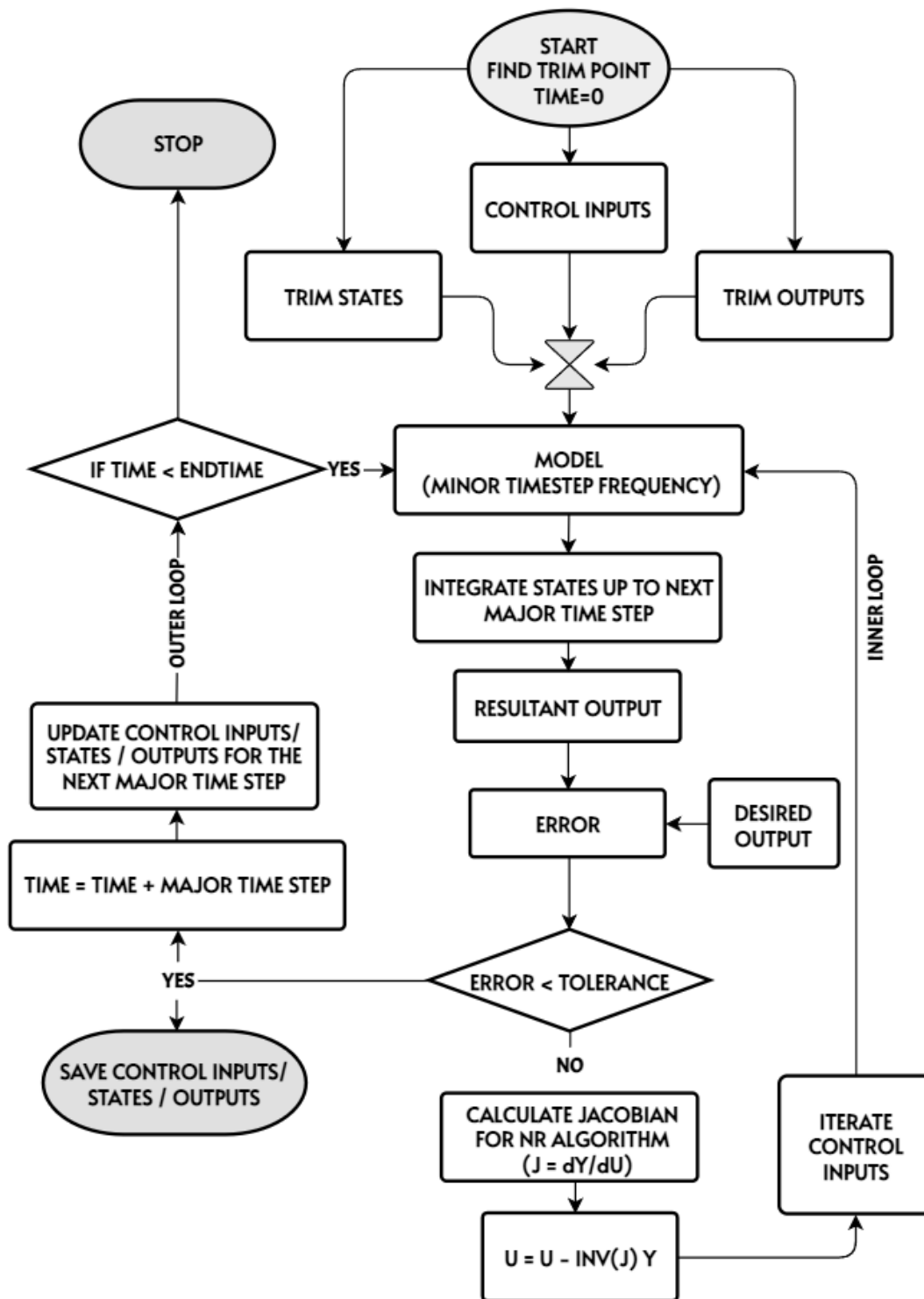


Figure 18: Inverse simulation control algorithm

The workflow of the inverse simulation control algorithm is figured out at Figure 18. The parameters which are used in the workflow are tabulated in Table 45 together with descriptions.

Table 45: Inverse simulation parameter descriptions

U	Control Input Parameters
J	Jacobian Matrix
Y	Output Parameters

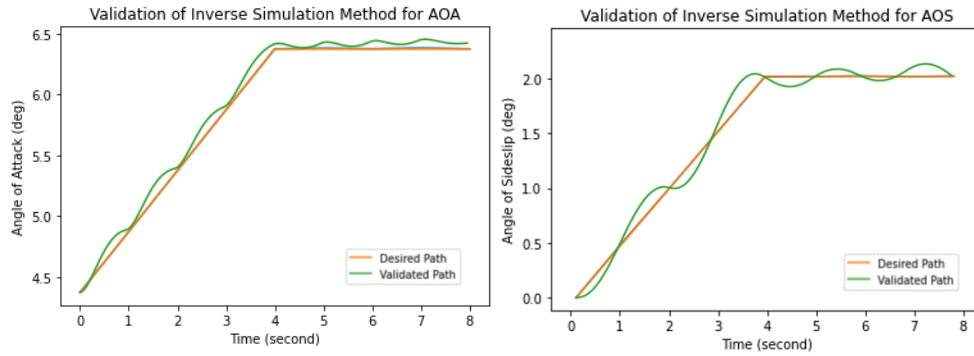


Figure 19: Inverse simulation method validation results

In MAD environment, the reference angle of attack and angle of sideslip commands are aimed to follow by using inverse simulation controller and instant simulation method. In Figure 19, the validated path shows that the algorithm works conveniently with a tolerance around 0.2 degrees.

2.3.7 Weight and Balance

For a complete analysis of a new concept aircraft, the weight and inertial properties of the geometry should be predicted from the first step of the design phase. In order to see effects of the weight properties over the stability and performance analysis,

Class II empirical weight prediction methods are utilized which is based on (Roskam, 2018). The methodology has the calculation sensitivity for different wing location, fuel tank location and type of the landing gear. To apply the effects of technological improvements to aircraft structural weight, MAD environment includes user defined technology factor parameter which decreases aircraft weight component-wise.

Table 46: Aircraft weight estimation formulations (Roskam, 2018)

WEIGHT ESTIMATION FORMULATIONS		
Wing	$W_W = 0.002933(S)^{1.018}(A)^{2.473}(n_{ult})^{0.611}$	(64)
Horizontal Tail	$W_h = \frac{3.184(W_{TO})^{0.887}(S_h)^{0.101}(A_h)^{0.138}}{174.04(t_{rh})^{0.223}}$	(65)
Vertical Tail	$W_v = \frac{1.68(W_{TO})^{0.567}(S_v)^{1.249}(A_v)^{0.482}}{639.95(t_{rv})^{0.747}(\cos\Lambda_{v\frac{1}{4}})^{0.882}}$	(66)
Fuselage	$W_f = 14.86(W_{TO})^{0.144}\left(\frac{l_{fn}}{p_{max}}\right)^{0.778}(l_{fn})^{0.383}(N_{pax})^{0.455}$	(67)
Main Landing Gear	$W_{mainLGs} = 0.013W_{TO} + 0.362(W_L)^{0.417}(n_{ult.l})^{0.950}(l_{sm})^{0.183}$	(68)
Nose Landing Gear	$W_{noseLG} = 6.2 + 0.0013W_{TO} + 0.007157(W_L)^{0.749}(n_{ult.l})(l_{sn})^{0.788}$	(69)
Power Plant	$W_e = K_p(P_{TO})$ Kp is changes from 1.1 to 1.8 for piston prop aircrafts.	(70)
Fixed Equipment	$W_{fc} = 0.0168(W_{to})$ $W_{els} = 0.0268(W_{to})$ $W_{iae} = 20 + 0.008(W_{to})$ $W_{api} = 2.5(N_{pax})$ $W_{ox} = 20 + 0.5(N_{pax})$ $W_{apu} = 0.0085(W_{to})$ $W_{fur} = 0.412 * (N_{pax})^{1.145} W_{to}^{0.489}$ $W_{pt} = 0.005(W_{to})$	(71)

In the design process, the weight calculation process is operated iteratively. By starting from an initial guess of the take-off weight, the algorithm tries to get a new guess. At the point where total weight converges, the algorithm stops and calculates center of gravity and inertia parameters. The empirical correlations of the component weights of the aircraft are stated at Table 46.

Thanks to the predicted values of the weight and center of gravity position of each component which is stated at Table 47, the overall center of gravity location of the aircraft is calculated by using, Equation (72).

$$X_{CG} = \frac{\text{Sum } W_i x_i}{\text{Sum } W_i} \quad (72)$$

Table 47 : The empirical predictions of CG point (Roskam, 2018)

CG positions of Components	
Wing	38 – 42 percent chord from the L.E. at 40 percent of the semispan
Horizontal tail	42 percent chord from the leading edge at 38 percent of semi-span
Vertical Tail	42 percent chord from the leading edge at 38 percent of semi-span from the root chord
Landing Gear	50 percent of strut length for gears with mostly vertical struts
Fuselage	32-35 percent of fuselage length (spinner excluded)

In order to calculate the inertia of the aircraft, Equations from (73) to (78) are performed accordingly (Roskam, 2018).

$$I_{xx} = \sum_{i=1}^{i=n} I_{xx_i} + \sum_{i=1}^{i=n} m_i \left((y_i - y_{cg})^2 + (z_i - z_{cg})^2 \right) \quad (73)$$

$$I_{yy} = \sum_{i=1}^{i=n} I_{yy_i} + \sum_{i=1}^{i=n} m_i \left((z_i - z_{cg})^2 + (x_i - x_{cg})^2 \right) \quad (74)$$

$$I_{zz} = \sum_{i=1}^{i=n} I_{zz_i} + \sum_{i=1}^{i=n} m_i \left((x_i - x_{cg})^2 + (y_i - y_{cg})^2 \right) \quad (75)$$

$$I_{xy} = \sum_{i=1}^{i=n} I_{xy_i} + \sum_{i=1}^{i=n} m_i (x_i - x_{cg})(y_i - y_{cg}) \quad (76)$$

$$I_{yz} = \sum_{i=1}^{i=n} I_{yz_i} + \sum_{i=1}^{i=n} m_i (y_i - y_{cg})(z_i - z_{cg}) \quad (77)$$

$$I_{zx} = \sum_{i=1}^{i=n} I_{zx_i} + \sum_{i=1}^{i=n} m_i (z_i - z_{cg})(x_i - x_{cg}) \quad (78)$$

2.3.7.1 Validation

As a validation case, Cessna 172N aircraft is based and (Roskam, 2018) is used to get weight breakdown of the aircraft. The actual component weights of the aircraft are compared to the weight prediction results of the MAD tool. The comparison results are tabulated at Table 48 and figured out at Figure 20.

Table 48: The weight prediction method validation of MAD with Cessna 172

Weight Description (lb.)	Cessna 172 Data	MAD Prediction
Empty Weight	1455	1430
Wing Weight	236	235
Empennage Weight	60	63
Fuselage Weight	367	432
Landing Gear Weight	115	121
Power Plant Weight	360	288
Fuel Weight	241	241
Payload Weight	606	606
Fixed Equipment Weight	165	289

According to Table 48 and Figure 20, the weight prediction method gives reasonable and acceptable results. The maximum error is recorded as approximately 15% at fuselage case. The total empty weight is predicted with an error of 2% which is a very good estimation for concept design phase.

Figure 21 is obtained with MAD tool by using different weight configurations of Cessna 172N aircraft. The weight configurations are defined by applying different alternatives of pilot, payload and fuel options on the aircraft.

According to Table 14, the real CG location of Cessna 172 aircraft is observed as varying from 2.23 meter to 2.54 meter. Moreover, the MAD tool predicts CG envelope of the Cessna 172 as from 2.22 meter to 2.55 meter, which is very close to actual results.

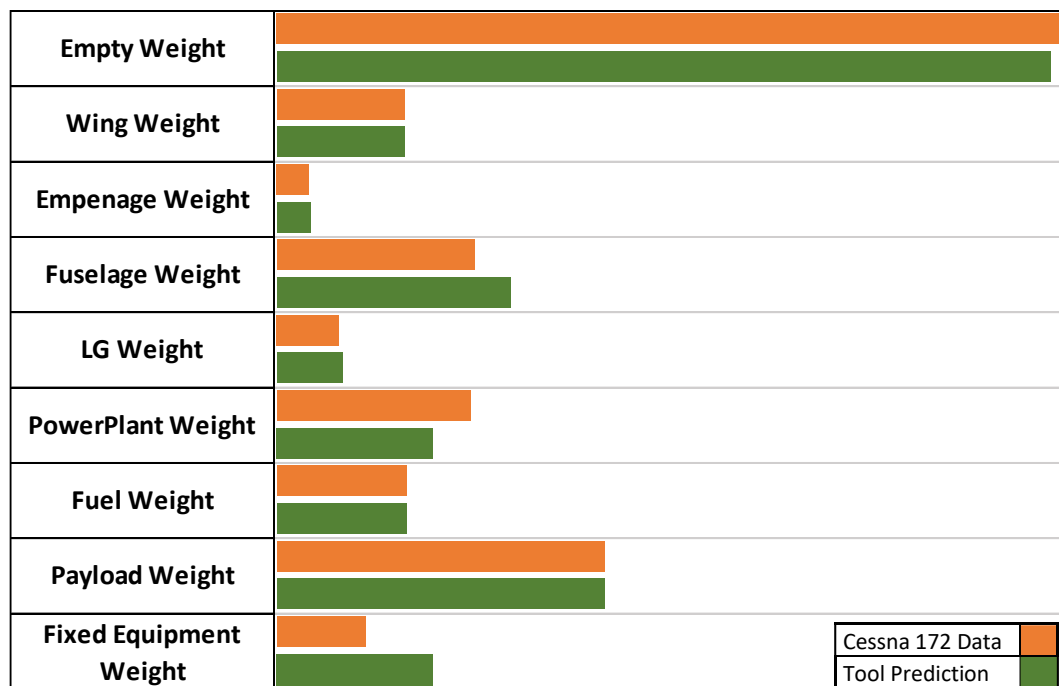


Figure 20: The comparison of weight prediction results of Cessna 172

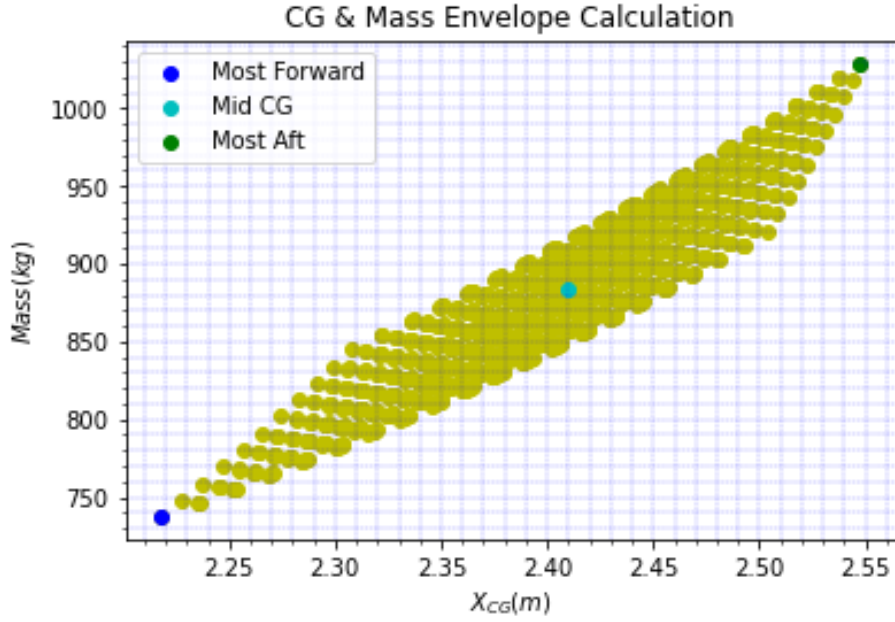


Figure 21: Cessna 172N mass & CG envelope analysis results of MAD tool

2.3.8 Cost Analysis

In the design process, one of the main parameters which affect the optimization results is cost of the aircraft. In this study, the price of the aircraft is predicted by using historical trends which is indicated in Figure 22. The cost of the aircraft is regarded as directly proportional with price. Thus, price parameters used to estimate cost in optimization algorithm.

According to Figure 22, the price of the aircraft is calculated by utilizing empty weight (in pounds) and engine power (in horsepower) parameters. Equation (79) and (80) indicates the formulations which are used for cost analysis of aircrafts in the general aviation category (Harris & Scully, n.d.). Moreover in Table 49, the sub-coefficients that is related to C_{GA} parameter are given.

$$Price = 192.38 C_{GA} (W_E)^{0.4854} (P_{BHP})^{0.5843} \quad (79)$$

$$C_{GA} = Engine\ Type \times Engine\ No \times Trainer \times Pressurization \quad (80)$$

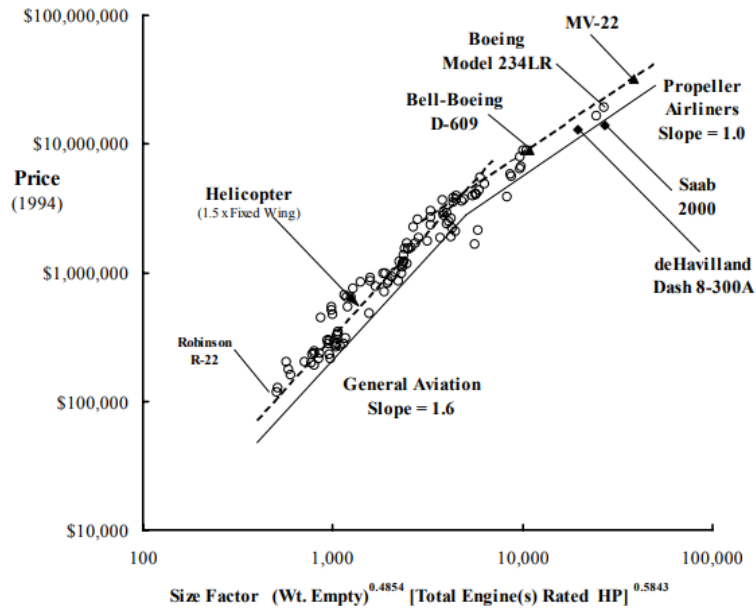


Figure 22: Aircraft pricing relation with respect to empty weight and engine horsepower (Harris & Scully, n.d.)

Table 49: C_{GA} Coefficient Sub-Coefficients (Harris & Scully, n.d.)

Engine Type		Engine Number		Trainer		Pressurized	
Piston	1.000	Single	1.000	No	1.000	No	1.000
Supercharged	1.249		1.352	Yes	0.710	Yes	1.135
Gas Turbine	2.101	Multi					

Figure 23 shows inflation of the products in the aviation industry. The inflation is important if the price of the aircraft is wanted to be calculated exactly for a specific time. However, price escalation effect is not implemented to analysis tool, since increment or decrement of the cost with respect to years does not affect the relation between design inputs and outputs. Thus, MAD software includes only main relation between design variables and price according to inflation in 1994.

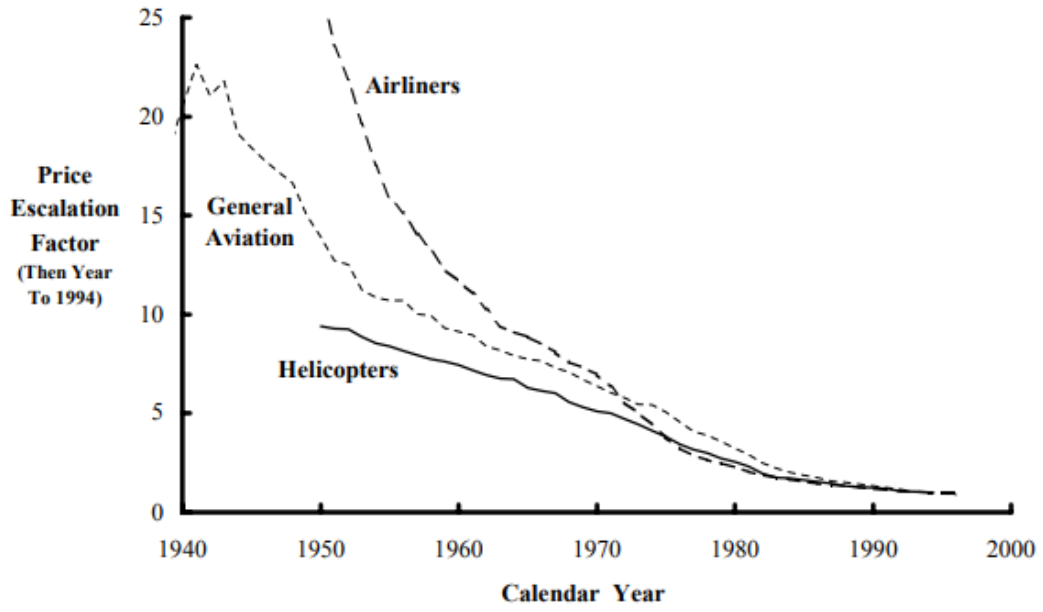


Figure 23: Price escalation factor change in time (Harris & Scully, n.d.)

CHAPTER 3

ANALYSIS CONDITIONS AND REQUIREMENTS

For an effective design methodology, it is very crucial to have wide range of physics-based analysis capability. In this scope, MAD environment has the competence to perform stability, performance, and control surface sufficiency analyses from conceptual to detailed design phase of a concept aircraft. List of the analyses for each discipline are tabulated at Table 50.

Table 50: Analysis capability of the MAD environment

Control Surface Sufficiency Analysis	Stability Analysis	Performance Analysis
NDR	Departure	Take off Distance
Max Roll Rate	FPS	Landing Distance
Crosswind Landing	FHQ	ROC
Controllability	Spin	Ceiling
		Stall Speed
		Max Cruise Speed
		Sustained Turn
		Range
		Endurance

3.1 Performance Analysis

In the literature, performance analysis is generally performed by using the point mass model which ignores moment equations and control surface effects. In this study, during the performance analysis it is aimed to see the required control surface deflections for related flight condition by using 6-DOF model. In the methods of calculations, theoretical formulations are utilized as well as trim and simulation analysis.

3.1.1 Range

Range is the distance an airplane can fly in a given time. This distance is of great importance in aircraft design and is often the parameter used to determine whether a particular design is viable (Gudmundsson, 2014). To predict maximum flight distance, the methodology which is stated from Equation (81) to (90), is followed up. In range analysis, velocity and angle of attack are kept constant with changing altitude profile.

$$\eta_{oswald} = 1.78(1 - 0.045 AR^{0.68}) - 0.64 \quad (81)$$

$$K = \frac{1}{\pi AR \eta_{oswald}} \quad (82)$$

To get $BHP_{Average}$ parameter for a specific airspeed, straight flight trim tabulated in Table 26, is used for W_c and W_l weight configurations. The average of the required horsepower values to trim the aircraft in related conditions, gives directly $BHP_{Average}$ parameter.

$$C_{BHP} = \frac{Lph}{BHP_{Average}} \quad (83)$$

$$\lambda_{tcr} = 0.1 \quad (84)$$

$$W_c = W_{TO} - (W_{Fuel(usable)} \lambda_{tcr}) \quad (85)$$

$$W_l = W_{TO} - (W_{Fuel_{total}} - W_{Fuel(unusable)} - W_{Fuel(reserved)}) \quad (86)$$

$$C_L = \frac{2W_c}{\rho V_{TAS}^2 S} \quad (87)$$

$$C_D = C_{Dmin} + KC_L^2 \quad (88)$$

$$C_t = V_{TAS} \frac{C_{BHP}}{745.7 \eta_p 3600} \quad (89)$$

$$Range = V_{TAS} \frac{C_L}{C_D C_t} \ln \left(\frac{W_c}{W_l} \right) \quad (90)$$

The range parameter calculated for constant velocity, constant angle of attack and changing altitude profile is figured out at Figure 24.

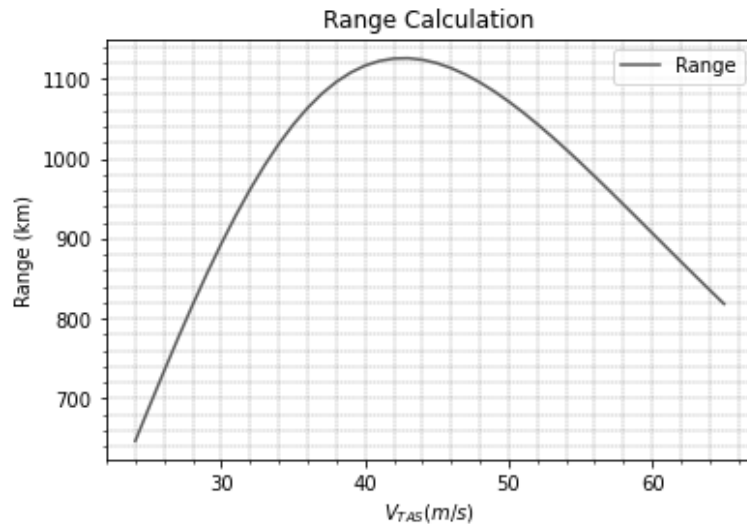


Figure 24: Range profile with respect to air velocity

According to Figure 24, the calculated maximum range of Cessna 172 is observed as 1125 km at 43 m/s air speed. Table 16 also shows the actual maximum range data of Cessna 172 which is 1064 km in 46.3 m/s speed. When the results are compared with actual aircraft data, it can be seen that the range analysis gives the range performance results with a reasonable accuracy.

3.1.2 Endurance

Endurance is the length of time that an aircraft can remain airborne for a given expenditure of fuel and for a specified set of flight conditions. For some mission types such as reconnaissance, surveillance, and border monitoring, the most important performance parameter is to be airborne as long as possible (Sadraey, 2013). The endurance and range calculation procedure are very similar to each other. From Equation (81) to (89), the steps are the same with range calculations process, however at the last step, endurance is obtained with Equation (91) instead of

Equation (90). In order to get maximum endurance performance in hours, the unit transformation should be applied from seconds to hours for related equation.

$$Endurance = \frac{C_L}{C_D C_t} \ln\left(\frac{W_c}{W_l}\right) \quad (91)$$

As a result of the calculation process, Figure 25 shows the endurance of Cessna 172 aircraft as 6.9 hours at 29 m/s airspeed. Moreover, in Table 16, the real data of Cessna 172N (Cessna Aircraft Company, 1978), states that the maximum flight time is 6.4 hours which is close to analysis result.

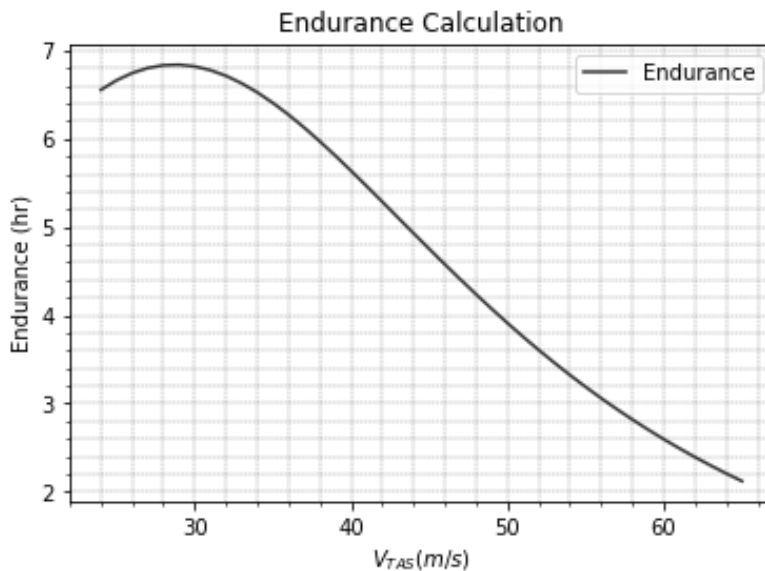


Figure 25: Endurance profile with respect to air velocity

3.1.3 Stall Speed Calculation

Stall Speed is defined in MIL-STD-3013 (U.S.A Department of Defense, 2003), for the condition of 1G flight normal to the flight path, for a specified altitude and weight configuration, as the highest of:

- a. The speed for steady, straight, and level flight at C_{Lmax} , the first local maximum of CL versus AOA graph

- b. The speed at which uncommanded pitching, rolling, or yawing occurs
- c. The speed at which intolerable buffet or structural vibration is encountered.

$$V_{stall} = \sqrt{\frac{2W_{TO}}{\rho_{SL}S_{ref}C_{Lmax}}} \quad (92)$$

To define stall speed, part (a) is referenced to determine minimum speed at steady level flight condition. In order to get this speed initially, angle of attack value which gives maximum lift coefficient are obtained for related flight condition. Since the Vortex Lattice Method is not capable to predict stall point, the MAD environment uses the angle of attack values obtained by DATCOM program to limit lift coefficient. By using this angle of attack as a user defined value, “Level Flight Speed Prediction” trim algorithm, which is stated at Table 29, finds the stall speed for 1G level flight.

In the validation process of the stall speed calculation, results are compared with flight manual of Cessna 172N. According to flight manual (Cessna Aircraft Company, 1978), for most aft cg and maximum mass configuration, stall speed is observed as 50 kts without flap deflection, 47 kts for semi-flapped configuration and 44 kts for full-flapped configuration. For the same conditions, the MAD tool calculates stall speed as 49.6 kts without flap deflection, 46 kts for semi-flapped configuration and 39 kts for full-flapped configuration.

According to model analysis results, it is seen that the configurations with the small flap deflections are predicted with maximum 1 kts error however, for full flap configuration, stall speed is underestimated with 5 kts error. It could result from the fact that nonlinear aerodynamic character at high flap deflections may not be calculated correctly with low fidelity aerodynamic calculation methods.

3.1.4 Maximum Cruise Speed

In MIL-STD-3013 (U.S.A Department of Defense, 2003), maximum cruise speed is defined as follows:

“The highest-level flight speed that can be maintained at the maximum thrust (power) setting at the specified configuration of weight and altitude”.

According to MIL-STD-3013 definition, “Max Speed Prediction” trim algorithm, stated in Table 30, is used to get maximum cruise speed. In the analysis procedure, throttle level is set as maximum at sea level and flaps up configuration.

$$V_{\max(cruise)} = \sqrt{\frac{2T_{max}}{\rho_{SL}S_{ref}C_{D}(V_{max})}} \quad (93)$$

The flight manual of Cessna 172N states that the maximum cruise speed equals to 125 kts at sea level condition, in other hand, the MAD tool calculates maximum cruise speed as 129.6 kts for takeoff weight configuration.

3.1.5 Sustained Turn

MIL-STD-3013 (U.S.A Department of Defense, 2003) states that: “Sustained load factor is defined as the number of G's attainable, without a change in energy ($P_s = 0$), during steady-state flight for a specified configuration of weight, altitude, speed, and thrust setting.”

According to this statement, “Steady Coordinated Turn” trim algorithm, which is defined in Table 32, is used to get limit conditions which result from the stall effect or insufficient power condition. The maximum trimmable load factors are figured out for each velocity condition at Figure 26.

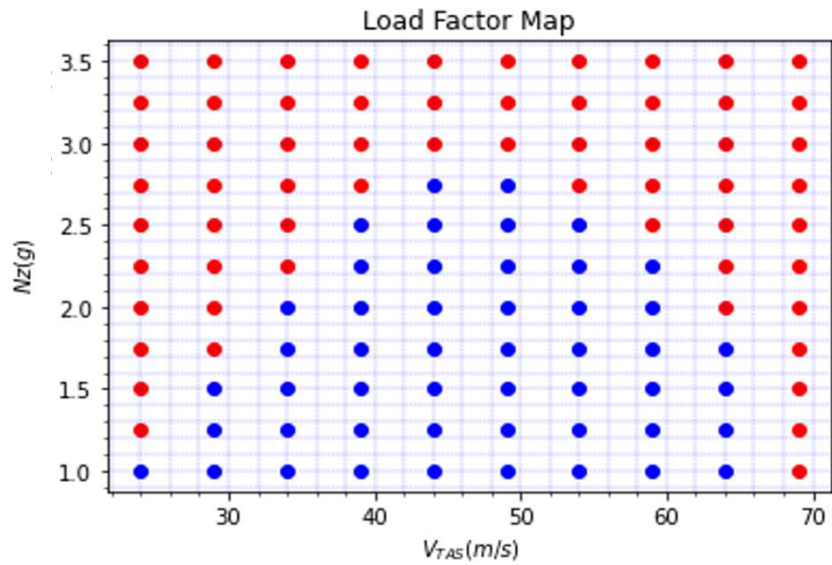


Figure 26: Sustain turn trimmable load factor map

According to Figure 26, the maximum load factor can be achieved as 2.8 G at 45 m/s velocity which is not exceed the limits in flight manual stated at Table 16.

3.1.6 Ceiling

According to MIL-STD-3013 definition, ceiling is the highest altitude where the aircraft has a specified, steady state rate of climb. In this scope, types of ceilings are tabulated at Table 51.

Table 51: Definitions of ceiling types

	Steady State Rate of Climb (fpm)
Absolute ceiling	0
Service ceiling	100
Cruise ceiling	300
Combat ceiling	500

The methodology which is applied to ceiling analysis is tabulated at Table 38. The methodology calculates the trim altitude by utilizing user defined climb rate input.

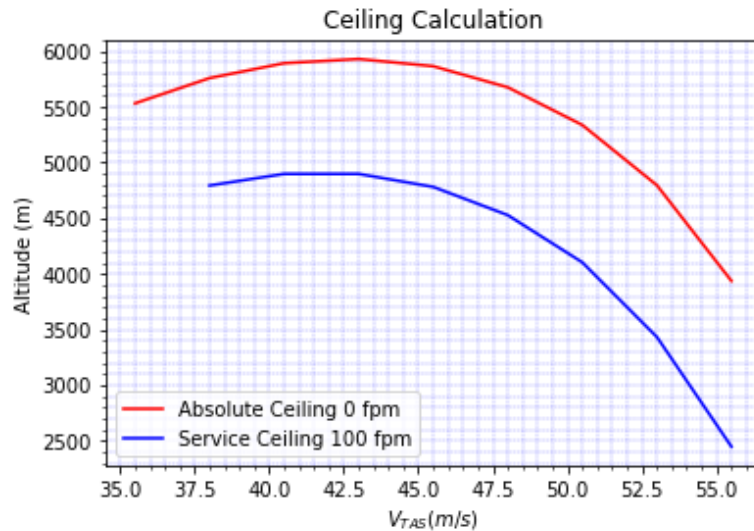


Figure 27: Ceiling performance of Cessna 172N aircraft

The flight manual of Cessna 172N gives service ceiling altitude as 4330 meters, however, MAD tool calculates the same parameter as 4910 meters at 42 m/s velocity which is figured out at Figure 27. The reason of the fact that the error norm is relatively higher, may be underestimated drag coefficient and deviation from the exact thrust value which is based theoretical formulations.

3.1.7 Rate of Climb

In military standards, maximum rate-of-climb is defined as the maximum time rate of change of geometric altitude for a given configuration, weight, altitude, speed, and thrust. In order to perform rate of climb analysis, the trim analogy, which is stated at Table 28, is utilized. In this trim condition, maximum throttle condition is accepted as the fixed trim state. Moreover, the time rate of change of altitude is defined as the main output of the trim calculation, which gives rate of climb

performance. The rate of climb parameter varies with respect to altitude condition. Thus, three different altitude condition are analyzed with MAD software. The best rate of climb performance is obtained at sea level condition. Figure 28 shows the rate of climb performance of Cessna 172N aircraft for the altitudes from sea level to 5000 meters.

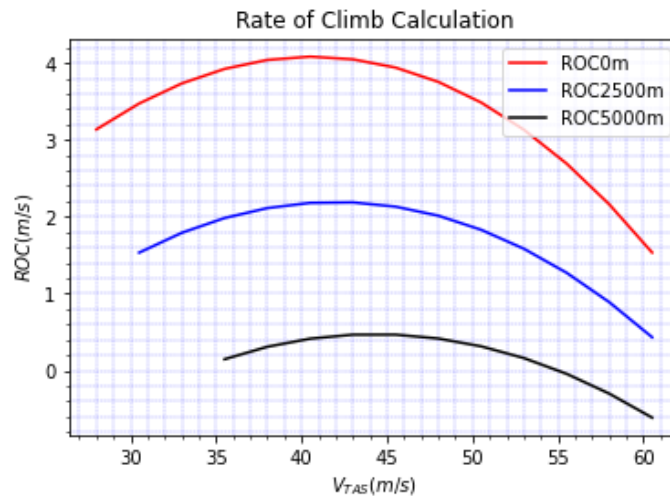


Figure 28: Cessna 172N rate of climb performance

According to Figure 28 results, the maximum rate of climb of Cessna 172N is observed as 4.08 m/s at 40.5 m/s velocity. On the other hand, flight manual data gives the best rate of climb as 3.91 m/s at 38 m/s.

3.1.8 Take of Distance

In the MAD environment, take-off analysis is mainly based on trim and simulation analysis. The general procedure to perform take-off simulation is stated as follows:

- Trim the aircraft at zero velocity at ground
- Flaps down (take-off settings)
- Use full throttle to accelerate
- When the aircraft reaches the rotation speed, use elevator to pitch up

- Control the aircraft by using elevator to get the target climb angle which is obtained at the trim point of 1.2 times stall speed.

Table 52: Take off speed definitions (Gudmundsson, 2014)

Take Off Speeds	
Rotation Speed	1.1 VS
Lift Off Speed	1.1 VS
Climb Speed	1.2 VS
Obstacle Clearance Speed	1.2 VS

Table 52 shows the take-off speed definition in terms of stall speed at flaps up configuration according to FAR 23 (Federal Aviation Administration, 2009) and MIL STD 3013. In order to obtain climb angle, the climb trim is utilized which is stated at Table 28, with maximum throttle settings at related speed condition and take-off flap configuration. Figure 29 shows the type of velocities which are important for take-off process.

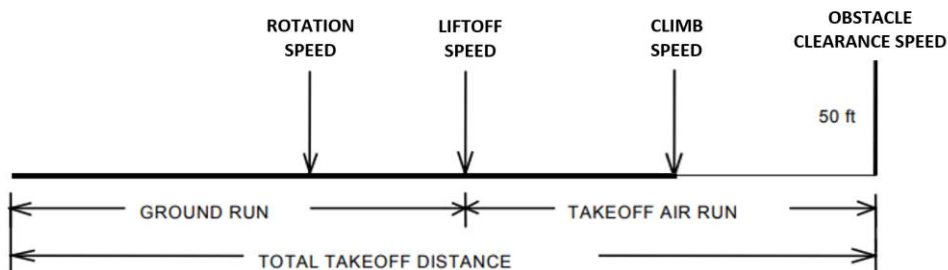


Figure 29: Take-off simulation procedure

Rotation speed is defined as the speed at which body rotation is initiated from the ground run attitude to the lift-off attitude, by using horizontal tail control. From the rotation speed to lift-off speed, pitch angle increases without changing flight path angle. Moreover, rotation speed must be greater than the ground minimum control speed to be able to generate sufficient moments to initiate rotation.

Lift-off speed is defined as the speed which aircraft leaves the ground totally. From lift off to climb condition, the flight path angle and velocity increase gradually. After the aircraft reaches the desired climb speed and climb angle simultaneously, flight path angle and speed are kept constant up to obstacle clearance point.

Obstacle clearance speed is defined as the speed at which the air vehicle clears a 50-ft height above the runway during climb out, for a specified altitude, weight, and configuration (U.S.A Department of Defense, 2003).

In the validation process of the takeoff distance analysis, the data taken from flight manual of Cessna 172, is utilized. From Figure 30 takeoff distance can be observed as 455 meters as a result of the MAD tool simulation. On the other hand, Cessna 172N flight manual states the takeoff distance as 438 meters.

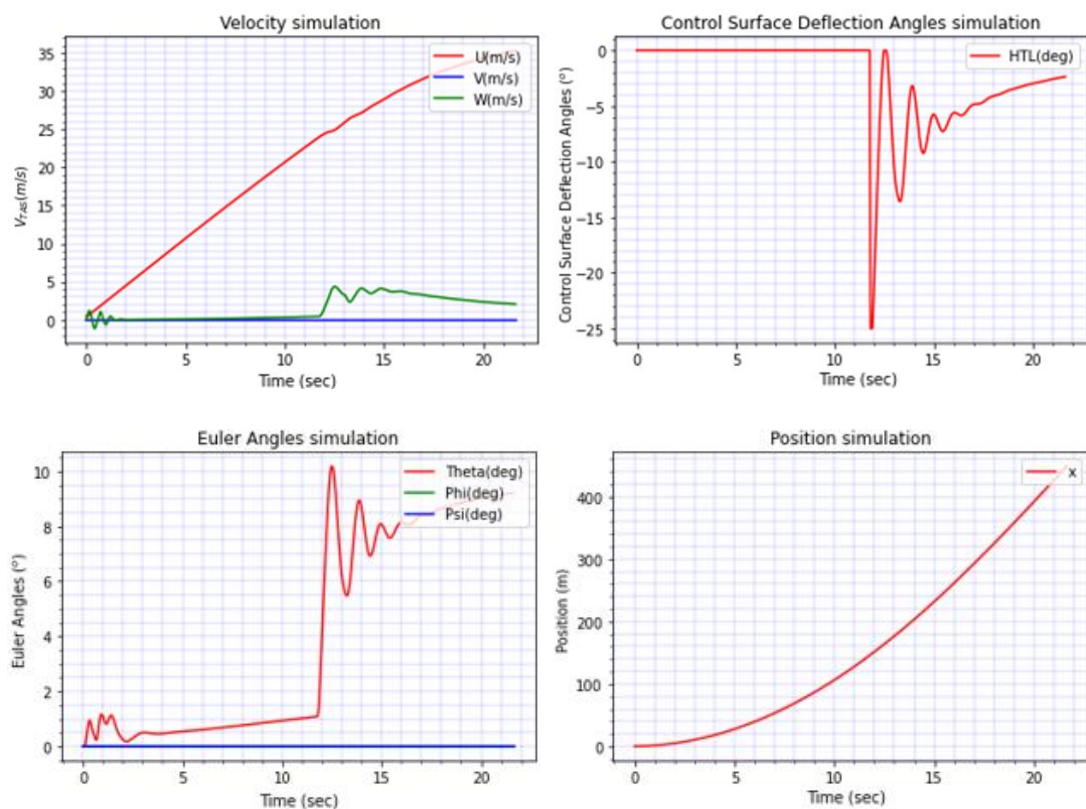


Figure 30: Take off simulation results

3.1.9 Landing Distance

In order to calculate landing performance, trim and simulation analyses are utilized at the specific weight and altitude conditions. The general stages of the landing distance analysis process are denoted as follows:

- Trim the aircraft at approach path angle (-3°), approach speed ($1.3 V_S$) and 50 ft obstacle clearance altitude for flaps down configuration (Gudmundsson, 2014)
- Flare just before touchdown (Flight path angle from -3° to -1°)
- Touchdown at $1.1 V_S$
- Set throttle to Idle (%5 of static thrust) (Gudmundsson, 2014)
- Neutralize control surfaces
- Brake / Stop

Table 53: Landing performance speed definitions (Gudmundsson, 2014)

Landing Speeds	FAR 23	MIL 3013
Approach	$1.3 V_S$	$1.2 V_S$
Flare	$1.3 V_S$	$1.2 V_S$
Touch Down	$1.1 V_S$	$1.1 V_S$
Braking	$1.1 V_S$	$1.1 V_S$

Table 53 exhibits the landing speeds, according to FAR 23 and MIL STD 3013 references. The speeds are defined in terms of stall speed at full flap configuration.

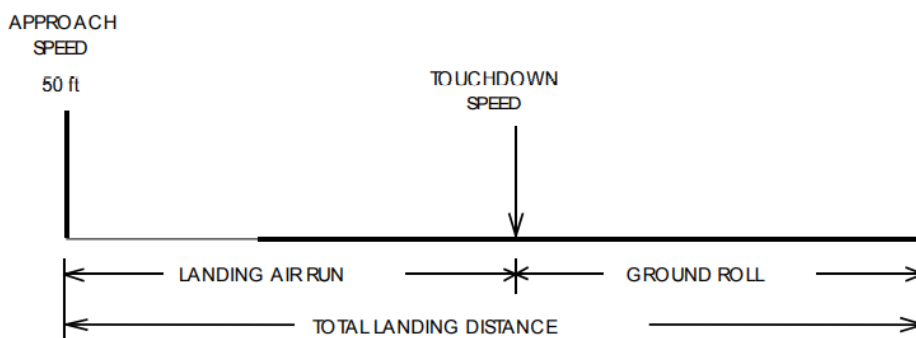


Figure 31: Landing distance analysis visualization

In Figure 31, the speeds and distance definitions are visualized. In landing distance calculation process, flare phase is ignored for the sake of simplicity. The landing simulation is initialized from approach trim, which is specified at Table 26, with full flap configuration. The distance travelled from the approach trim point to end of the landing process is calculated. The speed definitions which are utilized in landing simulations are explained according to MIL-STD-3013 as follows:

Touchdown speed is defined as the speed at which the air vehicle touches the ground, for a specified altitude, weight, and configuration.

Approach speed is defined as the speed which the air vehicle clears a 50-ft height above the runway during the approach to a landing for a specified altitude, weight, and configuration.

From Figure 32 to Figure 34, landing simulation results are figured out. As can be seen from Figure 34, landing distance is calculated as 426 meters via MAD tool. Also, the real landing distance data of Cessna 172N aircraft is indicated at Table 16 as 381 meters.

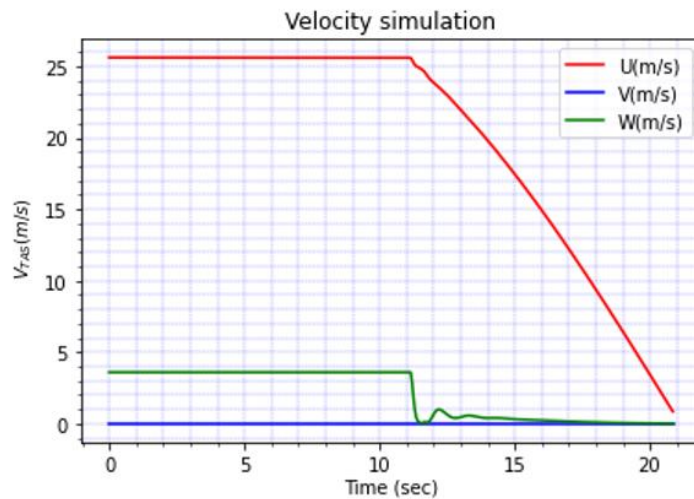


Figure 32: Landing simulation body velocities results

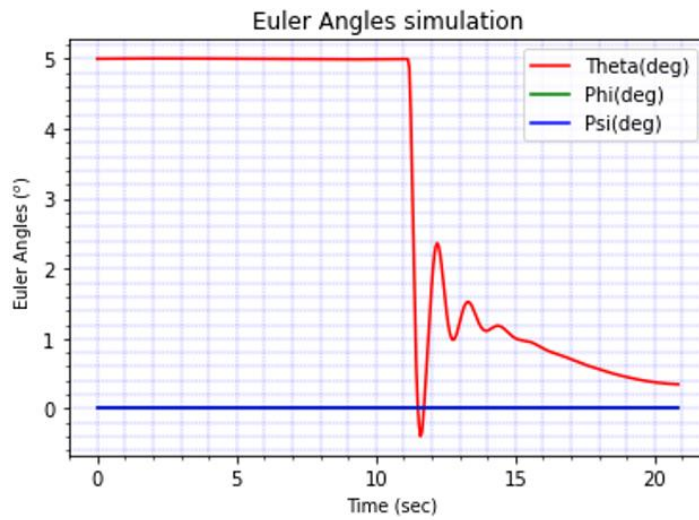


Figure 33: Landing simulation Euler angles results

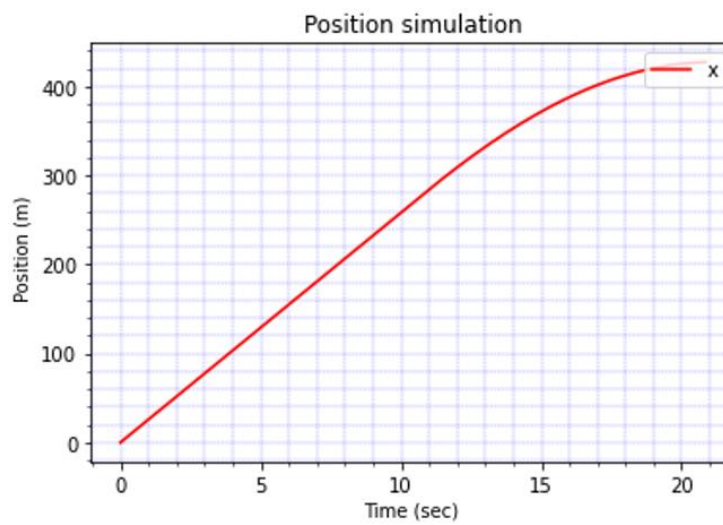


Figure 34: Landing distance simulation results

3.2 Stability Analysis

In the concept design phase of the aircrafts the first concern is generally performance calculations. However, stability analysis is also quite crucial for the design process. The flight character of the aircraft about equilibrium point indicates how much effort is required to handle the aircraft. With this standpoint, MAD environment classifies

the aircrafts according to the levels of acceptability related to the ability to complete operational missions by using stability analysis based on linearized 6-DOF dynamic model. The software includes three stability concern in it to evaluate the aircrafts at the conceptual design phase in detail (U.S.A. Department of Defense, 1980).

3.2.1 Flight Path Stability

According to MIL-F-8785C (U.S.A. Department of Defense, 1980), flight path stability is defined as flight path angle change with respect to the airspeed that is changed by use of pitch control only without changing throttle settings. In this scope, for the landing configuration, the curve of the flight path angle versus true airspeed shall have a local slope at $V_{o_{min}}$, which is less than the values defined in Table 54.

Table 54: FPS levels of acceptability (U.S.A. Department of Defense, 1980)

Level	Maximum Slope of $\left(\frac{\gamma}{V_{TAS}}\right)$
1	0.06 °/knot
2	0.15 °/knot
3	0.24 °/knot

The thrust setting shall be fixed at the required level to have the normal approach flight path angle at $V_{o_{min}}$. Also, the slope of the curve of flight path angle versus airspeed at 5 kts slower than $V_{o_{min}}$ shall not be 0.05 °/knots more positive than the slope at $V_{o_{min}}$ as illustrated by Figure 35.

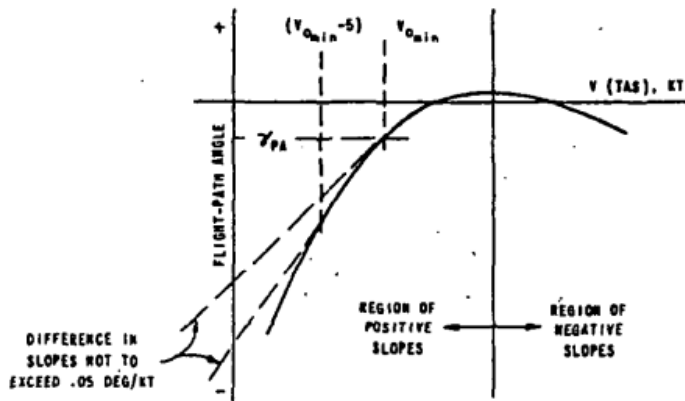


Figure 35: Flight path angle vs true airspeed (U.S.A. Department of Defense, 1980)

In order to perform flight path stability analysis, the straight flight trim is used with the fixed throttle and fixed gamma settings separately. The trim concepts are defined at Table 27 and Table 28.

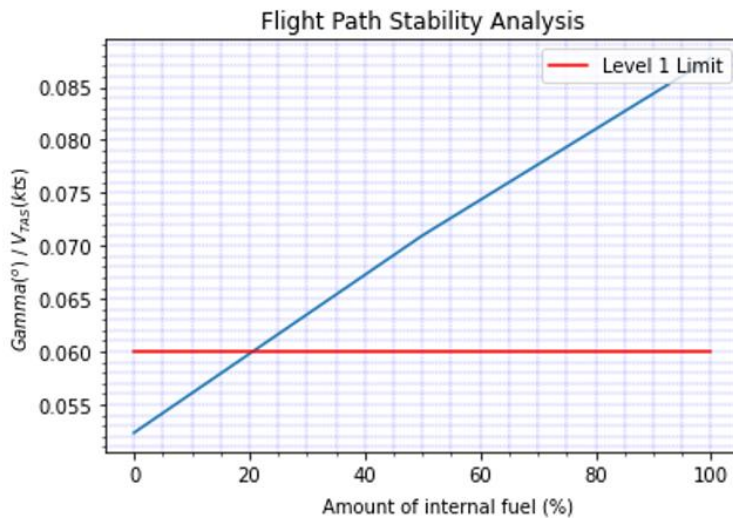


Figure 36: Flight path stability analysis output

The flight path stability analysis methodologies which are elaborated at this section is implemented to the MAD environment. The analysis results are figured out at Figure 36 for varying fuel percentage configurations.

3.2.2 Flying and Handling Qualities

Flying and handling qualities are vital for the maneuver simulation phase, which is the next step of trim analysis. In this phase, the aircraft should let the pilot to handle with the maneuver without loading him/her excessive work. Handling quality criteria serve to evaluate the stability and control characteristics of an air vehicle with respect to its suitability for completing different missions from a piloting point of view (Hasan et al., 2018). The precision tasks such as landing approach, tracking, and formation flying can only be accomplished successfully if the aircraft's dynamic stability characteristics are within acceptable ranges (Yechout et al., 2003).

In order to define this acceptable ranges, flight phases and class of the aircraft should be defined initially. Since the flying quality levels are meaningful within related class and flight phase only, which is shown at Table 55 and Table 56. Moreover, Table 57 is indicates flying quality levels definitions accordingly.

Table 55: Aircraft classes (U.S.A. Department of Defense, 1980)

Class	General Aircraft Types
Class I Small / Light Airplanes	Light Utility Primary Trainer Light Observation
Class II Medium Weight Airplanes Low-to-Medium Maneuverability Airplanes	Heavy Utility Search and Rescue Medium Transport Tactical Bomber Heavy Attack
Class III Large / Heavy Airplanes Low-to-Medium Maneuverability Airplanes	Heavy Transport Heavy Bomber Patrol
Class IV High Maneuverability Airplanes	Fighter Tactical Reconnaissance Observation

Table 56: Flight phase categories (U.S.A. Department of Defense, 1980)

Flight Phases		
Category	Definition	Included Maneuvers
A	Those nonterminal flight phases that require rapid maneuvering, precision tracking, or precise flight-path control.	Air-to-air combat (CO) In-flight refueling (receiver) (RR) Ground attack (GA) Terrain following (TF) Weapon delivery=launch (WD) Antisubmarine search (AS) Aerial recovery (AR) Close formation flying (FF) Reconnaissance (RC)
B	Those nonterminal flight phases that are normally accomplished using gradual maneuvers and without precision tracking, although accurate flight-path control may be required	Climb (CL) Descent (D) Cruise (CR) Emergency descent (ED) Loiter (LO) Emergency deceleration (DE) In-flight refueling (tanker) (RT) Aerial delivery (AD)
C	Those terminal flight phases that are normally accomplished using gradual maneuvers and which usually require accurate flight-path control	Takeoff (TO) Wave-off / go-around (WO) Catapult takeoff (CT) Landing (L) Approach (PA)

Table 57: Flying quality levels (U.S.A. Department of Defense, 1980)

Flying Quality Levels	
Level 1	Flying qualities clearly adequate for the mission flight phase
Level 2	Flying qualities adequate to accomplish the mission, but some increase in pilot workload or degradation in mission effectiveness exists
Level 3	Flying qualities such that the airplane can be controlled safely, but pilot workload is excessive, or mission effectiveness is inadequate, or both.

Level 1 is the highest level of flying quality. This level is required to satisfied for all points within operational flight envelope. Thus, level 1 flying qualities are used to define operational flight envelope.

Level 2 implies an increase in pilot workload or a degradation in mission effectiveness because of decreased dynamic stability or control power characteristics (Yechout et al., 2003). In fact, the aircraft, which is in the normal state, should satisfy at least level 2 flying quality requirements within the service flight envelope.

Level 3 flying quality requires that control of the airplane is maintained but cause excessive pilot workload or inadequate mission effectiveness. It is basically a “get home” level (Yechout et al., 2003). In the normal states, if the stability character is worse than level 3 flying quality requirements, it means the entrance of uncontrollable flight region. For this level of flying quality, Category A flight phases should be terminated safely, however Category B and C flight phases can be completed.

Table 58: Flight envelopes scope

Meanings of Flight Envelopes	
Satisfactory	Operational Flight Envelope
Tolerable	Service Flight Envelope
Recoverable	Permissible Flight Envelope

According to occurrence frequency of the states, for each flight envelope which is defined in Table 58, the required level of flying qualities is determined as in Table 59. Tables show that if the probability of encountering increases, then accepted maximum levels of flying quality is decreased.

Table 59 : Accepted levels of flying quality in related flight envelope

	Probability of Occurrence Per Flight	Within Operational Flight Envelope	Within Service Flight Envelope	Within Permissible Flight Envelope
Normal State	< 1	Level 1	Level 2	Level 3
Failure State	< 10 ⁻²	Level 2	Level 3	-
	< 10 ⁻⁴	Level 3	-	-

From Table 60 to Table 64 the specifications of the dynamic modes are denoted according to class and flight phase of the aircrafts for different flying quality levels. These specifications are critical to design the aircraft according to stability requirements of operational flight envelope.

Table 60: Short period mode flying quality levels in terms of damping ratio (U.S.A. Department of Defense, 1980)

	Category A and C		Category B	
	Minimum	Maximum	Minimum	Maximum
Level 1	0.35	1.30	0.30	2.00
Level 2	0.25	2.00	0.20	2.00
Level 3	0.15	-	0.15	-

Table 61: Phugoid mode flying quality levels (U.S.A. Department of Defense, 1980)

	Damping Ratio	Time to Double
Level 1	0.04	-
Level 2	0	-
Level 3	-	55

Table 62: Roll mode flying quality levels in terms of time constant (U.S.A. Department of Defense, 1980)

Flight Phase Category	Class	Level 1	Level 2	Level 3
A	I and IV	1.0	1.4	10
	II and III	1.4	3.0	10
B	All	1.4	3.0	10
C	I and IV	1.0	1.4	10
	II and III	1.4	3.0	10

Table 63: Spiral mode flying quality levels in terms of time to double amplitude (U.S.A. Department of Defense, 1980)

Flight Phase Category	Level 1	Level 2	Level 3
A and C	12s	8s	4s
B	20s	8s	4s

Table 64: Dutch roll mode flying quality levels (U.S.A. Department of Defense, 1980)

Category	Class	Minimum Damping Ratio	Minimum Natural Frequency
A	I and IV	0.19	1.0
	II and III	0.19	0.4
Level 1	B	0.08	0.4
	C	I and IV	0.08
	II and III	0.08	0.4
Level 2	All	0.02	0.4
Level 3	All	0	0.4

According to specified requirements included at tables from Table 60 to Table 64, flying and handling quality of the Cessna 172 aircraft is analyzed. At Figure 37 the comparison between eigenvalue analysis based on system identification method (Çetin, 2018) and MAD software prediction of the Cessna 172 are indicated.

According to results, the eigenvalues predicted by MAD software are found as reasonable, and compatible with system identification results (Çetin, 2018). In addition, the MAD environment provides to see all possible eigenvalues which corresponds to different velocities in the flight envelope. Figure 38 shows the eigenvalues at all speeds for most aft center of gravity configurations.

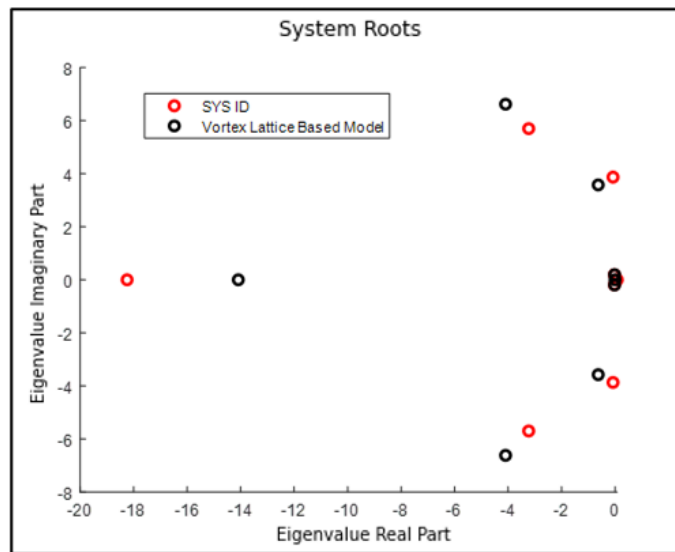


Figure 37: Eigenvalues of the Cessna 172 aircraft (Çetin, 2018)

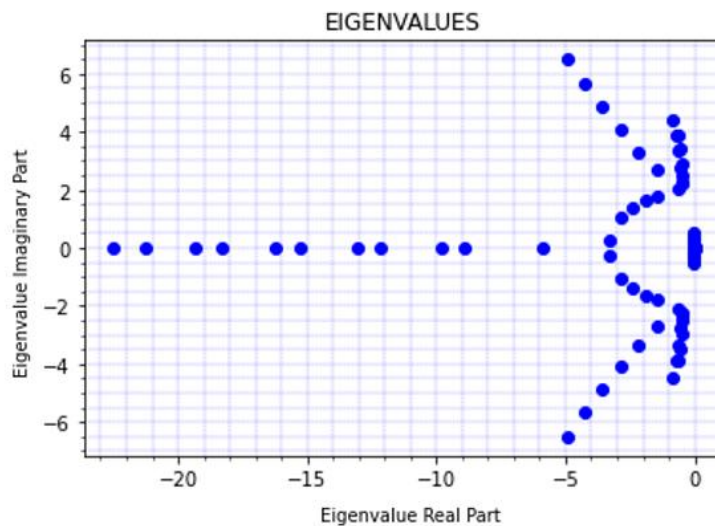


Figure 38: System eigenvalues predicted by MAD software

Figure 39 shows flying quality levels of each point in the flight envelope for most aft and most forward cg configurations. According to figures, the flight envelope is dominated by the trim points having level 1 and 2 flying qualities. In order to get flight characteristics of the related points in the envelope, trim analyses are performed for each speed and altitude combinations. Afterwards, the system is linearized at the trim point by using 6-DOF model. Thanks to linearized system matrix, longitudinal and lateral dynamic modes are obtained via MAD software. The dynamic modes are classified according to flying quality level requirements which is defined from Table 60 to Table 64. For each flight condition in the envelope, the levels of stability are figured out at Figure 39.

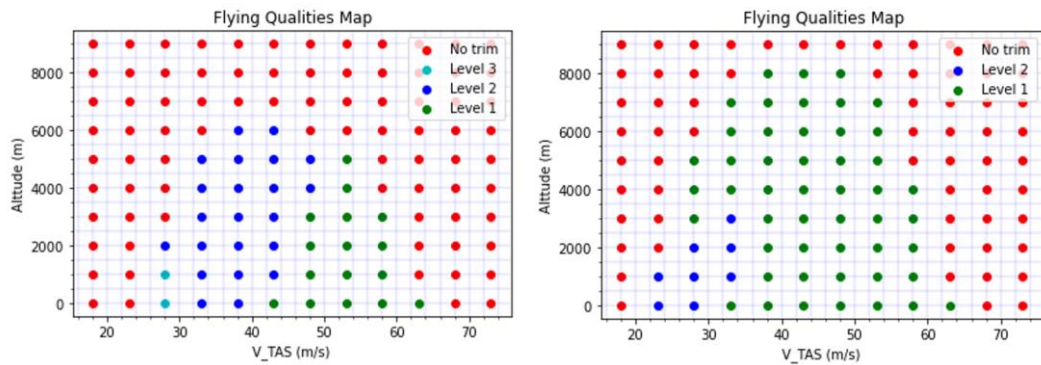


Figure 39: Flying quality map for most aft (left) and forward (right) cg

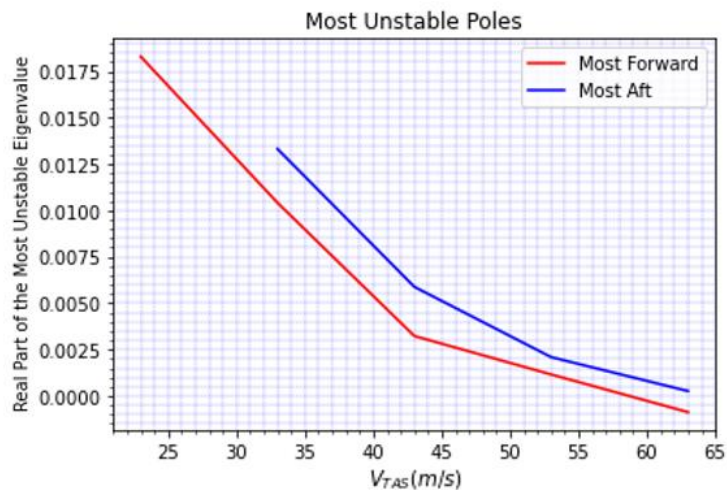


Figure 40: Most unstable pole with respect to airspeed

In addition, the most unstable poles are detected for each velocity in the envelope for most aft and most forward center of gravity configurations. The results are indicated at Figure 40.

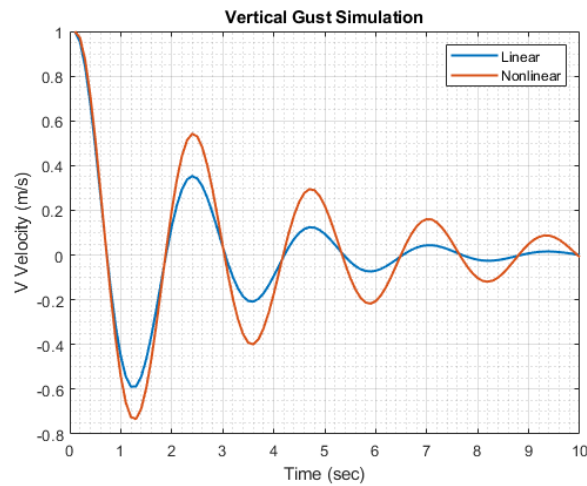


Figure 41: Linear and nonlinear model response to vertical gust perturbation

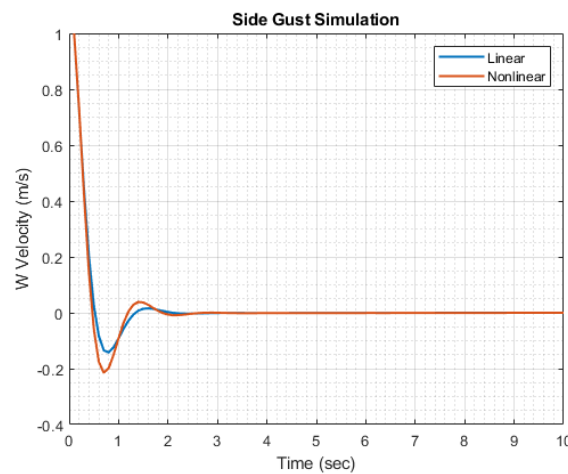


Figure 42: Linear and nonlinear model response to side gust perturbation

As a result of the handling quality study, linear and nonlinear models are compared to each other. For the comparison the velocities in body y and z axis are perturbed as 1 m/s from trim point. The results are figured out at Figure 41 and Figure 42. According to figures, frequency and amplitude of the linear and nonlinear model responses are observed as almost the same.

3.2.3 Spin

The spin is defined as a maneuver during which the aircraft descends rapidly in a helical movement, about a vertical axis, at an angle of attack greater than the aircraft stall angle of attack. Fundamentally an aircraft will enter a spin after stall occurs if the post-stall dynamics are characterized by rolling or yawing disturbances such that a phenomenon known as autorotation. The origin of these disturbances is most commonly due to an asymmetric stall progression that causes the sudden drop of one wing (Brinkworth & Uk, 2019). As a result of these attitudes, departures from controlled flight may lead to an undesirable trimmed flight condition which is named spin. In the existence of the post stall aerodynamic database, in order to observe spin character of the aircraft, trim and simulation analysis can be performed via MAD environment. In the software the trim algorithm which is used to get steady state modes is developed for spin condition specifically. The unknowns and constraints of spin trim, which is needed to get steady spin modes via 6-DOF mathematical model, is tabulated at Table 36.

After trim unknowns are obtained for the desired flight conditions, spin radius calculations can be performed by using Equation (94).

$$R_s = \left(\frac{\rho V_{TAS_{trim}}^2 S_{ref} C_{L_{trim}}}{2m\Omega^2} \right) \quad (94)$$

In order to obtain all possible spin modes, the altitude and weight combinations should be scanned via spin trim by changing flight path angle from -75 to -90 degrees. Each flight path angle input determines where spin trim optimization algorithm converges to. Moreover, in spin trim algorithm, initial conditions provide to change trim results critically. Because, for each altitude and weight combination, there are more than one equilibrium points. By manipulating initial condition of the trim unknowns, trim results can be obtained in desired flight region.

The steady or unsteady character of the spin modes can be determined by simulating the flight. According to MIL-F-83691, the mode character (steady or unsteady) can be interpreted by considering the variation in magnitude of the average angle of attack and yaw rate values throughout spin simulation (U.S.A Department of Defense, 1991).

3.2.4 Departure

In order to determine flight characteristics of the aircraft in departure prone regions, departure characteristics should be considered. In this study, quasi-trim algorithm, which is indicated at Table 37, is created to analyze departure characteristics of the aircraft by including control surface effects. For the evaluation of departure tendency, integrated Bihrlle-Weissman Chart, which is figured out at Figure 43, is benefited from. According to the chart, total seven categories are defined to classify the characteristics, expressed at Table 65.

Table 65: Bihrlle-Weissman chart class definition (Mason, 2006)

A	Highly departure and spin resistant
B	Spin resistant, objectionable roll reversals can induce departure and post stall gyrations
C	Weak spin tendency, strong roll reversal results in control induced departure
D	Strong departure, roll reversals and spin tendencies
E	Weak spin tendency, moderate departure and roll reversals, affected by secondary factors
F	Weak departure and spin resistance, no roll reversals, heavily influenced by secondary factors
U	High directional instability, insufficient data

The required parameters to interpret Figure 43, the relations which is defined in Equation (95) and (96) are utilized.

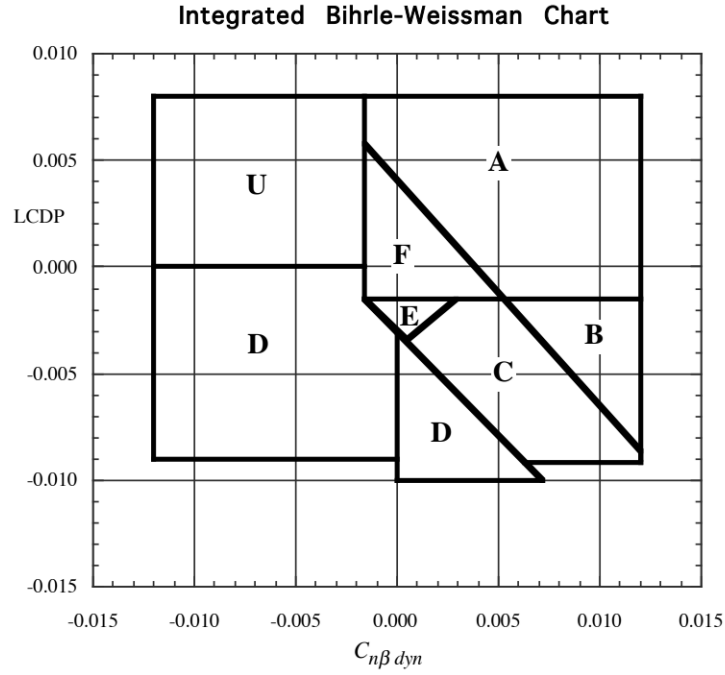


Figure 43: Bihrlé-Weissman chart (Mason, 2006)

$$C_{n\beta_{dyn}} = C_{n\beta} \cos \alpha - \left(\frac{I_{ZZ}}{I_{XX}} \right) C_{r\beta} \sin \alpha \quad (95)$$

$$LCDP_{open} = C_{n\beta} - C_{r\beta} \left(\frac{C_{n\delta_{aileron}}}{C_{r\delta_{aileron}}} \right) \quad (96)$$

If there is any aileron-rudder interconnection system in the aircraft, then effect of it should be included to $C_{n\delta_{aileron}}$ and $Cl_{\delta_{aileron}}$ parameters which is shown in Equation (97) (Mitchell & Johnston, 1980).

$$LCDP_{ARI} = C_{n\beta} - C_{r\beta} \left(\frac{C_{n\delta_{aileron}} + G_{ARI} C_{n\delta_{rudder}}}{C_{r\delta_{aileron}} + G_{ARI} C_{r\delta_{aileron}}} \right) \quad (97)$$

3.3 Control Surface Analysis

In an effective design process, it should be considered whether the aircraft has sufficient control authority to perform maneuvers throughout the flight envelope or not. In this scope, control surface sufficiency analyses are vital for control surface design at the early phase of the design. This capability provides designer to have a vision to see control surface effects over the aircraft performance and stability, besides general design inputs such as wing area or engine power.

3.3.1 Nose Down Recovery

To recover the aircraft from the stall, angle of attack must be reduced below the stalling angle. Nose-down pitch control must be applied and maintained until the wings are installed. In preliminary design phase, it is possible to check if pitch control is sufficient to recover the aircraft from the stall condition by referencing two base requirements. MIL STD 1797A (U.S.A Department of Defense, 2004) states that with full nose down control, the pitch moment should be at least a little negative at the most critical attainable angle of attack, for a center of gravity on the aft limit and nominal trim settings. With this standpoint, the minimum pitch acceleration and pitch rate requirements for the aircrafts from different classes are elaborated in Table 66 according to (Nguyen & Foster, 1990).

Table 66: Nose down recovery requirements (Nguyen & Foster, 1990)

Class	<i>Pitch acceleration</i> <i>(\dot{q}) rad/sec²</i>	<i>Pitch rate</i> <i>(q) rad/sec</i>
I	-0.28	
II	-0.20	
III	-0.08	-0.24
IV	-0.28	

Additionally required pitch acceleration because of inertial coupling should be added into the values which is specified at Table 66. According to (Nguyen & Foster, 1990), the pitch acceleration which is originated from inertial coupling effect can be calculated with Equation (98).

$$\dot{q}_{lc} = \frac{1}{2} \left(\frac{I_z - I_x}{I_y} \right) p_s^2 \sin(2\alpha) \quad (98)$$

3.3.2 Controllability

In order to see control surface sufficiency of the aircraft in the flight envelope, controllability study is performed via quasi-trim algorithm, which is defined in Table 37. Quasi trim algorithm provides to find a trim condition at the defined angle of attack, angle of sideslip, velocity and angular rates. Trim outputs show required control surface deflections to trim the aircraft in wings level condition. As a result of controllability trim study, the flight map, which is control surfaces are capable to keep angular rates constant, is created.

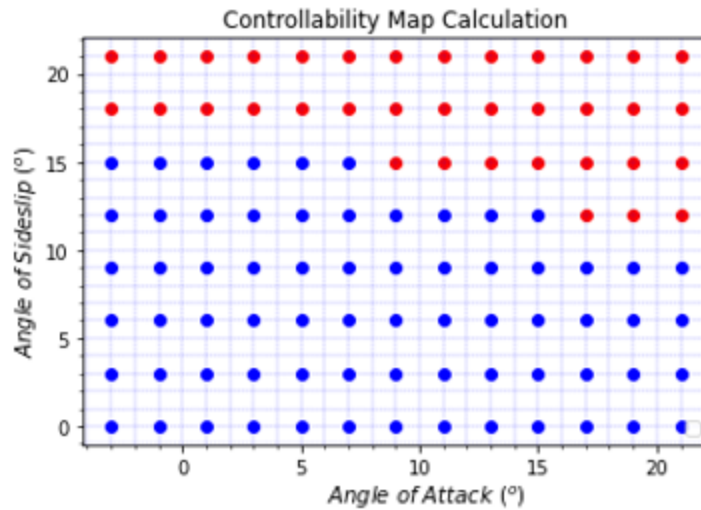


Figure 44: Controllable flight map

Figure 44 shows controllable region within flight envelope for various angle of attack and angle of sideslip conditions. The red dots represent untrimmed flight condition

because of insufficient control power. Also, blue dots show controllable conditions in the flight envelope. According to figure, control authority of the aircraft decreases as angle of attack increases.

3.3.3 Maximum Roll Capability

In the control surface design phase, roll capability is the one of the main concerns. In order to determine aileron size at the initial design phase of the aircraft, the roll rate requirements, which is tabulated at from Table 67 to Table 69, should be satisfied. The requirements are defined differently for each class and flight phase based on MIL STD 8785C (U.S.A. Department of Defense, 1980).

Table 67: Roll rate requirements for class I and II aircrafts (U.S.A. Department of Defense, 1980)

		Category A		Category B		Category C
		60°	45°	60°	45°	30°
Class I	Level 1	1.3		1.7		1.3
	Level 2	1.7		2.5		1.8
	Level 3	2.6		3.4		2.6
Class II	Level 1		1.4		1.9	1.8
	Level 2		1.9		2.8	2.5
	Level 3		2.8		3.8	3.6

Table 68: Required time to achieve 30° bank angle change for class III aircraft (U.S.A. Department of Defense, 1980)

Level	Speed Range	Category A	Category B	Category C
1	L	1.8	2.3	2.5
	M	1.5	2.0	2.5
	H	2.0	2.3	2.5
2	L	2.4	3.9	4.0
	M	2.0	3.3	4.0
	H	2.5	3.9	4.0
3	All	3.0	5.0	6.0

Table 69: Roll rate requirements for class IV aircrafts (U.S.A. Department of Defense, 1980)

Level	Speed Range	Category A			Category B	Category C
		30°	50°	90°	90°	30°
1	VL	1.1			2.0	1.1
	L	1.1			1.7	1.1
	M			1.3	1.7	1.1
	H		1.1		1.7	1.1
2	VL	1.6			2.8	1.3
	L	1.5			2.5	1.3
	M			1.7	2.5	1.3
	H		1.3		2.5	1.3
3	VL	2.6			3.7	2.0
	L	2.0			3.4	2.0
	M			2.6	3.4	2.0
	H		2.6		3.4	2.0

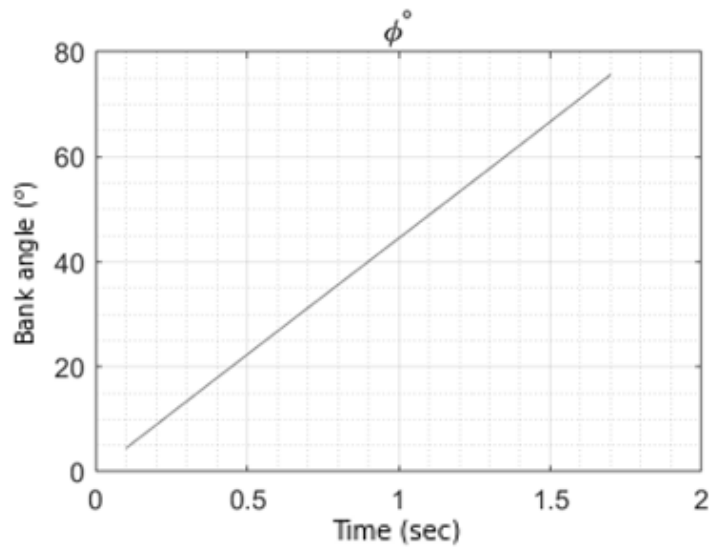


Figure 45: Bank angle response to maximum roll command

To determine maximum attainable roll rate by using all of the roll control power, steady roll trim algorithm is utilized, which is defined in Table 34. The bank angles with respect to time is figured out for maximum roll command condition at Figure 45. The figure shows that the Cessna 172N has 75° bank angle in 1.7 seconds which is the acceptable performance for the requirement, which is 60° bank angle should be reached in maximum 1.7 seconds with full aileron deflection.

3.3.4 Crosswind Landing

In the concept design phase of the aircrafts, in addition to the landing distance simulations, the crosswind condition at landing condition should also be checked from the standpoint of rudder authority sufficiency. In this part of the study, the methodology for evaluation of the landing characteristics under crosswind conditions is conducted, according to crosswind requirements specified in Table 70. The study is dedicated to crosswind landing since it is more critical phase when compared with takeoff.

Table 70: Crosswind requirement (U.S.A. Department of Defense, 1980)

	Class	Crosswind
Level 1	I	20 Knots
Level 2	II, III and IV	30 Knots
Level 3	All	One-half the values for Levels 1 and 2

The crosswind requirement at Table 70 is applicable for the 20 ft altitude where the wind speed measurement sensor is located, according to standards stated at MIL-STD-8785 (U.S.A. Department of Defense, 1980). Because of the wind shear effect, the reference airspeed will be decreased as approaching to ground. Thus, the wind shear effect should be calculated by utilizing Equation (99).

$$U_{ws} = U_{20} \frac{\ln\left(\frac{h}{z_0}\right)}{\ln\left(\frac{20}{z_0}\right)} \quad (99)$$

Where $z_0 = 0.15$ ft for Category C Flight Phase

$z_0 = 2.0$ ft for Category A and B Flight Phase

The MAD software performs crosswind landing analysis by using three different methodologies so called wing-low, crabbing and combination methods. In the validation study, combination method is benefiting from, which is defined at Table 35. According to trim analysis results, the combination of bank and crab angles are indicated at Figure 46 for the crosswind of 20 kts. Also, the required rudder deflection angle for each condition is shown in the same figure.

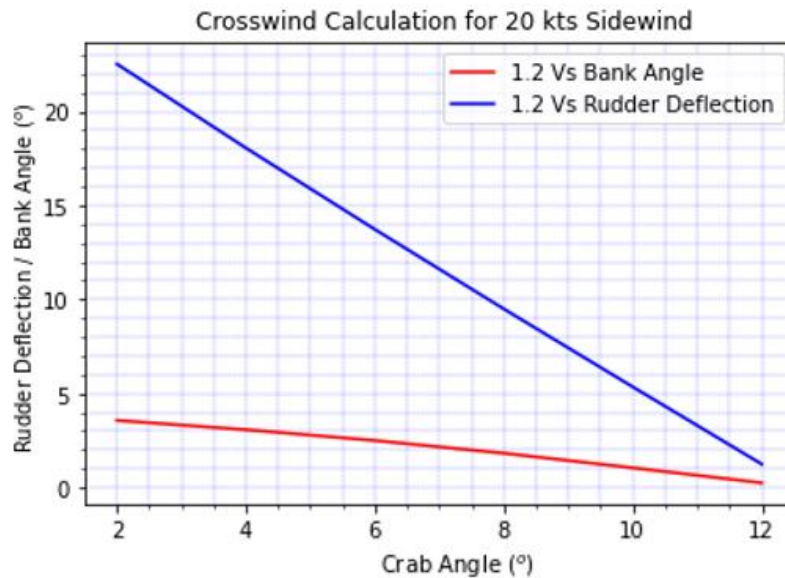


Figure 46: Crosswind landing analysis results

3.4 Model Validation Results

As a result of the validation process, flight manual performance data of Cessna 172N aircraft is compared with MAD software performance predictions. The results are tabulated at Table 71.

Table 71: Comparison between MAD prediction and Cessna 172 performance data

	Cessna 172 Flight	MAD	Mean Error
	Manuel	Prediction	Percentage
Take off Distance (m)	438	455	3.88
Landing Distance (m)	381	426	11.81
ROC (m/s)	3.91	4.08	4.35
Service Ceiling (m)	4330	4910	13.39
Stall Speed (Semi-Flap) (m/s)	24.2	23.7	2.07
Maximum Cruise Speed (m/s)	64	67	4.69
Range (m)	1064	1125	5.64
Endurance (hr)	6.4	6.9	7.81
Empty Weight (kg)	660	648	1.82

According to Table 71, while calculating performance characteristic of Cessna 172N aircraft, the maximum error norm of the MAD environment is observed as 13.4% which is reasonable for preliminary design phase. The result is regarded as acceptable because, MAD software performs analysis to know how a design input affects the design outputs. So, even the analysis results are different from the real performance data, the general approach to predict the relation between aircraft geometry and performance would be logical. By using this concept, the optimization process can be handled with ease by analyzing different alternative of geometries in early design phase.

CHAPTER 4

PRELIMINARY DESIGN AND OPTIMIZATION METHODOLOGIES

In this part of the study, the methodology of the design and optimization process for the fixed wing aircrafts is explained. The process, which is started with feasibility study and customer analysis, is completed by attaining the optimum design alternative which satisfies the related design requirements of the concept aircraft. In order to get optimum design for the aircraft, the physics-based analysis methods are used, which is investigated at Chapter 2 and Chapter 3.

4.1 Customer Requirements

In the concept design process, if the customer requirements are predicted accurately, then the design objective can be determined with ease. For this study, Cessna 172N aircraft is selected for optimization as a sample case. The main goal is determined as the improvements over the flight performance and stability properties of the Cessna 172N aircraft, by optimizing geometrical parameters according to customer requirements. With this standpoint, customer requirements and importance levels, which is created artificially, are tabulated at Table 72.

Table 72: Customer requirements and importance levels

CUSTOMER REQUIREMENTS	IMPORTANCE LEVELS
Affordable Price / Low Operational Cost	3
Good Handling Qualities	4
Predictable / Safe Flight	5
Durable / Long Lifecycle	5
Quite Operation Capability	2
Long Flight Duration Capability	4
Short Runway Operation Capability	2
Payload Capability	2
Fast Operation	3
Wide Range of Operation	5
Low vibration	1
Capable of Withstanding	4
Capability to low-speed operation	3
Capability to fly high Altitude	2

4.2 Competitors

Competitor aircraft survey is a significant phase of design, due to provide to see where the concept aircraft in the market when compared to other aircrafts in the same class. At Table 73, different competitor aircrafts which is in the same category with Cessna 172, are listed. In the table detailed specifications of the aircrafts are noted and various design concepts are discovered which is crucial for early phase of design.

Table 73: Specifications of competitor aircrafts (Wikipedia contributors, 2022)

COMPETITOR AIRCRAFTS SPECIFICATIONS							
	Cessna 172N	Grumman AA-5	Beechcraft Musketeer	Piper PA 28	Commander Aero 100	Diamond DA40	Vulcanair V 1.0
Gross Weight (kg)	1043	998	1089	975	1021	1198	1155
Empty Weight (kg)	658	577	624	545	581	795	763
Number of Passenger	4	4	4	4	4	4	4
Wing Area (m²)	16.17	13.0	13.6	15.0	17.0	14.0	-
Span (m)	11.0	10.0	10.0	9.1	11.0	12.0	10.0
Aircraft Length (m)	8.3	7.0	7.8	7.1	6.9	8.1	7.2
Max Engine HP	160	150	165	150	150	180	180
Range (km)	1063	930	1252	861	820	1341	1065
Take off Distance (m)	439	488	445	381	-	-	400
Landing Distance	381	335	384	335	-	-	480
Rate of Climb (m/s)	3.91	3.35	3.70	3.35	4.0	-	3.7
Service Ceiling (m)	4328	3855	3962	4358	3962	4876	4480
Stall Speed (kts)	44	50	63	47	48	49	48
Max Cruise Speed (kts)	125	130	127	123	116	151	128
LG Type	Tricycle	Tricycle	Tricycle	Tricycle	Tricycle	Tricycle	Tricycle
Wing Position	High	Low	Low	Low	High	Low	High

4.3 Configuration Selection

By considering customer requirements, the possible configuration alternatives are stated by observing the competitor aircrafts. A combination of different design options of each part of the aircraft is used to meet customer demands. The possible configuration alternatives are tabulated at Table 74.

Table 74: Fixed wing aircraft configuration alternatives

CONFIGURATION ALTERNATIVE						
Wing Position	Pitch Control Type	Vertical Tail Type	Motor location	LG type		Propeller Type
High	Canard	T	Fuselage Tip	Tricycle	Retractable	Fixed Pitch
Mid	Tail	H	Wing	Tail Dragger	Fixed	Variable Pitch
Low	Flying Wing	Conventional	Fuselage Aft			

From the different alternatives of configurations, the selected one is indicated at Table 75. According to the table, it can be seen that the chosen configuration is the same with the configuration which belongs to Cessna 172N aircraft. Because the optimization is aimed to perform with the different sizing alternatives of Cessna 172 aircraft without changing configurations. So, the further studies about preliminary design and optimization of Cessna 172N are completed by sticking to general configuration, which is defined Table 75.

Table 75: Selected configuration to optimization (Cessna Aircraft Company, 1978)

SELECTED CONFIGURATION					
Wing Position	Horizontal Tail Type	Vertical Tail Type	Motor Location	LG Type	Propeller Type
High	Tail	Conventional	Fuselage Tip	Tricycle, Fixed	Fixed Pitch

4.4 Quality Function Deployment Analysis

In this study, QFD matrix is utilized in order to analyze customer requirements. In the early phase of aircraft design, the verbal demands of the customers are quite challenging to turn them into the numerical engineering requirements. The QFD table makes a connection between customers and engineers by determining how the requirements can be satisfied and which type of analysis are needed for it. In this context, Table 76 is created to see the effects of customer needs on engineering parameters.

Table 76: Quality Function Deployment Analysis

QUALITY FUNCTION DEPLOYMENT										
Desired direction of improvement (↑,0,↓)		↓	↓	↑	↑	↑	↑	↓	↑	↓
1: low 5: high	Functional Requirements (How)	Empty Weight	Acquisition Cost	Range	Endurance	Ceiling Altitude	Stability	Take Off Landing Distance	Maximum Cruise Speed	Stall Speed
Customer importance rating	Customer Requirements - (What)									
3	Affordable Price / Low Operational Cost	9	9	1	1	1	1	1	1	1
4	Good Handling Qualities					1	9		1	1
5	Predictable / Safe Flight		1				3			3
5	Durable / Long Lifecycle		3	1	1	1	3			
2	Quite Operation Capability	1				3	1		1	
4	Long Flight Duration Capability	3		3	9	1		1	3	1
2	Short Runway Operation Capability	3						9	3	3
2	Payload Capability	1		3	3	3	1	3	3	1
3	Fast Operation	3	3	3	3	1	1	1	9	1
5	Wide Range of Operation	3		9	3	1		1	3	1
1	Low vibration	1					3		3	1
4	Capable of Withstanding		3			3	9	3		3
3	Capability to low-speed operation	3		1	1	1	1	1	3	9
2	Capability to fly high Altitude	3		3	1	9	1		3	3
	Technical importance score	89	68	89	79	69	120	54	93	88
	Importance %	12%	9%	12%	11%	9%	16%	7%	12%	12%
	Priorities rank	4	8	3	6	7	1	9	2	5
	OEC Coefficients	0.119	0.091	0.12	0.105	0.092	0.160	0.072	0.124	0.117

4.5 Overall Evaluation Criteria Equation

The technical importance scores of the performance outputs, that is included in the QFD table, is used to determine the coefficients of the OEC. OEC equation can be regarded as the objective function, which should be maximized. Equation (100) indicates the importance coefficients of the performance parameters together with overall evaluation criteria formulation.

$$\begin{aligned}
OEC = & 0.119 \frac{EmptyWeight\ ref}{EmptyWeight\ act} + 0.091 \frac{Cost\ ref}{Cost\ act} + 0.119 \frac{Range\ act}{Range\ ref} \\
& + 0.105 \frac{Endurance\ act}{Endurance\ ref} + 0.092 \frac{Ceiling\&ROC\ Alt\ act}{Ceiling\&ROC\ Alt\ ref} \\
& + 0.160 \frac{Stability\ act}{Stability\ ref} + 0.072 \frac{TO\&L\ Distance\ ref}{TO\&L\ Distance\ act} \\
& + 0.124 \frac{Max\ speed\ act}{Max\ Speed\ ref} + 0.117 \frac{Stall\ speed\ act}{Stall\ Speed\ ref}
\end{aligned} \tag{100}$$

OEC is an indicator of desirability level of the designed aircraft according to customer demands. Thanks to this concept, it can be seen which design alternative is more suitable with customer's requests, in a form of numerical value. Table 77 shows the outputs which is included to optimization process and importance levels of them.

Table 77: Design output parameters

Design Outputs	OEC Coefficient
Empty Weight	0.119
Cost	0.091
Take off & Landing Distance	0.072
ROC & Ceiling	0.092
Stall Speed	0.117
Max Speed	0.124
Range	0.119
Endurance	0.105
Stability (FPS & NDR & FHQ)	0.160

4.6 Design of Experiment

Design of Experiments is a mathematical methodology used for planning and conducting experiments as well as analyzing and interpreting data obtained from the experiments. It is multipurpose method that can be used in various situations such as

design for comparisons, variable screening, transfer function identification, optimization, and robust design (Durakovic, 2017). To benefit from these advantages of the statistical methods in the design process, design of experiment methodologies is utilized actively. In this scope JMP, which is an interactive data visualization and analysis tool, is used to implement statistical applications to overall design process. In this study, physics-based analyses are performed by MAD environment and the result of the analyses are used to feed JMP. As a result, MAD and JMP software are used to conduct design and optimization process collaboratively. Some of the statistical methodology alternatives, included in the DOE, are tabulated at Table 78.

Table 78: Statistical methodology alternatives in DOE

Level of Factorial	Type of Factorial	Fitting Model (RSM)	Fitting Methods
Two Level	Full Factorial	First order	Standard Least Square
Three Level	Fractional Factorial	First order with cross products	Generalized Regression
	Central Composite Design	Quadratic	

In Table 78, level of factorial concept stands for the number of levels which represents the whole range of each design variable. For the two levels factorial design, if temperature is a factor that varies from 30°C to 60°C, then the two levels used in the system would be 30°C and 60°C, which is the maximum and minimum values of the design variable.

Type of factorial represents the algorithms for design space creation. In the full factorial experiments all combination of the levels of the factors are analyzed (Kahn et al., 2017). To illustrate, in the two-level full factorial experiment with three factors, 2^3 cases are required to run. Statistical model of full factorial experiments having k factors, includes k main effects, $\binom{k}{2}$ times two-factor interaction, $\binom{k}{3}$ times

three-factor interactions, ... and $\binom{k}{k}$ times k-factor interaction. On the other hand, fractional factorial designs take into account only a low number of main effects and lower order interactions. The higher order interactions are ignored due to its negligible effects on the response variable (Bahçecitapar et al., 2016). In addition, central composite design consists of the additional axial and center points as well as full factorial model. In CCD the required number of analyses for k factors, can be expressed as in Equation (101).

$$CCD_{\# \text{ of run}} = 2^k + 2k + 1 \quad (101)$$

For two level experiment having three factors, CCD includes (2^3) corner points, (2×3) axial points and 1 center point. The axial and center points provide to represent system nonlinearity better. For three factor case, the central composite design totally includes 15 points which is figured out at Figure 47.

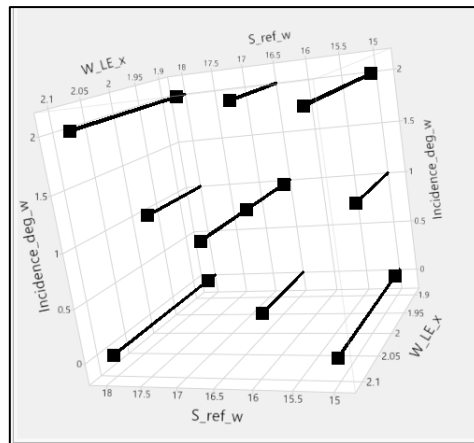


Figure 47: Central composite design structure

In the design process, the fitting models are used to represent the whole dynamic system of the aircraft by connecting design variables to design outputs directly with the analytical equations. The mathematical representation of the alternative fitting

models, in the polynomial forms, is stated at Equations (102), (103) and (104) (Alexander, n.d.).

First order(linear) model without cross product terms:

$$Y(x) = b_0 + \sum_{i=1}^k b_i x_i + e \quad (102)$$

First order(linear) model with cross product terms:

$$Y(x) = b_0 + \sum_{i=1}^k b_i x_i + \sum_{j=2}^k \sum_{i=1}^{j-1} b_{ij} x_i x_j + e \quad (103)$$

Second order quadratic model:

$$Y(x) = b_0 + \sum_{i=1}^k b_i x_i + \sum_{j=2}^k \sum_{i=1}^{j-1} b_{ij} x_i x_j + \sum_{i=1}^k b_{ii} x_i^2 + e \quad (104)$$

As can be seen from above relations, Equation (104) defines most inclusive fitting model by containing the other two equation in it, where b_i is regression coefficient for linear terms, b_{ii} is coefficient for pure quadratic terms, b_{ij} is coefficient for cross-product terms, x_i & x_j are the design variables and $x_i x_j$ are interactions between two design variables. In this study, in order to obtain the coefficients of the fitting equations, standard least square method is utilized. The method provides to minimize the sum of the difference between fitting equation and exact data points (SAS Institute Inc, 2018). By using all these methodologies, the statistical stages, which are implemented to design and optimization process of the concept aircraft, are stated as follows:

- Design Variable Reduction (Screening)
- Model Fitting (RSM)

4.6.1 Design Variable Reduction (Screening)

Screening study aims to determine most effective input set in the design process. According to “sparsity of effects” principle, most of the time, responses are influenced by a small number of main effects and lower order interactions, while higher order interactions are relatively unimportant. Thus, in the early stages of the experimentation, usually large number of potential factors are investigated to discover “vital few” factors. With this standpoint, the two-level fractional factorial design is used for screening to identify the important factors that can then be investigated more deeply in subsequent experiments (Kahn et al., 2017).

As a summary, the screening steps which are followed up in the process, are stated as follows:

- Chose potential design input parameters
- Select factorial type: Two level fractional factorial design
- Select resolution: Two Factor Interaction
- Perform the analysis for each design variable combination
- Fit model for related analysis outputs
- Check level of residual (error norm)
- Reduce number of factors to investigate with RSM

In the study initially 15 design variables, tabulated at Table 79, is investigated with screening methodology. In this process, instead of 2^{15} design points, 2^{15-8} points are analyzed with MAD environment by using fractional factoring model. The analysis results of each input combination are scored according to mean of the design outputs. In order to fit a model between design variables and OEC values, first order linear fitting model is utilized which is formulized at Equations (102). By using fitting model, effects of each factor on OEC are figured out as Pareto plot at Figure 48. From the figure the most effective factors are detected.

Table 79: All Design Input List

All Design Inputs	
Wing Reference Area (m ²)	Horizontal Tail LE Position (m)
Wing Leading Edge Position (m)	Vertical Tail LE Position (m)
Wing Incidence (°)	Aileron Area
Wing Aspect Ratio	Rudder Area
Horizontal Tail Area (m ²)	Elevator Area
Vertical Tail Area (m ²)	Taper Ratio
Maximum Engine Horsepower	Dihedral Angle
Fuel Weight (kg)	

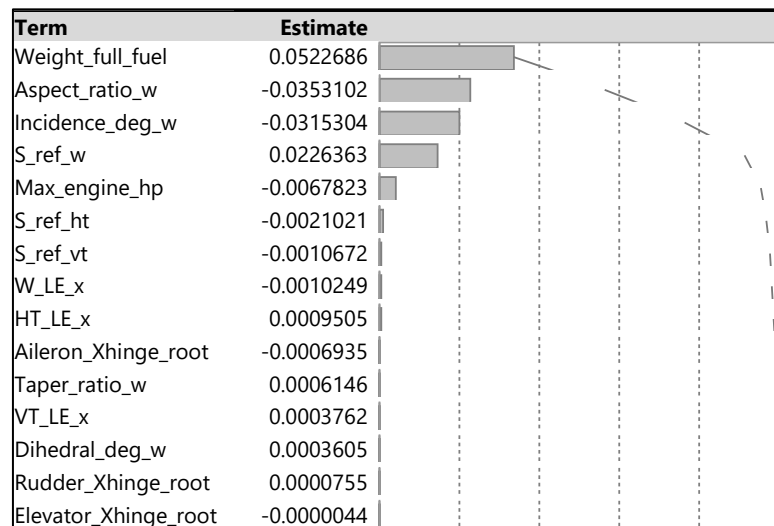


Figure 48: Pareto plot

As a result of the screening study the most effective 8 factors are obtained. Selected design variables and analysis intervals for each variable are indicated at Table 80.

Table 80: Selected design input parameters and optimization intervals

Selected Design Inputs	Interval
Wing Reference Area (m ²)	[15 - 18]
Wing Leading Edge Position (m)	[1.9 – 2.1]
Wing Incidence (°)	[0 - 2]
Wing Aspect Ratio	[6 - 9]
Horizontal Tail Area (m ²)	[3 - 4]
Vertical Tail Area (m ²)	[1.5 - 2]
Maximum Engine Horsepower	[150 - 180]
Fuel Weight (kg)	[90 - 120]

4.6.2 Response Surface Function

In the study, response surface method is utilized to predict to system response to any design variable inside of the limits. In the response surface methodology, the central composite design experiment is used by building a second order quadratic model without needing to use a complete three-level factorial experiment. Although the response surface is very effective and useful method, it can be used effectively only within a limited envelope. In this context, response surface designs are available for only continuous factors, and they support up to eight factors. Thus, in order to use response surface method, the screening study is mandatory to reduce number of design variable for the systems having more than 8 factors. In our case the reduced factors and related design space are visualized at Figure 49.

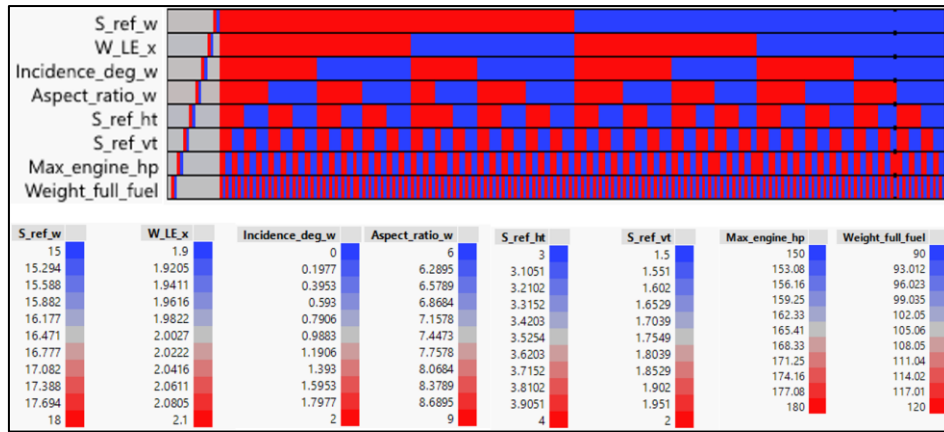


Figure 49: Response surface method design space

In Figure 49, there is 273 unique vertical lines which are composed of different level of factors. These points can be classified as 2^8 corner points, 2×8 axial points, and 1 center points, which is formulized at Equation (101). In the figure, blue, red, and grey colors represent maximum, minimum and center values of the design variables respectively. After defining design space, the coefficients of quadratic response surface function can be obtained via standard least square method. Thanks to this stage, the response surface function is obtained completely. As an example of the factor interaction level of the RSM for the system with three factor is tabulated at Table 81. At the table “x”, “o” and “v” symbols are representing regression coefficients for cross product terms, pure quadratic terms, and linear terms respectively.

Table 81: Considered factor interactions by response surface method

	Factor A	Factor B	Factor C	1
Factor A	o	x	x	v
Factor B		o	x	v
Factor C			o	v

In summary, the steps for implementation process of the Response surface method are stated as follows:

- Determine important design variables according to screening study
- Select Factorial Type: Central composite design
- Run the analyses for the points determined with CCD
- Select fitting model: Second order quadratic
- Exclude the deviated points from fitting model
- Get response surface function for each output separately

In summary, the ultimate objective of the Response Surface Method is to use a sequence of designed experiments to obtain an optimal response. Besides RSM, in order to get optimal response of the system, it is also required to have the optimization algorithms which are used to attain global minimum or maximum point of the objective function in the design space.

4.7 Optimization

The optimization stage of the design process is required to obtain the best design alternative which meets the needs optimally. In this scope, the main objective of the optimization process is determined as to maximize the result of desirability function. The desirability functions are used to combine the response surface functions according to importance levels of each specific design objectives. If the importance values are defined for each design output, then they can be integrated into the overall desirability function. The overall desirability function can be defined as a weighted geometric mean of the individual response surface functions as shown in Equation (105). In the equation, the scaled importance values are denoted by w_1, w_2, \dots, w_k . (SAS Institute Inc, 2018a)

$$D = r_1^{w_1} r_2^{w_2} \dots r_k^{w_k} \quad (105)$$

In the optimization process, the objective of each response surface function can be specified as maximizing, minimizing, or achieving target value. In desirability profiling, the desirability functions can be defined for each response separately or as an overall function. The optimization of the overall desirability function is conducted by gradient descent algorithm for continuous factors (SAS Institute Inc, 2018a). In summary, overall design and optimization workflow is figured out at Figure 50.

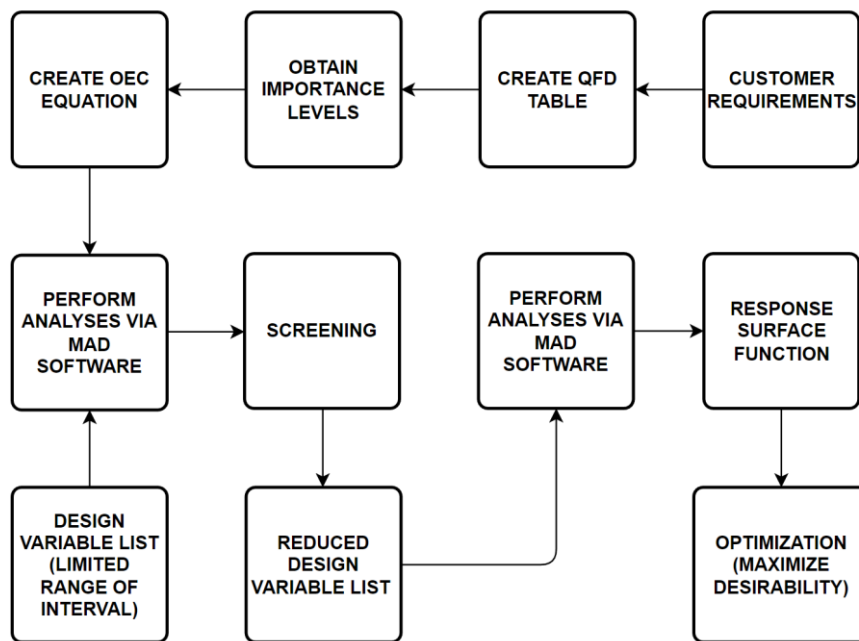


Figure 50: Design and optimization flowchart

In the optimization process, three type of overall system analysis technics are utilized so called contour plot, maximum desirability plot and surface plot. The contour plots show the relations between all design input and outputs instantly by benefiting from response surface functions. Thanks to the fact that all dynamic system is represented as analytical fitting functions, it is possible to observe the effects of each design variable on different design outputs. This capability provide designer to see the characteristics of the whole system without wasting time and money. In addition, by specifying the lower and upper bounds of the output parameters, the related design

input region which satisfies the defined limits can be observed at the visualization part. Figure 51 indicates the contour profiler which is created by using JMP software.

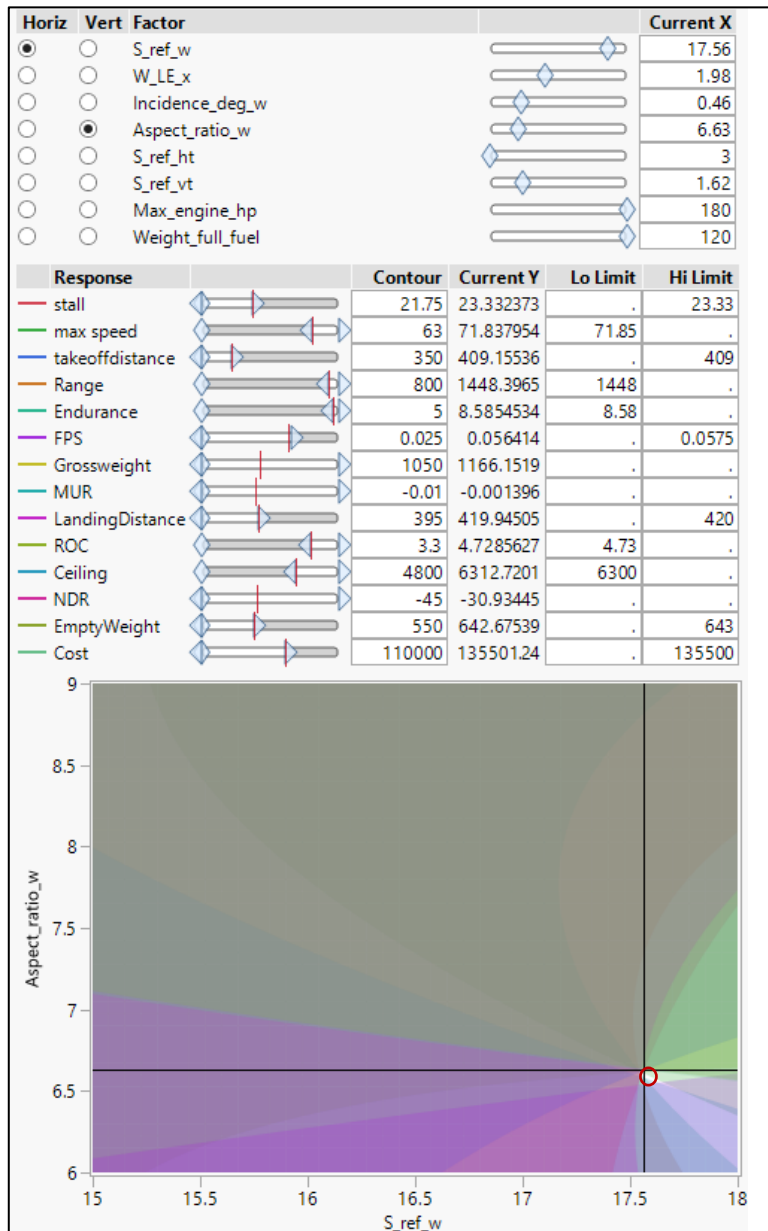


Figure 51: JMP contour profiler

The second system analysis technic of the optimization process is maximum desirability concept. In this concept the design variable values which provides the maximum value of desirability function is founded via JMP without exceeding defined limits for each factor. Figure 52 shows all interaction combinations between design input and outputs by visualizing each of them. Moreover, the system response to the optimum design variables is indicated at the same figure. In addition, Table 82 shows the most affected design outputs for five powerful design variables. In the table “min” and “max” subscripts are represents the optimization objective for related design output. Moreover, upper script shows the effects of the input parameters on related design outputs.

Table 82: Most affected design outputs for main design factor

Parameter	Most Affected Design Output
Wing Area	$Stall_{min}^-$, $LandDist_{min}^-$, $Ceiling_{max}^+$, $Endurance_{max}^+$, $Range_{max}^+$, GW_{min}^+ , $MaxSpeed_{max}^-$
Wing Position	NDR_{max}^- , FPS_{min}^-
Incidence Angle	$MaxBank_{max}^-$, MUR_{min}^+ , $LandDist_{min}^-$
Aspect Ratio	EW_{min}^+ , FPS_{min}^-
Max Engine Power	$MaxSpeed_{max}^+$, ROC_{max}^+ , $Ceiling_{max}^+$, $TakeOffDist_{min}^-$, EW_{min}^+

The last technic of the system analysis is called as surface plots. The main advantage of the surface plot is the capability to visualize the natural response of the system. Figure 53 shows the surface plot of ROC parameter with respect to reference wing area and aspect ratio.

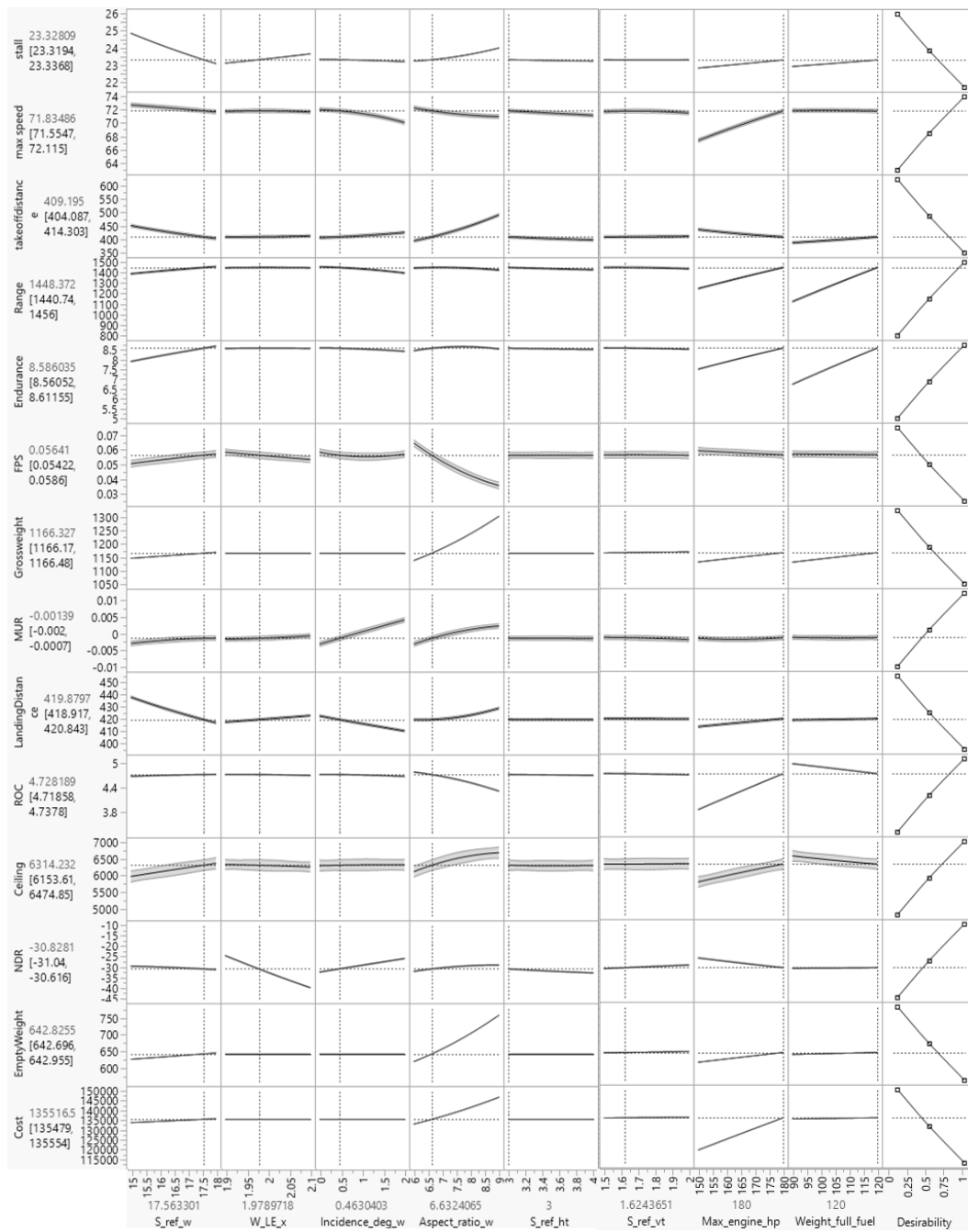


Figure 52: JMP maximum desirability results

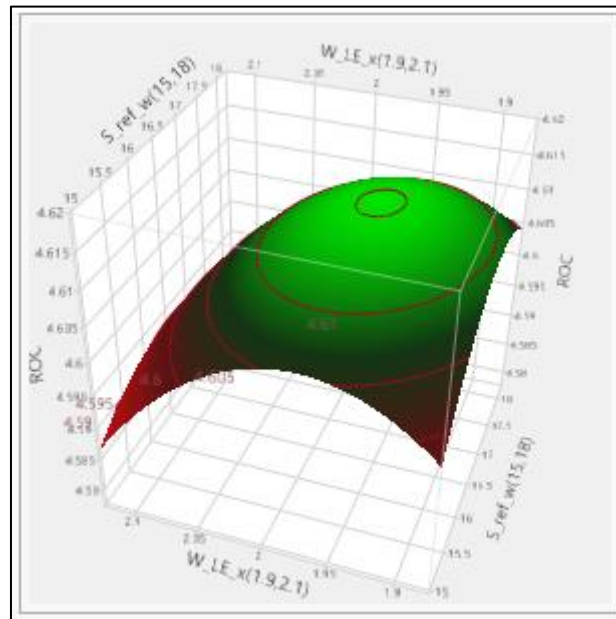


Figure 53: ROC surface plot

As a result of the optimization part of the study, optimum design variables are obtained according to customer demands by following up a systematic methodology. The performance values which are calculated with MAD software for base geometry, are tabulated at Table 83 as well as the optimized design outputs. Moreover, the design variables which correspond to optimized geometry of Cessna 172N can be observed from the Table 84.

Table 83: Performance enhancements of Cessna 172N aircraft

	Cessna 172 Base Performance (MAD)	Optimized Performance (RSF)	Improvement Percentage (%)
Take off Distance (m)	455	409	10.11
Landing Distance (m)	426	420	1.41
ROC (m/s)	4.08	4.73	15.93
Absolute Ceiling (m)	5930	6314	6.48
Stall Speed (m/s)	23.69	23.33	1.52
Max Cruise Speed (m/s)	67	72	7.46
Range (m)	1125	1448	28.71
Endurance (hr.)	6.9	8.59	24.49
Empty Weight (kg)	648	643	0.77
Cost (1000\$)	126.7	135.5	-6.95
FPS (°/knot)	0.088	0.057	35.23

Table 84: Design variables of optimized Cessna 172N geometry

	Cessna 172 Base	Cessna 172 Optimized
Reference Wing Area (m²)	16.10	17.56
Wing Aspect Ratio	7.50	6.63
Wing Incidence Angle (°)	1.50	0.46
Wing LE position (m)	2.00	1.98
Horizontal Tail Area (m²)	3.6	3.0
Vertical tail area (m²)	1.71	1.62
Maximum Engine HP	160	180
Fuel Weight (kg)	109	120

Table 85: MAD analysis and response surface function prediction comparison

	Cessna 172 Optimized Performance Of Analysis Tool	Cessna 172 Optimized Performance Of RSF	Prediction Tolerance (%)
Take off Distance (m)	412	409	0.73
Landing Distance (m)	415	420	1.20
ROC (m/s)	4.74	4.73	0.21
Absolute Ceiling (m)	6425	6314	1.73
Stall Speed (m/s)	23.35	23.33	0.09
Max Cruise Speed (m/s)	71.9	72.0	0.14
Range (m)	1458	1448	0.69
Endurance (hr.)	8.64	8.59	0.58
Empty Weight (kg)	642	643	0.16
Cost (1000\$)	135.4	135.5	0.07
FPS (°/knot)	0.057	0.057	0.00

Table 85 shows the performance predictions of response surface function and MAD software. The results indicate the error norm percentage of the fitting function which is in a reasonable range.

Also, an alternative case study for a different customer profile is shown in Table 86 and Table 87. Importance levels are changed according to new customer profile as can be seen from Table 86. Related QFD matrix is created by using alternative importance levels table. In fact, the change in importance levels does not affect response surface function of each design output. However, it can change the coefficients of OEC equation which is the desirability function of optimization process. According to updated OEC equation, optimization is completed, and results are tabulated at Table 87. From the results, it can be seen that the increment in importance level of price parameter provides to decrease cost. Also decreasing the importance level of “wide range operation capability” enables to decrease maximum range performance as expected. These results show that, any optimization case can be performed via MAD software by considering customer demands.

Table 86: Alternative customer importance levels

CUSTOMER REQUIREMENTS	IMPORTANCE LEVELS
Affordable Price / Low Operational Cost	5
Good Handling Qualities	4
Predictable / Safe Flight	5
Durable / Long Lifecycle	4
Quite Operation Capability	2
Long Flight Duration Capability	3
Short Runway Operation Capability	2
Payload Capability	2
Fast Operation	2
Wide Range of Operation	3
Low vibration	1
Capable of Withstanding	4
Capability to low-speed operation	3
Capability to fly high Altitude	2

Table 87: Performance enhancements results of Cessna 172N aircraft according to alternative customer importance levels

	Cessna 172 Base Performance (MAD)	Optimized Performance (RSF)	Improvement Percentage (%)
Take off Distance (m)	455	438	3.74
Landing Distance (m)	426	417	2.11
ROC (m/s)	4.08	3.86	-5.39
Absolute Ceiling (m)	5930	6120	3.20
Stall Speed (m/s)	23.69	23.29	1.69
Max Cruise Speed (m/s)	67	67.8	1.19
Range (m)	1125	1220	8.44
Endurance (hr.)	6.9	7.26	5.22
Empty Weight (kg)	648	591	8.80
Cost (1000\$)	126.7	116.5	8.05
FPS (°/knot)	0.088	0.062	29.55

CHAPTER 5

CONCLUSION

In this study design and optimization process of a fixed wing propeller driven aircraft is explained. Model Based Design (MAD) environment, which is created specifically for this study, is elaborated in two parts as model structure and analysis methodology. Capabilities of the alternative design software are investigated and compared to MAD tool. According to literature study it is seen that there is numerous alternative design software, however, any software apart from MAD, does not have the capability of performing instant trim and simulation via six degrees of freedom dynamic model. This capability provides user to analyze any unconventional unique design in detail without needing a pre-calculated database.

The MAD software is created by using mathematical dynamic model in Python environment. In addition, MATLAB, AVL and DATCOM software are utilized actively within the structure of MAD software. In the model structure, eight main disciplines are utilized to see the response of the dynamic system of the concept aircrafts. These disciplines are used to calculate force and moment on the aircraft and to simulate the flight.

In the study, the analyses are divided to three parts which are performance, stability and control surface sufficiency. Inside of these sections analysis methodologies are elaborated. Moreover, in order to validate the model and analysis methodologies, Cessna 172N aircraft is analyzed in detail. The results obtained from MAD environment are compared with the data in flight manual of Cessna 172N aircraft. According to comparison results, the MAD software predictions are observed as reasonable.

In design and optimization process, customer profile and requirements are determined as an initial step. With the help of QFD matrix, coefficients of OEC

equation are obtained. After this stage, Design of Experiment (DOE) concept are utilized for statistical analysis of the system via JMP. Initially screening study conducted with 129 different geometric alternatives, by using first-degree polynomial model which benefits from the fractional factorial design. This is sufficient to determine which explanatory variables affect the response variable of interest. Once it is suspected that only significant explanatory variables are left, then more complicated central composite design is implemented to estimate a second-degree polynomial model, which is named as Response Surface Method (RSM).

In order to use response surface methodology, initially 273 different geometric alternatives are analyzed, and desirability functions are defined to obtain maximum desirable point within the design space. In order to get global optimum point, optimization method is selected as to maximize or minimize for each design outputs according to desirability concept.

As a result, the optimized design variables provide more desirable design outputs when compared to base performance of Cessna 172N. In the whole analysis and optimization process, it is noticed that the instant trim and simulation algorithm of MAD environment works effectively within an acceptable tolerance.

In order to reach ultimate maturity level of MAD environment, in the future, following actions are planned to perform:

- To change motor dynamics with X_{rotor} or selectable real engine data
- To perform load and structural analysis
- To add SU2 analysis capability to use in further design phases
- To use advanced weight calculation methodologies
- To enlarge the scope of the software for supersonic or transport aircraft
- To develop graphical user interface for MAD software
- To make automatic the process between JMP and MAD environments

REFERENCES

- Afsar, R., Rumi, J., Salam, A., & Banna, H. (2013). *CEASIOM: An Open Source Multi Module Conceptual Aircraft Design Tool*. www.ijert.org
- Alexander, M. T. (n.d.). *RESPONSE SURFACE OPTIMIZATION USING JMP SOFTWARE*.
- Bahçecitapar, M. K., Karadağ, Ö., & Aktaş, S. (2016). Estimation of sample size and power for general full factorial designs. *Journal of Statisticians: Statistics and Actuarial Sciences*. www.istatistikciler.org
- Böhnke, D., Nagel, B., Zhang, M., & Rizzi, A. (2013). Towards a collaborative and integrated set of open tools for aircraft design. *51st AIAA Aerospace Sciences Meeting Including the New Horizons Forum and Aerospace Exposition 2013*. <https://doi.org/10.2514/6.2013-222>
- Brinkworth, B., & Uk, W. (2019). On the early history of spinning and spin research in the UK. *Journal of Aeronautical History*.
- Budziak, K. (2015). *Aerodynamic Analysis with Athena Vortex Lattice (AVL)*. <http://nbn-resolving.org/urn:nbn:de:gbv:18302-aero2015-09-20.015>
- Cessna Aircraft Company. (1978). *Cessna 172N Pilot's Operating Handbook*.
- Çetin, E. (2018). *SYSTEM IDENTIFICATION AND CONTROL OF A FIXED WING AIRCRAFT BY USING FLIGHT DATA OBTAINED FROM X-PLANE FLIGHT SIMULATOR*. Middle East Technical University.
- Chudoba, B. (2019). *Stability and Control of Conventional and Unconventional Aerospace Vehicle Configurations*. <https://doi.org/https://doi.org/10.1007/978-3-030-16856-8>
- Chudoba, B., & Cook, M. v. (2003). *Trim Equations of Motion For Aircraft Design: Steady State Straight-Line Flight*.

- Cook, M. v. (2013). *Flight Dynamics Principles* (3rd ed.).
 (<https://www.sciencedirect.com/science/article/pii/B978008098242700002X>)
- DARcorporation. (2018). *Advanced Aircraft Analysis User's Manual*.
- Drela, M., & Youngren, H. (2004a). *AVL User Primer*.
- Drela, M., & Youngren, H. (2004b, September 1). *AVL Overview*.
<https://web.mit.edu/drela/public/web/avl/>.
- Durakovic, B. (2017). Design of experiments application, concepts, examples:
 State of the art. *Periodicals of Engineering and Natural Sciences*, 5(3), 421–
 439. <https://doi.org/10.21533/pen.v5i3.145>
- ESDU 77022. (2003). *Equations for calculation of International Standard
 Atmosphere and associated off-standard atmospheres*.
- Fasanella, E. L., & Jackson, K. E. (2016). *4 th International LS-DYNA Users
 Conference Crash Testing and Simulation of a Cessna 172 Aircraft: Pitch
 Down Impact onto Soft Soil*.
- Federal Aviation Administration. (2009). *PART 23-AIRWORTHINESS
 STANDARDS: NORMAL, UTILITY, ACROBATIC, AND COMMUTER
 CATEGORY AIRPLANES*.
- Finck, R. D., Ellison, D. E., & Malthan, L. v. (1978). *USAF STABILITY AND
 CONTROL DATCOM*.
- Galbraith, B. (2004). *DATCOM Predicted Aerodynamic Model*. www.holycows.net
- Gudmundsson, S. (2014). *GENERAL AVIATION AIRCRAFT DESIGN: APPLIED
 METHODS AND PROCEDURES*.
<http://booksite.elsevier.com/9780123973085>
- Harris, F. D., & Scully, M. P. (n.d.). *Rotorcraft Cost Too Much*.
- Hasan, Y. J., Flink, J., Freund, S., Klimmek, T., Kuchar, R., Liersch, C. M., Looye,
 G., Moerland, E., Pfeiffer, T., Schrader, M., & Zenkner, S. (2018). Stability

- and control investigations in early stages of aircraft design. *2018 Applied Aerodynamics Conference*. <https://doi.org/10.2514/6.2018-2996>
- Jafari, H., & Shahmiri, F. (2019). Examination of Quadrotor Inverse Simulation Problem Using Trust-Region Dogleg Solution Method. *JAST*, *12*(1), 37–51.
- Kahn, C., Guo, H., Racaza, K., Hacker, L., & Caroline, M. (2017, August 10). *Two Level Factorial Experiments*.
<https://www.reliawiki.com/index.php?oldid=65247>.
- Liersch, C., & Hepperle, M. (2011). A distributed toolbox for multidisciplinary preliminary aircraft design. *CEAS Aeronautical Journal*, *2*(1–4), 57–68.
<https://doi.org/10.1007/s13272-011-0024-6>
- Lukaczyk, T., Wendorff, A. D., Botero, E., Macdonald, T., Momose, T., Variyar, A., Vegh, J. M., Colonna, M., Economon, T. D., Alonso, J. J., Orra, T. H., Ilario Da Silva, C., & Embraer, S. (n.d.). *SUAVE: An Open-Source Environment for Multi-Fidelity Conceptual Vehicle Design*.
- Lycoming. (2007). *Operator's Manual Lycoming O-320 Series*.
<http://www.lycoming.com>
- Mason, W. H. (2006). *High Angle Of Attack Aerodynamics*.
- McDonald, R. A., & Gloude-mans, J. R. (2022). Open vehicle sketch pad: An open source parametric geometry and analysis tool for conceptual aircraft design. *AIAA Science and Technology Forum and Exposition, AIAA SciTech Forum 2022*. <https://doi.org/10.2514/6.2022-0004>
- Mingtai, C. (2012). *Static Thrust Measurement for Propeller-driven Light Aircraft*.
- Mitchell, D. G., & Johnston, D. E. (1980). *Investigation of High Angle of Attack Maneuver Limit Factors*.
- Moerland, E., Zill, T., Nagel, B., Moerland, E., Zill, T., Nagel, B., Spangenberg, H., Schumann, H., & Zamov, P. (2012). *Application of a Distributed MDAO*

- Framework to the Design of a Short-to Medium-Range Aircraft.*
<https://www.researchgate.net/publication/259896668>
- Nguyen, L. T., & Foster, J. v. (1990, February). *Development of A Preliminary High Angle of Attack Nose Down Pitch Control Requirement for High Performance Aircraft.*
- Özdemir, M., & Kurtulus, D. F. (2021). *GENERIC TRIM ANALYSIS AND SIMULATION ALGORITHM CREATION FOR DESIGN AND OPTIMIZATION OF THE FIXED WING AIRCRAFT.*
<https://www.researchgate.net/publication/354451387>
- Pester, M. (2010). *Multi- Disciplinary Conceptual Aircraft Design using CEASIOM.*
- Richardson, T. S., Beaverstock, C., Isikveren, A., Meheri, A., Badcock, K., & da Ronch, A. (2011). Analysis of the Boeing 747-100 using CEASIOM. *Progress in Aerospace Sciences*, 47(8), 660–673.
<https://doi.org/10.1016/j.paerosci.2011.08.009>
- Rocca, G. la, Zill, T., Rocca, G. la, Jansen, J., & Zill, T. (2013). *Investigation of multi-fidelity and variable-fidelity optimization approaches for collaborative aircraft design.* <https://www.researchgate.net/publication/259176444>
- Roskam, J. (1997). *Airplane Design Part I Preliminary Sizing of Airplanes.* DARcorporation. <https://books.google.com.tr/books?id=GIHHFkd829cC>
- Roskam, J. (2018). *Airplane Design Part V: Component Weight Estimation* (Vol. 5). DARcorporation.
- Sadraey, M. H. (2013). *Aircraft design: a system engineering approach.*
- SAS Institute Inc. (2018a). *Desirability Profiling and Optimization.*
- SAS Institute Inc. (2018b). *DISCOVERING JMP.* SAS Institute.

- Siddiqui, B. A., Kassem, A. H., & Al-Garni, A. Z. (2010). Using USAF DATCOM to Predict Nonlinear Aerodynamics of Structurally Impaired Aircraft. *International Review of Aerospace Engineering (I.RE.AS.E)*, xx.
- Suit, W. T., & Cannaday, R. L. (1979). *NASA Technical Memorandum 80163*.
- U.S.A. Department of Defense. (1980). *MIL-F-8785C Flying Qualities of Piloted Airplanes*.
- U.S.A Department of Defense. (1991). *MILITARY SPECIFICATION FLIGHT TEST DEMONSTRATION REQUIREMENT'S FOR DEPARTURE RESISTANCE AND POST-DEPARTURE CHARACTERISTICS OF PILOTED AIRPLANES*. <http://www.everyspec.com>
- U.S.A Department of Defense. (2003). *PRACTICE GLOSSARY OF DEFINITIONS, GROUND RULES, AND MISSION PROFILES TO DEFINE AIR VEHICLE PERFORMANCE CAPABILITY*. <http://www.everyspec.com>
- U.S.A Department of Defense. (2004). *FLYING QUALITIES OF PILOTED AIRCRAFT*. www.dodssp.daps.mil.
- Vecchia, P. della, Ciampa, P. D., Prakasha, P. S., Aigner, B., & van Gent, I. (2018). MDO framework for university research collaboration: AGILE academy initiatives & outcomes. *2018 Multidisciplinary Analysis and Optimization Conference*. <https://doi.org/10.2514/6.2018-3254>
- Wikipedia contributors. (2022a, February 13). *Cessna 172 Related Developments*. Wikipedia, The Free Encyclopedia.
- Wikipedia contributors. (2022b, June 10). *Cessna 172*. https://en.wikipedia.org/w/index.php?title=Cessna_172&oldid=109240310
- 1.
- Yechout, T. R., Morris, S. L., Bossertt, D. E., & Hallgren, W. F. (2003). *Introduction to Aircraft Flight Mechanics: Performance, Static Stability,*

Dynamic Stability, and Classical Feedback Control (J. A. Schetz, Ed.; 2nd ed.). American Institute of Aeronautics and Astronautics.

Zur, S. (2013). *RCE-Distributed, Workflow-driven Integration Environment*.
www.rcenvironment.de